Sheffield Hallam University

A Sheffield Hallam University thesis

Experimental and theoretical modelling of cancellous bone structure for the ultrasonic assessment of Osteoporosis

Malcolm Anthony Whitehead

A thesis submitted in partial fulfilment of the

requirements of

Sheffield Hallam University

For the degree of Master of Philosophy

In collaboration with the

University of York

May 1997

ABSTRACT

This study describes the use of the Stereolithography (SL) process to produce what are probably the first realistic mimics of trabecular bone, with a precise predefined structure, for use in the modelling of BUA in the calcaneus. This is part of the ongoing investigation of the role of ultrasound in the assessment of Osteoporosis.

It has been shown that Broadband Ultrasonic Attenuation (BUA) measurements of the calcaneus have a similar diagnostic accuracy to ionising radiation measurements of spinal bone density, in predicting fracture risk due to Osteoporosis. There is evidence that BUA measurements are related to structure as well as bone mineral density and if this structural information can be isolated, osteoporotic fracture risk predictions will be enhanced.

The actual ultrasonic attenuation mechanisms occurring in cancellous bone (thought to be mainly scattering) are not fully understood at present and further research is hampered by the lack of suitable samples. The available bone samples tend to be of elderly or diseased origin and so there is, therefore, a need for a bone mimic with similar acoustic properties to cancellous bone whose structure can be carefully controlled.

Previous attempts to model cancellous bone using perspex and a composite epoxy resin did not produce acoustic characteristics sufficiently close enough to natural tissue and so an alternative approach was required.

The Stereolithography (SL) process is a form of rapid prototyping that allows complex solid objects to be made directly from 3D computer models, by laser scanning of liquid light cured resins. The smallest wall thickness of this system is 0.3mm

A literature search of calcaneal trabecular bone was unable to supply the detailed structural information required to produce a design for a cancellous bone model, and so a modified histomorphometrical analysis procedure was used.

Two cancellous core samples, one high density and one low density, were analysed using digital imaging techniques and the majority of the trabeculea in both models were found to be less than the 0.3 mm resolution of the SL system. This ruled out a full 3D reconstruction of the samples and so a model, similar to but not exactly like, cancellous bone was designed, based on the skeleton of the low density sample.

The basic model, using castor oil as a marrow mimic, was found to be stable and the ultrasonic characteristics were compatible with natural tissue.

In order to look at the relationship between ultrasonic parameters and porosity, a family of models, based on the basic design, was produced. The porosity of the models was 70% (basic design) 50%, 30%, 80% and 85%.

BUA showed a non linear relationship with porosity with a minima at 0 and 100%, and a maxima at 70%. This is very similar to natural tissue which has a peak BUA at 75%. Velocity showed a linear relationship with porosity and the values, within experimental limits, followed the theoretical model. These results validated the use of the SL process as a modelling medium.

Two further models, with a different structure but the same porosity as the basic model, were produced, and the three models showed a 7% spread of BUA, confirming the structural dependence of BUA.

Using the precise structural details extracted from the computer model, the best structural indicator of BUA for the SL models was found to be Trabecular Surface Area, with a high correlation of $r^2 = 0.92$.

This would seem to confirm that the attenuation mechanism in cancellous bone is governed by architectural complexity as well as porosity.

AIMS

The aims of this project are:

- To investigate the Stereolithography process with a view to producing a cancellous bone model for use in the assessment of Osteoporosis.

- To provide specific structural data from human calcaneal cancellous bone to form an SL model design.

- To produce a basic SL model and carry out an evaluation in terms of ultrasonic velocity and BUA.

- To evaluate the effect of altering porosity whilst maintaining constant structure, and vice versa, on ultrasonic parameters by producing variations of the basic SL model.

ACKNOWLEDGMENTS

CONTENTS

3

List of Figures

6

List of Tables

CHAPTER ONE

The Assessment of Osteoporosis using

Broadband Ultrasonic Attenuation (BUA).

1:1 Introduction

Osteoporosis, or brittle bone disease, affects approximately one in four women over 60

years old and one in two over seventy years old at a cost of over £640 million per annum

to the National Health Service[1]. Until recently the first indication of the presence of the

disease was a non traumatic fracture, usually at the hip or wrist. At this advanced stage

of the condition, recovery and subsequent preventative treatment is very difficult and so

non invasive methods of predicting those at risk at an earlier stage were sought.

Bone density is the parameter most commonly used to predict fracture risk at present

and may be measured by ionising radiation techniques, such as dual energy x-ray

absorptiometry (DXA) or Quantitative Computerised Tomography (QCT)[2], and the area

of interest in this thesis, Quantitative Ultrasound (QUS).

This first chapter begins with an overview of osteoporosis followed by a description of

Broadband Ultrasonic Attenuation (BUA), including the 3 main commercial systems on

the market. Section 4 introduces the concept that BUA is also dependent on bone

structure as well as density and finally section 5 looks at the problems associated with

measuring the internal structure of bone and specifies the need for the development of a

physical bone model with a controlled structure.

1:2 Osteoporosis - An Overview

Osteoporosis literally translates to porous bone and can be defined as a disease characterised by low bone mass with micro-architectural deterioration of bone tissue, leading to enhanced bone fragility and a consequent increase in fracture risk[3]

The direct cause of the condition is an imbalance in the normal renewal process that the skeleton is continually undergoing, leading to a gradual reduction in bone mass.

Bone is composed of collagen, an organic fibrous matrix, impregnated with inorganic mineral, mainly calcium and phosphate, and exists in two forms, cortical and cancellous. The compact cortical bone forms the outer shell of the skeleton and accounts for the greatest proportion of long bones such as the femur and humorous. The second type of bone, cancellous, takes the form of a honeycomb type structure made of small plates and rods called trabeculea. This three dimensional structure is indispersed with bone marrow and fat and forms the greater part of vertebrae and the heel bone. It is also found at the ends of long bones where stresses are applied over large areas. See figure 1:1

Figure 1:1 Examples of a normal and Osteoporotic Femur.

Normal   Osteoporotic
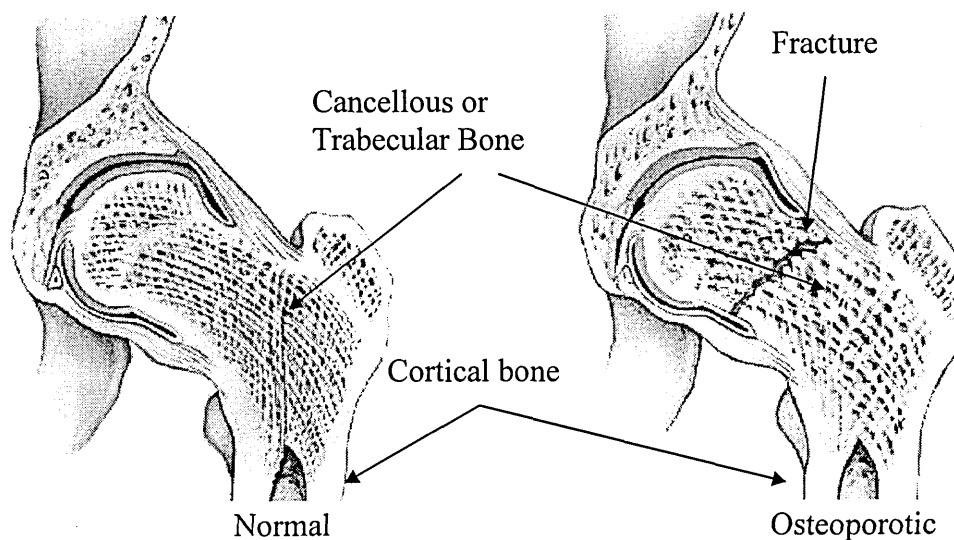
It can be seen in the diagram that the trabeculea are orientated along the lines of principle stress.

The constant renewal of bone within the skeleton is carried out by two cell types, osteoclasts and osteoblasts, in a process known as remodelling. The osteoclasts absorb the bone to form microscopic cavities which are then infilled by the osteoblasts.

Peak bone mass is achieved at between 30 and 40 years for both men and women with a gradual decline thereafter due to an imbalance in remodelling.

Once a certain level of bone has been lost, the risk of fracture increases significantly and this is known as primary osteoporosis. It is found mainly in post menopausal women and very elderly men. Osteoporosis may also be caused by factors other than age, e.g., digestive disorders, immobility, rheumatoid arthritis and steroid therapy. It is then classified as secondary osteoporosis.

The condition is also classified by the main type of bone loss:

Type I Osteoporosis   Perforation of the trabecular framework where complete rods or plates disappear.

Type II Osteoporosis Overall thinning of the whole trabecular structure.

During remodeling, the turnover rate in cancellous bone is eight times that of cortical bone[4], and this, combined with the greater surface area of the trabeculae, means that sites with large amounts of cancellous bone are more sensitive to osteoporotic changes. The calcaneus, or heel bone, is over 90% cancellous bone with a thin cortical shell. There is limited soft tissue around it and it is easily accessible, making it the logical site for ultrasonic measurements.

the calcaneum.

Figure 1:2 Normal Calcaneal Trabecular bone
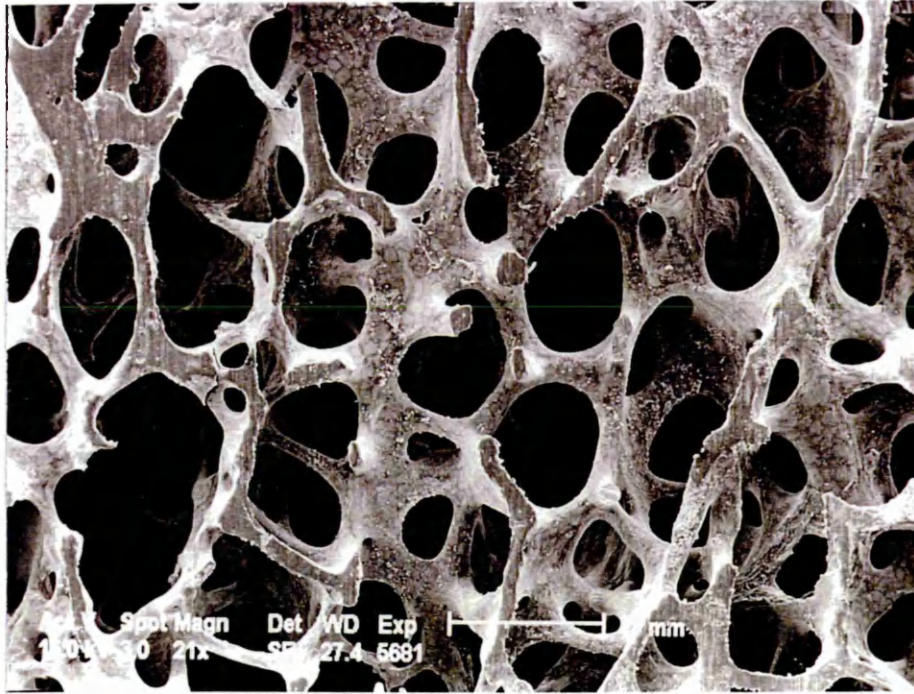
Figure 1:3 Osteoporotic Calcaneal Trabecular bone
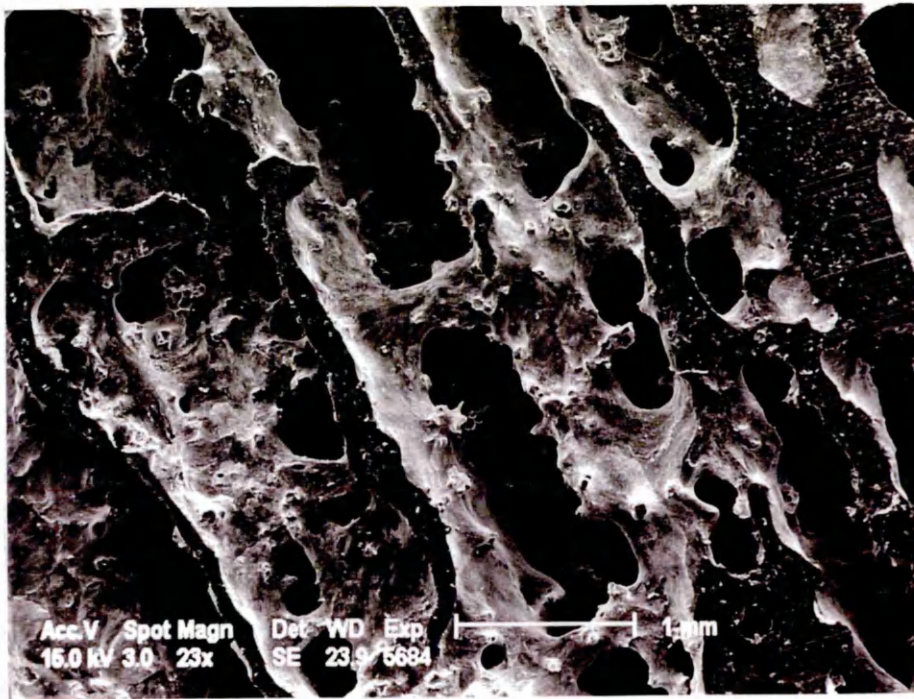
1:3 Broadband Ultrasonic Attenuation (BUA)

In 1984 C M Langton *et al*[5] demonstrated that there is a linear relationship between ultrasonic attenuation and frequency in the calcaneus.

Using a temperature controlled water bath and two 25 mm diameter broad band transducers, measurements were taken through the calcaneus in the frequency range 0.2 MHz to 1mhz.

Figure 1:4 Schematic diagram of the ultrasonic system
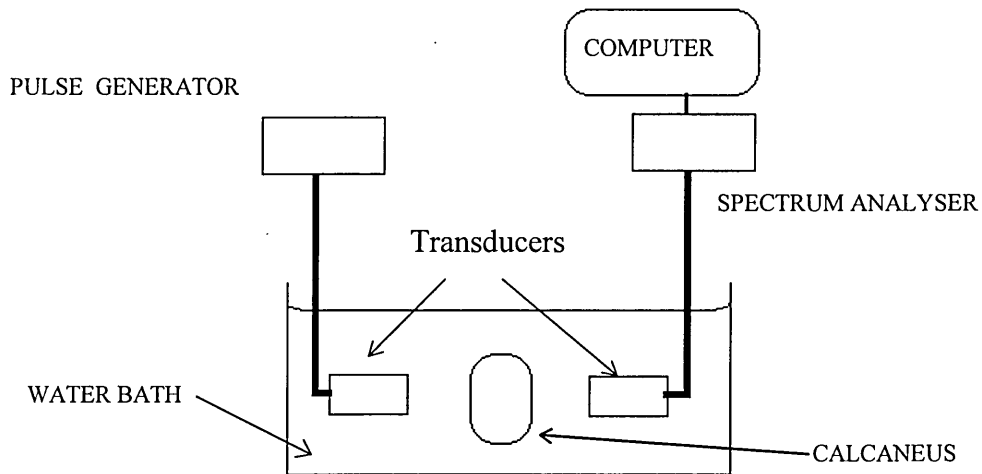
The transmit transducer is excited by a fast rising 1KV spike which produces a short broadband ultrasonic pulse. The output signal from the receive transducer, which detects the propagated ultrasonic pulse, is fed into a spectrum analyzer and the resulting attenuation information stored in the computer.

To account for the frequency response of the transducers, a 'reference trace' is first taken across the frequency spectrum through the water in the bath, i.e. without the foot in place. Subtracting the spectrum obtained with a foot in place from the reference trace directly yields the relationship between ultrasonic attenuation and frequency for that

12

subject. The slope of this linear relationship is termed the Broadband Ultrasonic Attenuation, BUA, measured in dBMHz^{-1}.

An initial *in vitro* study was carried out on cylinders of bovine cancellous bone which showed that BUA was directly related to the total bone volume through which the ultrasound propagates and is therefore an indicator of bone mineral content (BMC). Since the total bone volume is dependent on the sample width as well as the relative density, absolute measurements of BMC require the BUA to be divided by the width of the sample to give a normalised BUA reading (nBUA, dBMHz^{-1}cm^{-1}).

Following this, an *in vivo* study was carried out on 60 females from three populations:

a)   20 healthy women between 20 and 50 years

b)   20 healthy women between 55 and 85 years with no history of fracture

c)   20 women within four weeks of sustaining a fracture of the neck of the femur, between 63 and 93 years of age.

Fig 1:5 shows typical plots of attenuation vs frequency for young females and post femur neck fracture patients, from which BUA is derived. Fig 1:6 shows the results for all sixty patients and demonstrates the highly significant age and fracture related dependence of BUA

Langton *et al* concluded that BUA measurements of the calcaneus are directly related to BMC and so could be used as an indicator in the assessment of osteoporosis. Further more, non invasive ultrasound measurements are inherently safer than ionising techniques and so have the potential to provide a better method for large scale screening of those at risk from osteoporosis.

Figure 1:5 Comparative traces for a typical young female adult and typical fractured neck of femur female patient

Error bars show variation within the population tested
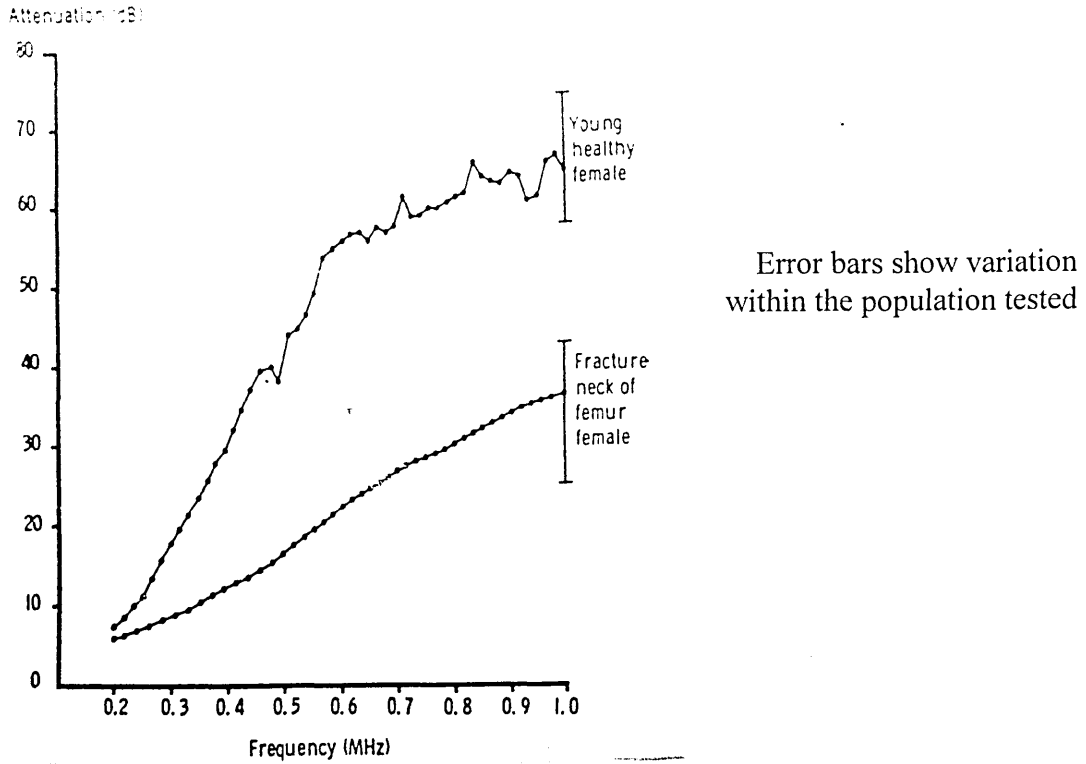
Figure 1:6 BUA as a function of the subject age and fracture occurrence
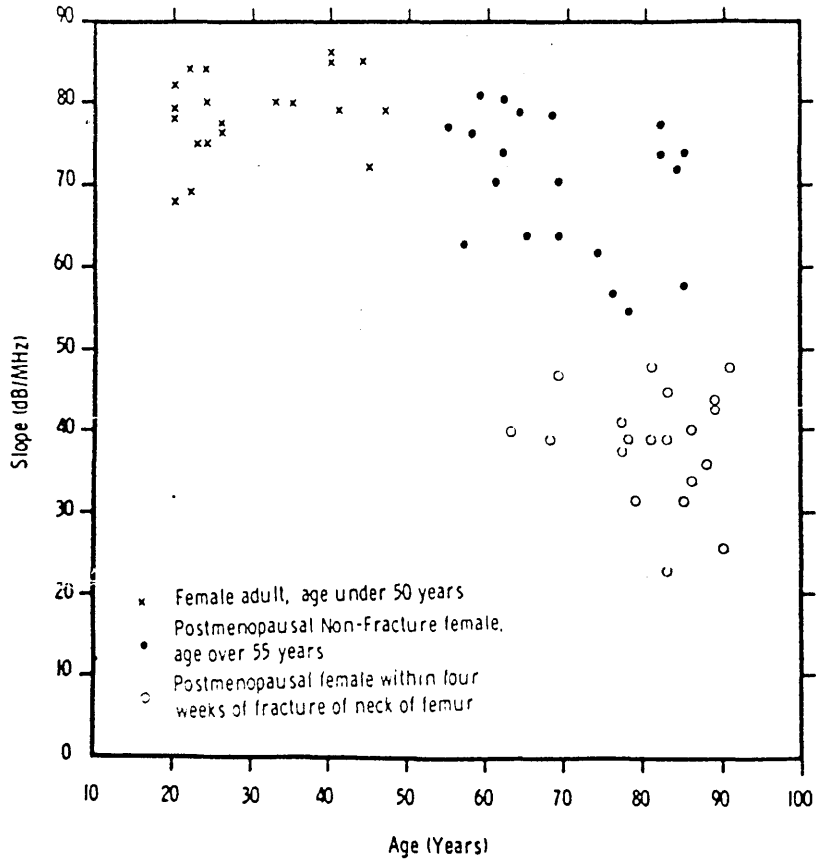
1:3:1 Commercial BUA systems

The work carried out by Langton *et al* in 1984 led to the development of three

commercial ultrasound systems that measure the calcaneus, shown in table 1:1. Clinical

trials are being carried out at centres throughout the EC and many of the centres will

have more than one system.

Table 1:1 Comparison of Commercial Ultrasound systems that measure the

Calcaneus

System	Measurement site	Parameters measured	Coupling	QA Phantom
Walker Sonix UBA575+ (Hologic as of 28/12/96)	Rectilinear scan of posterior region	BUA and velocity	water	Glass beads in silicone rubber
Lunar Achilles	Static across central waist	BUA and velocity	water	Solid urethane polymer
McCue CUBAclinical	Static across central waist	BUA and Velocity	Silicone pads and gel	Perspex block for velocity and porous plastic filters in water for BUA

Although the three system all measure across the heel there are several important

differences worth noting:

The walker Sonix system measures in a different place to the other two, slightly below

and behind.

The Achilles system modifies the BUA data, apparently to improve the coefficient of

variation (CV%), whilst CUBA(Contact Ultrasonic Bone Analyser) Clinical measures

15

true BUA. (Incorporation of dynamic range to standardise the CV% shows the two systems to be equal).

Each system is supplied with its own Quality Assurance phantom, however there is no standard against which these may be referenced.

The consequence of this is that each machine will give a different reading for the same patient and, since there is no standard reference, there is no direct way of comparing data between different systems at the same Centre, or data from different Centres.

1.4 The Structural dependency of BUA

1.4.1 Clinical Trials

As commercial ultrasound systems became available, clinical trials were instigated to evaluate the diagnostic accuracy of BUA in predicting those at risk from osteoporosis. Using Receiver Operating Characteristics (ROC) analysis[6] it has been shown that BUA has very similar diagnostic accuracy to spinal bone mineral density(BMD) measurements. Correlation studies between BUA, measured at the calcaneus, and DXA bone mineral measurements of the spine show a range of coefficients from r = 0.4 with 2.6% precision[7],(Massie *et al* 1993), to r = 0.83 with 2.9% precision[8] (Baran *et al* 1991), which would seem to indicate that BUA is affected by other factors in addition as BMD. To better understand this variance and hence determine what BUA actually measures, more detailed studies are required.

1.4.2 In Vivo Studies

One of the main causes of ambiguity in the previous correlation studies was the fact that the measurement sites were different for the different systems. Furthermore the total volume of bone interrogated was different in each case. To overcome this Gluer *et al*[9] (1992) carried out measurements using BUA and SXA (single photon Absorptiometry) at the same skeletal site, the calcaneus.

A group of 33 volunteers with a wide range of ages and bone mineral densities were used, 25 were female, 16 being 40 or more years old.

BUA measurements were carried out using a Walker Sonix UBA 575 which performs a rectilinear scan with 19mm diameter circular transducers, giving a 22mm diameter region of interest (ROI).

The normal ROI for SXA measurements covers an area 40 x 27mm, 3 times the size of the BUA measurements, and was used for normal correlation. The results were re-analysed to give a square ROI covering virtually same area as the ultrasonic ROI, which gave a site-matched correlation.

Reproducibility of measurements also plays a part in determining correlation coefficients and so an algorithm to correct for precision errors was developed and applied to the results.

The overall site-matched and precision corrected correlation coefficient was r = 0.58 with a coefficient of variation (CV%) of 17.08%. The sub group of 25 women showed a better correlation, r = 0.72 and CV% = 14.33%. The group of most interest from osteoporosis risk, those 40 years or older, gave r = 0.68 with CV% = 16.93%.

The difference in correlation between the normal and sitematched ROI for SXA showed a slight downward trend, but not enough to be significant.

Gluer *et al* concluded that the correlation coefficient in the order of r = 0.7 between the two systems is significant but 50% of the variance is unexplained. This variability indicates that BUA is affected by factors, such as bone strength and structure, other than BMD, or other outside influences.

A similar, separate survey of the calcaneus was carried out by Waud *et al*[10] (1992) who looked at 64 women in the age range 35 to 83 years. Again the Walker Sonix UBA 575 was used for the ultrasonic measurements, but this time dual energy X-ray absorptiometry (DXA) provided site matched BMD measurements.

Comparisons were made between BMD, BUA and Velocity of sound (VOS); BMD vs BUA r = 0.73, BMD vs VOS r = 0.66 and BUA vs VOS r = 0.74. This shows that there

is a high degree of correlation between BMD and both VOS and BUA, however density only accounts for about 50% of the ultrasonic measurements.

These results agree with the findings of Gluer *et al* that ultrasound measures some other property of bone, and this is further demonstrated by the correlation between BUA and VOS, r = 0.74, which suggests that these two parameters measure further different aspects of the bone.

1.4.3 In Vitro Studies

During work carried out to assess the ability of ultrasound velocity and attenuation to predict fracture risk in humans and race horses, Langton *et al*[11] carried out a study on eight cubes of equine cancellous bone. The aim of the study was to investigate the proposal that ultrasonic velocity was related to density and elasticity whilst BUA is related to density and structure.

The density of the eight de-fatted cubes was measured by Archimedes' principle and Young's modulus was measured for each cube in each orthogonal direction. The outer faces of the cubes were analysed for mean intercept length of the trabuculea to give an indication of the cancellous structure. BUA measurements between 0.2 to 0.6 MHz, and ultrasonic velocity measurements were made through all three axes of all eight cubes using CUBA.

The results showed significant variations in BUA for the 3 axes which demonstrates a structural dependence as the density is constant. There was no significant relationship between BUA and elasticity.

The theoretical values for velocity were calculated from the formula

$$\text{Velocity (C)} = (\text{Elasticity(E)}/\text{Density}(\rho))^{1/2} \qquad\qquad (1.1)$$

Comparison with the measured values for the three orthogonal directions gave correlation coefficients better than 0.9. These finding confirm that BUA is related to structure and density, whereas velocity is related to elasticity and density.

Continuing on from his *in vivo* work, Gluer *et al*[12-13] carried out two *in vitro* studies on bovine trabecular specimens. The first study (1993) looked at the effect of bone structure, in the form of trabecular orientation, on BUA and BMD. Ten 1.2cm^3 specimens were cut from fresh bovine proximal radii and defatted. The specimens were cut so that the trabecular plates were aligned with one of the three major axes of each cube. BUA measurements from the three axes of all the samples were taken using a Walker Sonix UBA 575, followed by a similar set of BMD readings using DXA. Conventional high resolution radiographs of the three axis of the specimens were used in conjunction with an alignment scoring system to determine the orientation of the trabeculea.

BUA variability was found to be 27.6 dBMHz^{-1}, with inter and intra specimen variability at 18.2 dBMHz^{-1}(38.7%) and 19.4 dBMHz^{-1}(41.3%) respectively. The reproducibility error was 2.1%. Along the axis aligned with the trabeculae BUA, was 44% to 54% higher compared to the other two directions and a significant association between BUA and alignment was observed. A change in alignment from parallel to perpendicular gave a difference of 36.1 dBMHz^{-1}.

The inter and intra sample variability for the BMD measurements were 18.2% and 2.9% respectively with a reproducibility error of 1%.

The association with alignment and the comparatively large intra specimen variation indicates that BUA measurements are affected by the anisotropic nature of cancellous bone and are dependent on trabecular orientation. Further, the relatively small intra

specimen variation of the DXA measurements shows that this structural dependence of BUA is independent of bone density.

The second study (1994) looked at several different ultrasound measurements and more detailed structural parameters. 20 samples similar to the first study were used and the structure was assessed by microcomputed tomography (μCT) with approximately 80μm spatial resolution. Structural parameters were determined from the reconstructed 3 D images of the samples, including trabecular thickness and spacing, anisotropy and connectivity.

The quantitative ultrasonic (QUS) parameters consisted of BUA, UVB and UAB. UVB is the ultrasonic velocity through bone and is slightly different from the normal velocity measurements as it gives the velocity of sound in the cancellous bone only. (Normal velocity measurements include soft tissue and cortical bone.) UAB is the ultrasound attenuation in bone and is the average attenuation in the range 0.2 to 0.6 MHz.

Bone mineral density was measured using DXA.

The results showed all three ultrasonic parameters to be significantly associated with bone structure independently of BMD. UVB was largely influenced by trabecular separation, UAB by connectivity and BUA by a combination of both.

Multivariate models of QUS versus BMD combined with bone structure parameters showed squared correlation coefficients of $r^2 = 0.70 - 0.85$ for UVB, $r^2 = 0.27 - 0.56$ for UBA and $r^2 = 0.30 - 0.68$ for BUA compared to $r^2 = 0.18 - 0.58$ for UVB, $r^2 < 0.26$ for UAB and $r^2 < 0.13$ for BUA for models including BMD alone.

Although these studies were carried out on 1.2cm^3 samples of bovine cancellous bone they demonstrated that BUA does measure structure as well as density and similar effects can be expected when measuring the human calcaneus *in vivo*.

1.5 Physical Cancellous Bone Models

Having established the link between BUA and the structure of cancellous bone further studies are needed to better understand the interaction between the two.

In order to quantify the effects of structure on ultrasonic measurements, a deeper analysis must be carried out. To be of value the study must look at structures very similar to the cancellous bone found in the calcaneus and this presents the problem of obtaining suitable samples. Since there is no way at present of obtaining the detailed structural information *in vivo, in vitro* samples must be used. The majority of *in vitro* samples are either equine or bovine, slightly different structurally from human cancellous bone, and the human samples that are available tend to be of elderly origin. This limits the amount of structural variation found and presents difficulties in measuring and defining those differences.

To overcome this, there is a need for a physical model of cancellous bone whose structure may be accurately defined and controlled. The model would allow the various structural parameters to be altered independently in a precise fashion, rather than the structural 'lottery' of *in vitro* samples.

The model must be capable of providing open cell structures with the following properties:

- A dynamic BUA range of 20 - 120 MHz^{-1}
- Stable with respect to water immersion and time.
- Repeatably high precision manufacture.

Furthermore such a model could be used to produce cancellous bone phantoms for use in the quality control of commercial ultrasound systems and more importantly provide a means of directly comparing inter and intra system data.

Modelling of the Calcaneus - A review of previous studies

2.1 Introduction

The most relevant previous studies into producing a cancellous bone phantom were carried out by Njeh[14] (1994), at Sheffield , and Clark *et al*[15] (1994) in Leeds. Njeh used a machined cortical matrix, a solid block of material with similar acoustic properties to cortical bone, which was then drilled to introduce pores. Clark *et al* used a composite consisting of epoxy resin mixed with a granular material which was then cured in a mould.

2.2 Machined Cortical Matrix

2.2.1 Plaster of Paris (POP)

The first material Njeh looked at was POP (Calcium Sulphate), using a ratio of 3:2 powder to water by weight. The mixture was cast into 40 mm cubed blocks then soaked in water for an extended period to eliminate residual air. Measurements were carried out on six complete blocks and two with holes drilled in them. For the solid blocks the mean BUA was 46 dB MHz^{-1} with a CV of 45.8%, the velocity was 2056 ms^{-1} with a CV of 9% and the density was 1736 Kgm^{-3} with a CV of 3.1%

The two blocks with drilled holes, A, 9 x 3 mm dia and B, 16 x 4.1 mm dia, were measured at the start and finish of a 108 day period. The BUA for A and B, respectively, was 83.43-47.05 $dBMHz^{-1}$ and 90.86-106.22 $dBMHz^{-1}$. The introduction of the holes showed a large alteration in the BUA, however the inability to produce identical samples (CV of BUA = 45.8 %) precludes POP from being used as the cortical mimic.

2.2.2 Perspex

Since POP was not useable, Njeh looked at a selection of thermoplastics including;

Polyethylene, Polyvinyl chloride, Nylon and Polymethylmethacrylate (Perspex).

The properties of Perspex were the closest to cortical bone, see table 1, and this was

selected as a suitable matrix.

Table 2.1 Properties of Perspex

	Density $Kg\,m^{-3}$	Velocity ms^{-1}	E GPa
Cortical Bone	1800 - 2000	3000 - 4000	4 - 25
Perspex (PMMA)	1180	2670	3.3

A solid block of Perspex, 41 mm cubed, was drilled with an array of vertical holes (6x6

giving 36 total). Starting at 1 mm diameter the holes were successively drilled out in 0.5

mm stages to a maximum diameter of 5.5 mm. This gave a relative density range of 295

to 1180 $Kg\,m^{-3}$, which is within the range of cancellous bone. BUA and velocity

measurements were taken at each stage using the CUBA system with the perspex block

immersed in degassed water.

BUA was found to increase with hole diameter up to 3.5 mm (30% porosity) thereafter

it decreased rapidly. Attenuation was attributed mainly to scattering for hole sizes less

than 3.5 mm and mainly absorption for higher porosities. Velocity remained virtually

constant up to 4 mm diameter then decreased.

Having shown that Perspex blocks with holes drilled in them behaved in a manner

similar to cancellous bone, Njeh then made several more models with different hole

patterns to look at structural effects. He found that BUA varied with the number of

holes, the spatial distribution and the inter hole spacing. This showed the structural dependence of BUA, however his study was not deep enough to quantify these effects.

2.3 Composite Materials

The main aim of the work carried out by Clarke *et al* (1994) was to produce a material that mimicked cancellous bone for use in the routine monitoring of commercial ultrasound scanners.

Their approach used an epoxy resin as the bone material which was indispersed with a granular marrow mimic. Altering the relative volumes of epoxy resin and granules (constant size) provided the variation in porosity for the model.

Araldite 1302 liquid resin and hardener, mixed as per the manufacture's instructions, was used as the bone matrix and a gelatine water mixture provided the marrow mimic. The gelatine water mixture, 11g dry gelatine powder to 150 ml of water, was selected as the best compromise between mechanical stiffness, to give stable granules, and acoustic properties which are not ideal but are close enough to marrow to be practical.

The gelatine water mix was extruded twice through a mesh which produced cubic granules approximately 1 mm^3. The correct volumes of resin and granules for a given porosity were mixed together until a uniform distribution of particles was achieved, then left to harden in a mould. The closed cell structure so formed is similar to, but not exactly like, the open cell cancellous bone.

Eight samples measuring 50 mm x 50 mm x 20 mm were produced with porosity's in the range 10% to 80%, and ultrasonically tested through the 20 mm thickness.

The ultrasonic velocity was found to follow a fairly linear inverse relationship with porosity, starting at 3118 ms^{-1} for zero and 1844 ms^{-1} for 100%. This agrees with the

proposal that the velocity in a porous material may be predicted by the following expression:

$$Vp = Va(1-f) + Vbf \qquad (2{:}1)$$

where Vp is the predicted Velocity, Va is the velocity of the matrix, Vb is the velocity of the pore material and f is the porosity of the material.

Attenuation measurements were made at spot frequencies in the range 0.5 to 0.9 MHz, (usually the calcaneus is measured over the range 0.2 to 0.6 MHz, Langton *et al* 1984). The results for all frequencies showed an increase in attenuation with porosity, peaking at roughly 50%, then a similar decrease. As expected the greatest attenuation coefficient was for the higher frequency, 36 dBcm^{-1} at 0.875 MHz with 18 dBcm^{-1} for 0.5 MHz. The eight samples were then measured on a commercial system (Walker Sonix UBA 575) and again a peak BUA of 77 dBMHz^{-1} was seen at around 50% porosity, dropping to between 20 and 30 dBMHz^{-1} at 10 and 80% porosity.

Clarke *et al* proposed that the peak seen at 50% could be explained by the dominant attenuation mechanism being scattering. Up to 50% porosity the epoxy resin formed the matrix with the marrow granules acting as scatterers, above 50% porosity the marrow granules would tend to homogenize and the more dispersed resin would become the net scatterer. In either case the maximum number of scatterers occurs at the 50% cross over point. The author agrees that at some point the resin will become the net scatterer but feels that the cross over point would be higher, 60 to 70%, rather than exactly 50%.

2.4 Limitations

Although both methods demonstrated similar characteristics to cancellous bone neither are ideal for modelling purposes. Perspex blocks may be drilled very accurately

however the structure is made of regular cylindrical pores, unlike cancellous bone. Also the minimum size pore that can be drilled accurately is 1 mm, (at smaller diameters the drill bit is prone to deviate), which is significantly larger than the pore size found in the calcaneus. It is therefore not possible to produce a controlled phantom of the calcaneus using this method.

The composite material developed by Clarke *et al* has a structure much more similar to cancellous bone except that all the pores are the same size, closed and cubic. The main draw back is that the only the porosity may be controlled. The actual structure, or architecture, of the model cannot be controlled and samples with the same porosity but significantly different structures cannot be produced. The granular nature of the marrow mimic also limits the choice of materials to those with less than ideal acoustic properties.

CHAPTER THREE

Stereolithography

3.1 Introduction

StereoLithography (SL) is a recent technology that allows complex solid objects to be made directly from 3D computer models. The process involves 'printing' successive layers of the model, by laser, onto liquid light cured resin. Where the resin is exposed to the laser it solidifies and each layer bonds to the previous to form a single solid object. Stereolithography was patented by Charles Hull[16] in 1986 with the first commercial systems available by 1987.

Initially SL was used in the automotive and aerospace industries to make conceptual models and prototype parts. As the number of SL applications increased and it's unique ability and potential began to be realised, it formed the foundation and cornerstone of a wider technology called Rapid Prototyping and Manufacture. (RP&M)

More recently RP&M techniques have been developed to produce fully functional components including casting masters and replacement human skeletal parts. Also several similar systems such as Selective Laser Sintering (SLS), and Laminated Object Manufacture(LOM) have been developed.

With this technology, previously impractical complex structures can be manufactured with high precision. This coupled with the ability to make precise structural changes to subsequent models provides, for the first time, the potential to experimentally model cancellous bone structure.

3.1.1 Overview

The first section of this chapter looks at the wider field of RP&M in industry and the 3 main systems, SL, SLS and LOM. Next, the SL process is described in detail, followed by the three main technologies involved, lasers, photopolymers and computers. Section five covers part building and post processing, and section six discusses accuracy. Finally the production and measurement of several test pieces is described followed by a comparison of the material properties of the SL resin and cortical bone.

Figure 3:1 The basic Stereolithography system

CAD design to STL format
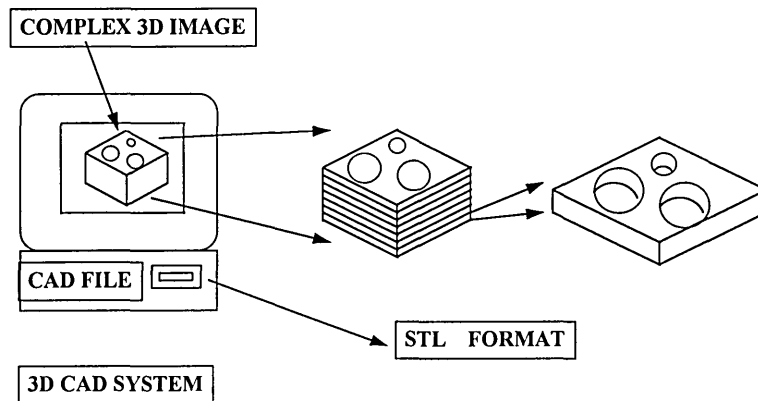
Model manufacture
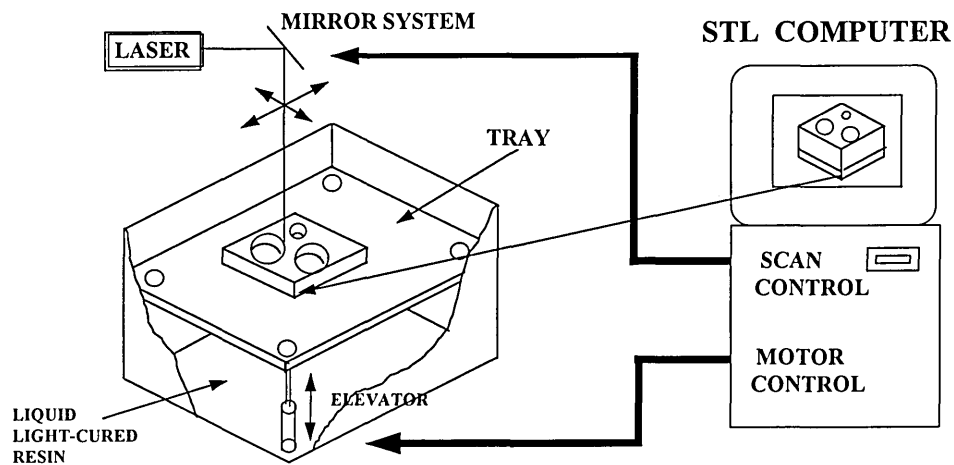
3.1.2 Rapid Prototyping and Manufacture (RP&M)

Stereolithography is the foundation of RP&M[17] and its development was brought about by advancements in a combination of three major technologies, photopolymers, lasers and computing. Driving the development was the potential of SL to bridge the historic gap between product design and manufacture.

The basic components of the SL system are:

A vat of liquid photopolymer resin.

A tray in the resin with vertical control, the elevator.

A laser with a scanning optical system.

Two computers, a) CAD model slicing, b) laser and elevator control.

3.1.3 The basic layering process

The 3D CAD file of the object to be produced is loaded into the first computer which forms a 'Slice' file[18]. This cuts the object into a series of slices which, starting with the lowest, are printed in order onto the resin surface. Slice thickness is in the range 0.1 to 0.5mm. At the start of the building process the elevator, controlled by the second computer, is placed just below the resin surface at exactly the slice thickness. The laser scans out or 'prints' the first slice onto the resin surface, causing the exposed area to solidify. When the slice has been scanned the elevator is lowered into the resin to cover the newly formed layer, then repositioned so that the top of the first layer is exactly one slice thickness below the resin surface. A recoating system skims the resin surface to ensure an even layer across the solidified first slice.

The second and subsequent slices are then scanned in the same fashion until the model is complete. The overlapping areas of adjacent slices bond together during curing so that

30

the finished model is one complete object. Once the build is completed the elevator is raised above the vat to allow unused resin to drain. At this stage the resin is about 60% cured so once the model has been drained it is fully cured in an ultra-violet flood oven. The maximum model envelope is governed by the vat size , the most common model being 250mm x 250mm x 250mm. Small models take several hours to build whilst larger items can be completed overnight.

3.1.4 Industrial applications.

Using rapid prototyping helps to shorten time, lower costs and improve quality of new products being brought to market[19]. Even with CAD, conventional model making involves producing drawings which are then passed to skilled model makers for manual crafting of the object. This can be a long, costly process, taking weeks or months, and each stage is open to error that may only be discovered once the model is made. The RP&M system uses the CAD data directly, reducing the potential for error, and the rapid build time allows design faults to be discovered and corrected quickly throughout the design procedure.

Initially conceptual models can be produced very quickly, this allows both manufacturer and customer to get the feel of a product and give feedback about prototype designs. Once the design engineer has completed the prototype model in CAD, physical models can then be quickly produced and tested for form and fit. For example complex engine inlet manifolds that would take weeks to make conventionally can be made overnight. The model can then be offered up to the engine and any faults or unforeseen problems such as access can be identified straight away. Correction is a simple matter of altering the CAD model and a revised part can be produced overnight. Problems can be solved

in days rather than weeks or months using conventional methods at great cost savings. Also, since RP&M methods are relatively low cost and rapid, it becomes feasible to produce several iterations of a design allowing optimisation and hence a better quality product.

Further potential saving in time and money can be gained by using SL models in testing automated production systems. If a product is used in an automated system, that system can only be tested when the product is available. This is usually quite some time after design completion due to the delay involved in tooling up. By using SL models the automated system can be tested and corrected if required whilst the product tooling is being completed, ready to use as soon as the product is available. This again saves the all important time to market.

As the accuracy and surface finish of the SL models was improved it became feasible to use them as masters in standard casting and molding methods. Room temperature vulcanised (RTV) silicone rubber is used to form a mold from which wax casting are made for the lost wax process and the SL model itself can be consumed in investment casting systems.

Limited number production runs can be made using any suitable pourable plastic resin in a mold made from an SL model in a much shorter time.

The SL master can be used directly as a mold in the vacuum forming process. Plastic sheets are made pliable by heating then drawn under vacuum into a mould. The working temperature is around 55^-C which is tolerable for SL resins.

3.1.5 Medical Applications

The SL process readily lends itself to applications in medicine using computerised 3 dimensional imaging systems[20]. X ray Computerised Axial Tomography, (CAT scan), and Magnetic Resonance Imaging , (MRI), provide detailed 3D data about the internal anatomy which can be translated into the SL format. Exact replicas of the skeleton can be produced from this data which is of great benefit in both prothesis and reconstruction.

The use of RP&M speeds up the whole design process of replacement joints in general and the speed of iteration allows greater optimisation providing better quality. Special benefits are gained when standard sizes cannot be used and a custom joint must be made. An SL model of the diseased area helps the surgeon and engineer to design the replacement joint quickly. The new joint can then be cast from an SL master in a fraction of the time taken using conventional methods, thus reducing the patient's suffering.

The SL process is especially useful in reconstructive surgery where a 3D model could be used to preview an operation. Facial reconstructions can be simplified as 3D data of one side of the face can easily be mirrored in the software and a symmetrical SL master very quickly produced.

Stereolithographic models can also be used for dry runs of complex operations. For example CAT scan data of a patient with a brain tumor can be used to build an exact replica of the scull with the tumor in place which can then be used by the surgeon to rehearse the actual procedure.

3.1.6 Alternative Systems

As the field of RP&M grew, various other technologies similar to SL were being developed. The two most important are Selective Laser Sintering[21], (SLS), and Laminated Object Manufacture[22], (LOM). Like SL they both work on the layering principle.

3.1.7 Selective Laser Sintering (DTM Corp. of Austin, Texas)

This system uses infrared heat from a CO_2 laser to fuse together fine particles of thermoplastic material[21]. The material is used in powder form and the laser energy is absorbed by the particles causing them to fuse together at the points of contact. This process is known as sintering and forms a slightly porous solid structure.

Figure 3:2 Schematic of the Selective Laser Sintering process

34
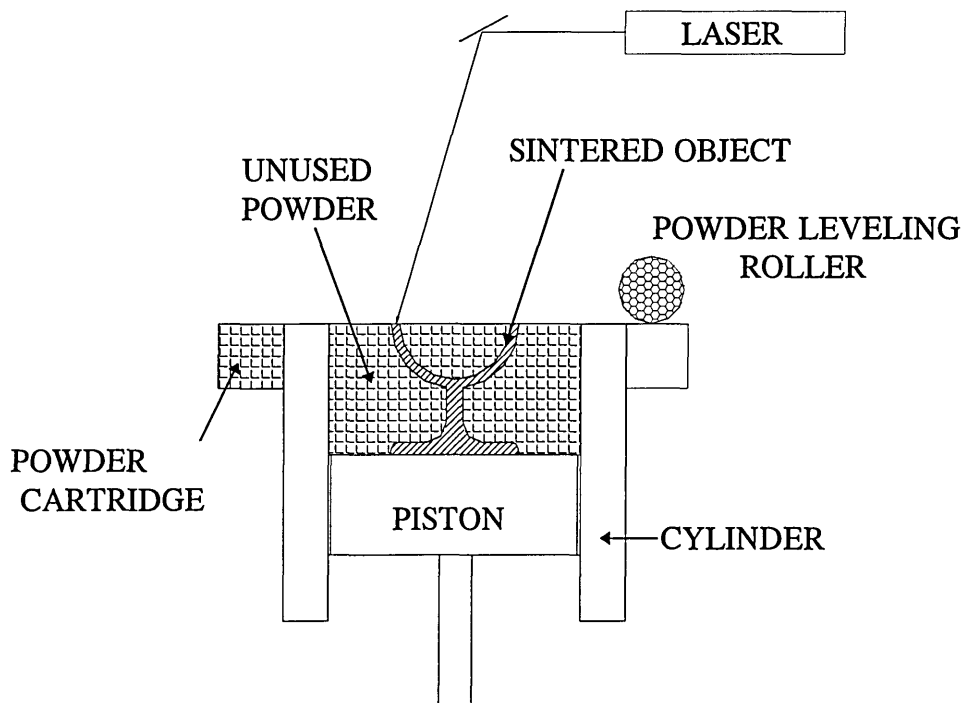
The first layer of powder is placed on a piston which is sitting inside a vertical cylinder and the lowest slice of the object is scanned out by the laser on to the powder. The piston is lowered slightly into the cylinder and another layer of powder is deposited over the first. This is similar to the elevator action in the SL process. Successive slices of the object are scanned onto new layers of powder until the object is complete. At this point the solid structure is in the cylinder and completely surrounded by powder. The piston is raised and the object gently lifted to allow the majority of the excess powder to fall away. Any remaining powder is very carefully removed using brushes and scrapers. This can be quite a problem if the object has complicated internal cavities.

The object build times of this system are faster than SL and there is a greater variety of thermoplastic materials available. The main disadvantages are a rough surface finish and unpredictable density due to the sintering action. This slight porosity makes SLS unsuitable for ultrasonic modeling.

3.1.8 Laminated Object manufacture(Helisys, Inc. of Torrance, CA)

The Helisys[22] system uses sheet material that is laminated with thermal adhesive. The outline, or contour, of each slice is cut into the sheet by laser trimming, which is then laminated to a new sheet. The next slice is cut into the new sheet which is again laminated. The areas of the sheet outside the object are cut into tiles to help with removal of excess material once the object is complete. A heated roller is used, under slight pressure, to laminate the sheets together to ensure bubble free adhesion.

The basic materials used are paper and plastic films and are relatively cheap. Large models may be made using this system and build time is quite short as only the outline is scanned by the laser, not the full cross section of each slice.

Figure 3:3 Schematic of the Laminated Object Manufacture process
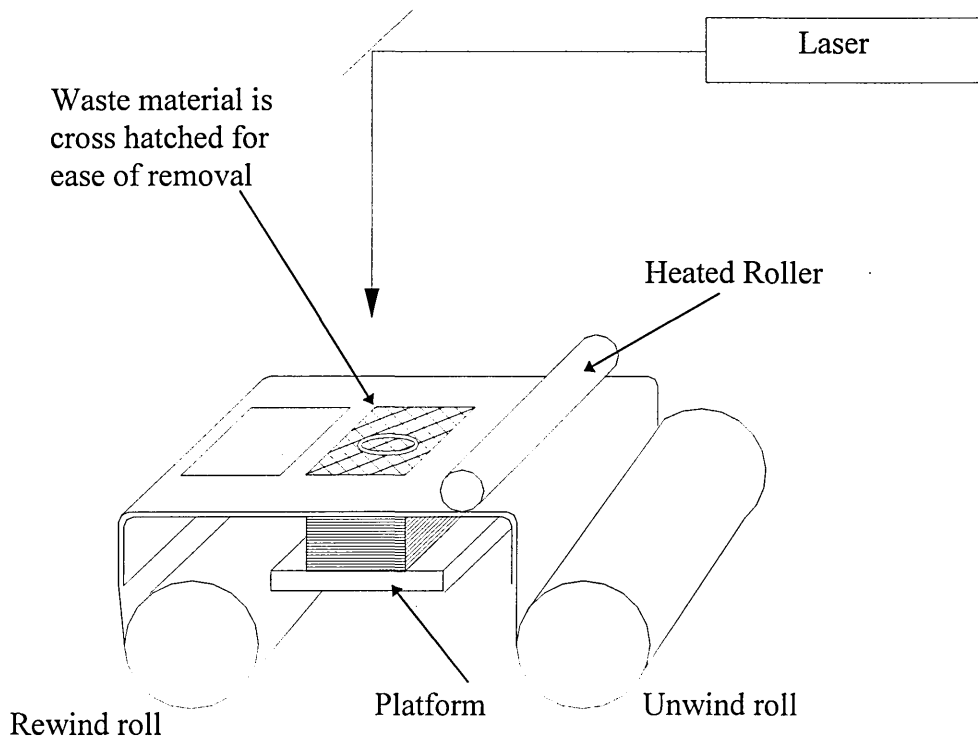
The completed object consists of layers of material separated by adhesive, not a solid

structure as in the other two systems, and shear forces can be a problem as part strength

is geometry dependent. Excess material is not reusable and can be difficult to remove

from internal cavities and large vertical faces. The materials used and the laminar

nature of these parts make them unsuitable for ultrasonic use.

3.2.1 Stereolithography

The Stereolithography system[19] was developed during the early 1980s by Charles Hull

of Ultra Violet Products, Inc (UVP) in California. It was patented in 1986 and 3D

Systems, Inc, was formed to produce commercial systems with the SLA-1 being

introduced in 1987. An upgraded version, the SLA-250, became available in 1989 and

in 1990 the SLA-500, (double the vat capacity of the SLA-250) was added to the range.

The SLA-250 is the most widely used system in the world and is the basis for the

following description.

Figure 3:4 The Stereolithography Apparatus (SLA 250,Nottingham University)

The main components of the system, collectively known as the stereolithography apparatus (SLA), are as follows:

A vat of photo-sensitive resin.

An elevator and a resin recoating system.

A LASER with optical scanning.

Two computers;   a) Model preparation and production of slice file.

b) Build control - Scanning, elevation and recoating.

3.2.2 CAD Model preparation

The CAD file of the design model must be translated into the .STL[23] format before it can be imported into the SLA. The .STL format represents the boundary surfaces of the CAD model by triangles in a process known as tessellation. The translation is usually performed in the CAD software.

Once the model has been imported into the SLA the first part of the preparation is the addition of a supporting structure. The supporting structure is a fine lattice used to isolate the model from the elevator. This nullifies any small distortions in the elevator plate and aids the removal of the model after completion. Overhanging areas of the model that would form an isolated island until the bridging to the main object was built must also be supported. All the supports are generated in a separate file that is indexed to the model.

When the supports have been added both files are then 'sliced' to produce a series of crossectional layers that the build computer uses to 'print' onto the resin. The layer thickness, build style and system parameters are selected and added to the slice file.

The SLA is capable of making several models on the elevator platform at the same time and at this point all the slice files for all the models and supports are merged ready for the build to begin.

3.2.3 Model Building

Before the polymerisation is started, the elevator platform, under the control of the build computer, is positioned exactly one layer thickness below the resin surface. The Z level of the resin surface is measured and adjusted to ensure optimum laser focus. Adjustment is made through an incremental plunger dipped in the resin that displaces more resin as required. The resin level is constantly checked throughout the build as polymerisation causes volumetric shrinkage, approximately 3% during laser cure. Once the platform is in the correct position the first layer is printed by the laser and the resin is polymerised. Laser scanning is controlled by X and Y galvanomic mirrors and the outline of the solid areas within the slice are written first followed by cross hatching of the remaining solid areas. To save time the scan lines of the hatching are slightly separated forming small cells of uncured resin. This saves scanning the entire cross section but provides sufficient green strength to complete the model. The remaining resin is polymerised during the post cure process. On up or down facing surfaces a series of parallel touching lines, called skin fill, are used to improve strength and finish as well as preventing loss of uncured resin from the hatching.

When the laser writing is complete the first layer must be lowered and coated with resin ready for the next layer.

The recoating process begins with a deep dip, the elevator is lowered into the resin by approximately 7.5mm forming a depression in the surface of the resin. This depth is

sufficient to allow the resin to overcome surface tension and close the depression formed over the first layer. The elevator is raised until the previous layer is above the level of the liquid resin and exactly one layer thickness below the recoating blade. The recoating blade is swept across the vat and removes any excess resin from the previous layer leaving a coating one layer thick. The elevator platform is then lowered back into the resin so that the top of the previous layer is a layer thickness below the free resin level. At this point the resin level should be completely planar, however due to surface tension effects, slight perturbations in the form of creases are formed around the outline of the previous layer. The finite surface tensions forming the non uniformity will relax with time and so a pause, called the Z wait, is included in the building procedure to allow for this. Lifting the model clear of the resin for the recoat sweep helps to reduce the amount of resin disturbed and so reduces Z wait time. Typically Z wait times are 15 to 30 seconds depending on layer thickness and surface tolerance. At the end of the Z wait, the build computer then scans the next layer onto the resin and the whole process is repeated for successive layers. When the object is complete the elevator platform is raised above the level of the resin and the model allowed to drain.

3.2.4 Post cure and finishing

The elevator platform with the completed model attached is removed from the SLA to a cleaning station and washed with down with solvent. When all the residues have been removed the part is dried with low pressure air jets, then separated from the platform by cutting through the supports with a sharp knife.

At this point the part is approximately 60% cured and to complete the polymerisation process it is placed in a post cure oven and flooded with broadband ultraviolet light.

Postcure timing depends on the size of the model and is generally one to two hours, however very large items may take as much as ten hours.

Finally the support structures are removed with a sharp knife leaving the finished object. Depending on the application the surface of the model may then be polished, sanded and painted, or spray metal coated.

3.3 Light Cured Resins

Light sensitive resins consist of a liquid monomer and a photo initiator. When the photoinitiator is exposed to ultraviolet light it acts as a catalyst that causes the liquid monomer molecules to link together to form a solid polymer[24]. Polymerisation starts when the initiator has absorbed a certain level of energy. At a slightly higher level a gel begins to form and this level is called the critical energy. The amount of absorption by the initiator is a function of incident light power and wavelength. This process is known as photopolymerisation and was originally developed for paints, adhesives and inks.

The vast majority of SL resins available are acrylate monomers with a free radical initiator. More recently epoxy monomers that use cationic initiators have become available and these increase the range of mechanical properties of the cured resin.

All resins shrink during polymerisation, (acrylic polymers, 5 to 7%, epoxy compounds, 2 to 3 %), and in layered systems this can lead to curling distortion. The amount of internal stress developed is dependent on the shrinkage rate of the particular resin and how the laser energy is introduced into the photopolymer. Shrinkage rates and optimum laser settings for the various resins are included in the build software to compensate for overall accuracy and minimise distortion. Changing from one resin to another usually involves recalibrating the SLA and users tend to stick to a single resin where possible. The resin most commonly used in this country at the present time is CIBA-GEIGY XB 5154 which is acrylic and has a cured density of 1.12 g/cc.

Photoinitiators that are sensitive to invisible ultraviolet light at laser power levels are used so that the resins remain stable out of direct sunlight and no safelight systems are needed.

3.4 Laser and Optical system

The Laser and optical components are perhaps the most critical part of the SLA as these control the minimum feature size, overall resolution and speed of build[25]. A Helium-Cadmium laser is used in the SLA 250 which delivers about 16mW on the resin surface at a wave length of 325 nm. There is also an output at 442 nm which gives a visual (blue green) indication of the beam position.

Figure 3.5 SL optics and focus curve

Even at the extremes of the build envelope the beam diameter is still relatively constant

Soft focus gives constant beam diameter through the curing depth in the resin
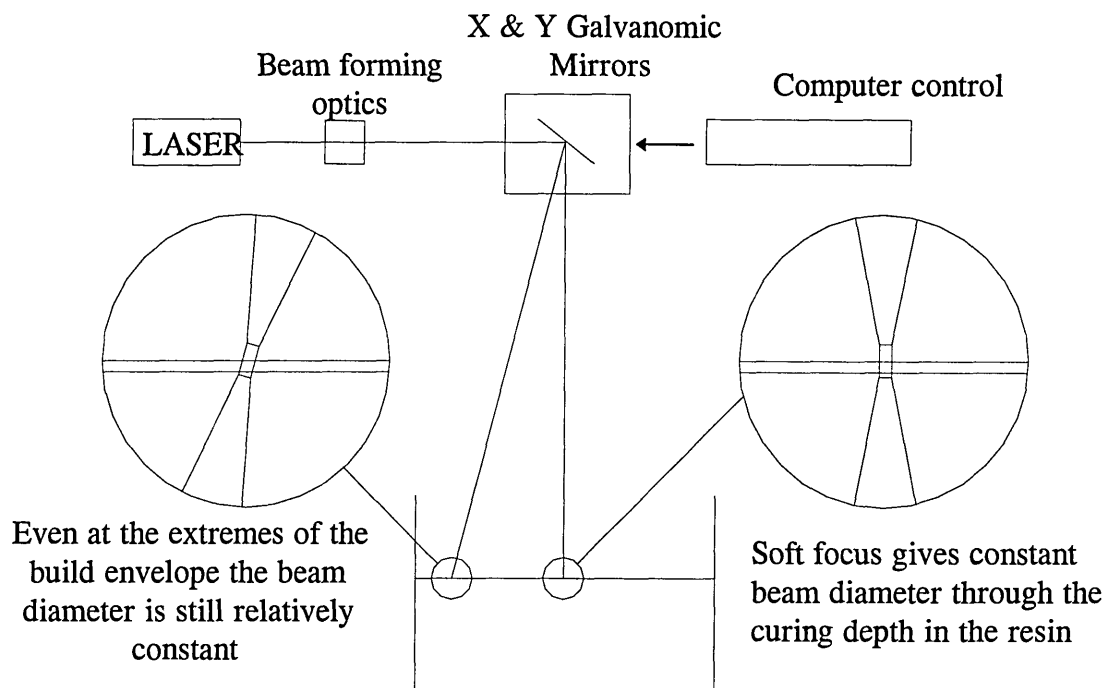
The laser energy is passed through a focusing lens then reflected by galvanomic mirrors for X-Y scanning on to the resin surface. The focal plane of the lens describes an arc centred on the mirrors and to compensate for this a soft focus is employed, this provides sufficient depth of field so that the beam diameter is constant across the whole build area. The beam diameter governs the minimum feature size and for the SLA-250 is

0.3mm. Smaller spot sizes are possible (0.05mm) however this means tighter focus of the laser and the need for for flat field correction which is not practical for commercial systems.

Part resolution is determined mainly by the angular accuracy of the scanning system but is affected by changes in intensity and distribution of power in the laser spot. Typically the laser source is replaced after 2000hrs and the computer automatically adjusts the scan speed to ensure the correct exposure for each resin and layer thickness as the power decreases with age.

Stereolithography only became possible since the development of modern, relatively stable laser systems.

3.5 Stereolithography Computing

Modern computer systems form an integral part of the SL system providing precise control of the SLA, the medium to produce the CAD model, and transformation of the CAD data to produce a solid object[26]. The SLA control systems are straight forward and can be run from a 386 PC, however CAD modeling and transformation is more complex and a work station must be used.

CAD systems use a variety of methods to describe designs from simple 2D blue prints, to 3D wire meshes or surfaces and 3D solids. Whichever system is used the CAD data must be converted into an intermediate format from which a slice file can be produced.

3.5.1 The STL format

The STereoLithography format (.STL) [23,26] is the RP&M industry standard and uses triangles to represent the surface boundaries of the object in a process known as tesselation.

Figure 3:6 TESSELATION
(The representation of outside boundaries by triangulation used in the .STL format.)

MAX CHORD
HEIGHT →

Original object with
curved face

LARGE MAX CHORD
gives **LOW** resolution
representation

SMALL MAX CHORD
gives **HIGH** resolution
representation
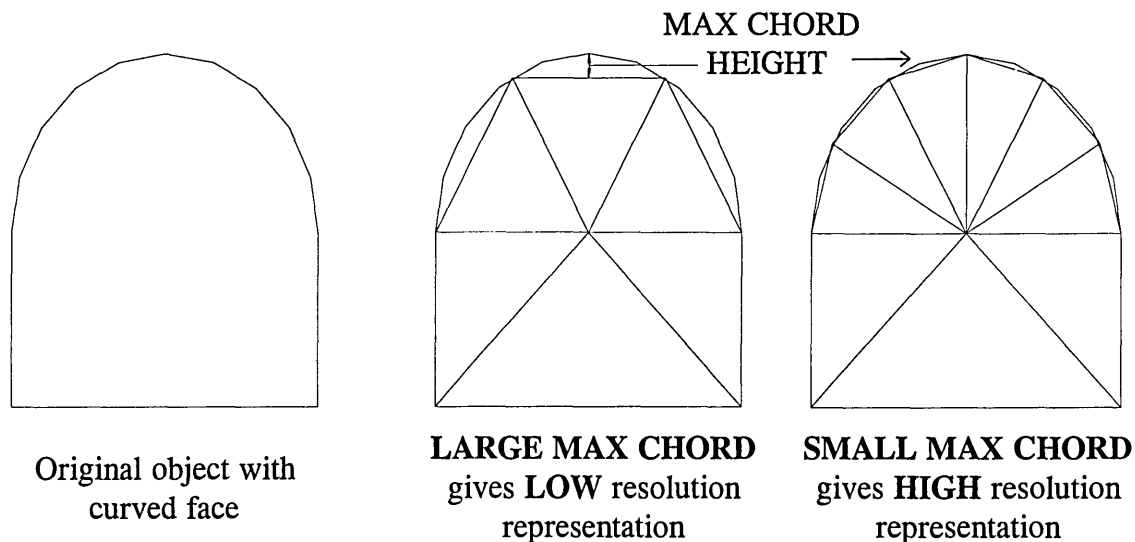
During tesselation the outside boundaries of the object are node sampled then the nodes are triangulated. Planar surfaces can be faithfully represented but curved areas can only be approximated. The level of approximation is determined by the number of nodes used along the curve and is described by the distance between triangle side and actual curve. The maximum chord length can be specified within limits in the software before conversion takes place. Each triangle has a normal associated with it that indicates which side is solid for use in the slicing process. Translators to convert CAD files to the STL format are usually supplied as add on's for the CAD package and once the model is in this form it is ready to be passed from designer to production. This maybe in-house or through a bureau service. For a list of RP&M service providers see reference 27.

3.6 Evaluation of test samples

In order to evaluate the SL system, the Rover Car group, one of only three bureau services in the UK in 1993, was contacted and they kindly agreed to provide some test samples. Based on a 3D rod lattice, two models representing the porosity of healthy and osteoporotic bone were designed. Both models used 3mm centres for the lattice with rod sizes of 1.09mm (70% porosity for healthy bone) and 0.4mm (95% porosity for osteoporotic bone). STL files for the models and a solid cube 23mm^3 were provided by the PROTOMOD design agency and two of each built on Rover Group's SLA 500, using XB 5154 acrylic resin. The models were measured and then tested ultrasonically with the following results.

Table 3:1 Results of the Ultrasonic tests carried out on the SL samples

	Solid cube	70% porosity	95% porosity
BUA dB Mhz^{-1}	10.26	21.1	8.88
Velocity m s^{-1}	2800	1767	1499

Outside dimensions of the cubes were all within 0.1mm (better than 0.5% accuracy) measured by vernier gauge.

Since the outside dimensions were greater than the ultrasonic wavelength the elasticity (E) was calculated from the velocity (V) and the Density (D) using the formula (1.1) (Langton *et al* 1990)

Figure 3.7 The Rover Test Pieces
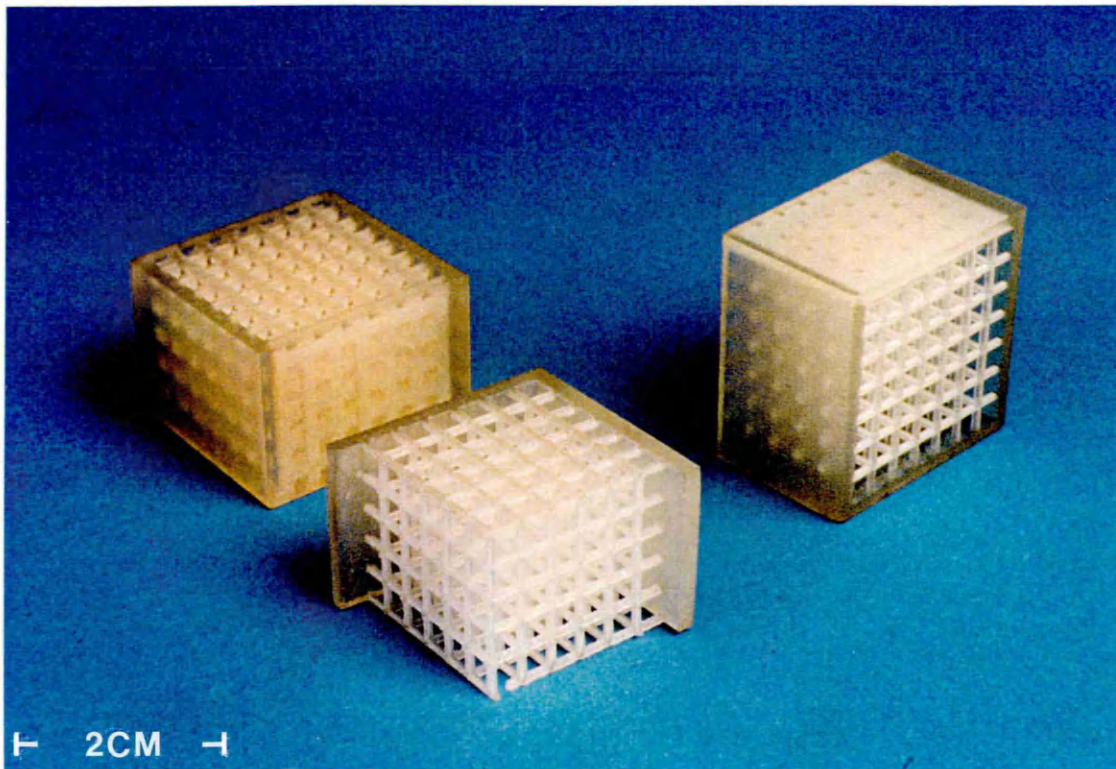
3.7 Conclusion

The stereolithography process is capable of producing controlled porous structures similar to human cancellous bone. Of the three main RP&M systems it is the only one compatible with ultrasonic testing and is the most widely available through bureau services.

The accuracy of test models compared to the CAD file was better than 0.5% and the smallest feature size, guaranteed repeatable, is 0.3mm.

Ciba Giegy XB5154, an acrylic polymer, is the preferred resin of the service providers and, although other resins are available, the extra cost to change over would be prohibitive. The ultrasonic properties of the resin are not the same as cortical bone however the differences are not thought to be significant.

48

CHAPTER FOUR

HISTOMORPHOMETRIC ANALYSIS OF THE CALCANEUM

4.1 Structural Analysis of the Calcaneus

In order to produce a design for an SL model based on the calcaneus, detailed structural information regarding cancellous bone must be obtained. The main parameters required are the frequency and distribution of trabecular and pore thickness, with some indication of 3 D connectivity. This section describes how that information was gained using histomorphometric analysis and looks at the design limitations imposed by the results.

A literature review for the trabecular structure of the calcaneus showed that the required information was not available and that further analysis had to be undertaken.

Starting with a general overview of Histomorphology, (Histology and Morphometry), the usual method of sample preparation is described, followed by a look at the parameters measured.

Next, a detailed description of the preparation, sectioning and imaging of two samples of human calcanium is given with the results of the computerised structural analysis that followed.

4.2 Literature Review of the Trabecular Structure of the calcaneum

General interest in cancellous bone was only generated once the role in skeletal strength was realised and much of the analysis tended to be qualitative rather than quantitative. The trabecular structure of the calcaneus was brought under the spotlight after the evidence suggested that BUA measurements were dependent on structure as well as density.

The first in depth description of the architecture of cancellous bone was given by

Singh[28] (1978) after a study of large numbers of macerated adult human bones from

various skeletal sites. He found that the architecture of cancellous bone takes the form

of one of three groups, with the second and third groups divided into three further sub

groups.

Figure 4:1 The Architecture of Cancellous bone (Singh 1978)
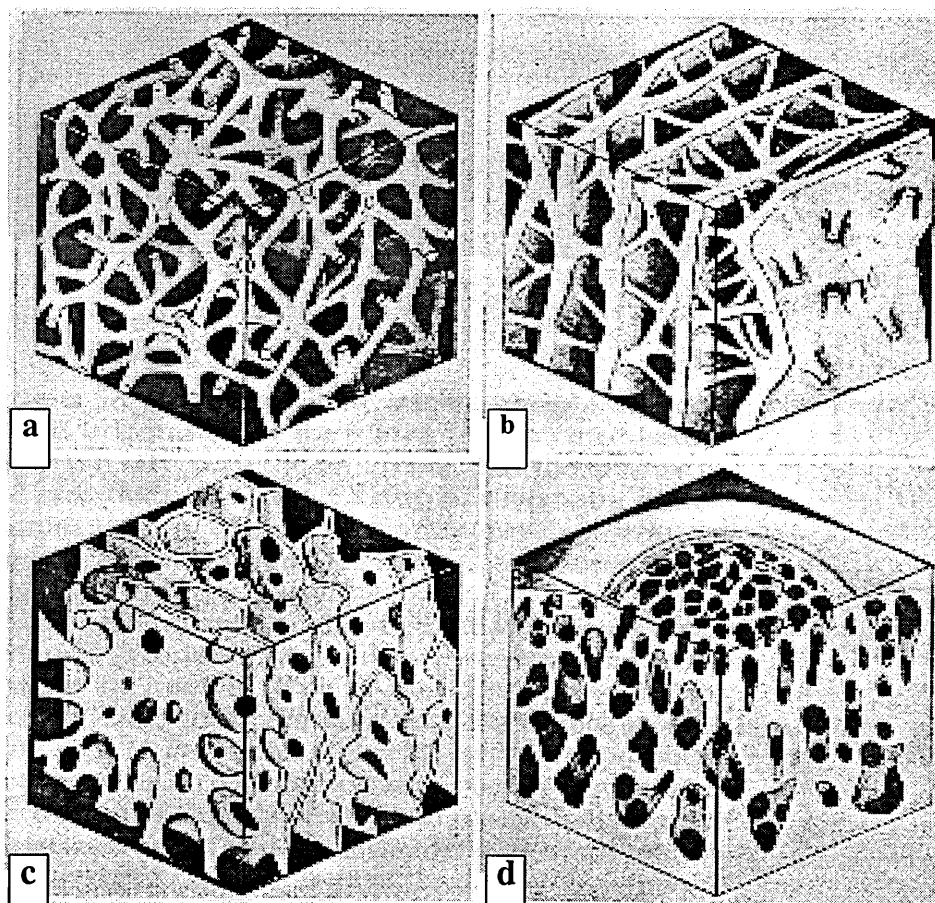
The first type of cancellous bone, Type I, is made up exclusively of fine, straight or

curved rods 0.08 to 0.14 mm in diameter and about 1mm in length. This is shown in

figure 1a, and is found mainly in the deeper parts of long bones.

Type II consists of both rods and plates and is divided into three sub groups: Type IIa is

similar to Type I but some of the rods are replaced by small plates 0.1 to 0.2 mm thick.

This type is found mainly in the ends of long bones.

Type IIb has more extensive plates that show a well marked orientation, with thicker rods that give a ladder like appearance. The plates and rods were up to 0.5 mm thick. This type is found mainly in the calcaneus. See figure 1.2. Type IIc is made up of parallel plates with interlinking rods and is found at the lower end of the femur. The plate thickness ranges from 0.16 to 0.3 mm with 0.4 to 0.8 mm spacing. See figure 4.1b. Type III is made up entirely of plates that anastomise to form a cellular structure, the plate thickness for the three subtypes are; 0.1 to 0.2mm for Type IIIa, 0.12 to 0.24 mm for Type IIIb and 0.2 to 0.4mm for Type IIIc. See figure 4.1c and d

A more theoretical approach was taken by Gibson and Ashby[29] when they looked at cancellous bone as a cellular solid. Models were developed for the analysis of mechanical parameters based on the structural features of cancellous bone that determine stiffness and strength. The four models are shown in figure 4.2 and represent the following:

Figure 4.2a   Low density equiaxed cells (rods).

Figure 4.2b   High density equiaxed cells (perforated plates).

Figure 4.2c   The prismatic structure (stress orientated).

Figure 4.2d   The parallel plate structure (stress orientated

Figure 4:2 Theoretical models of Cancellous Bone (Gibson and Ashby 1988)

51
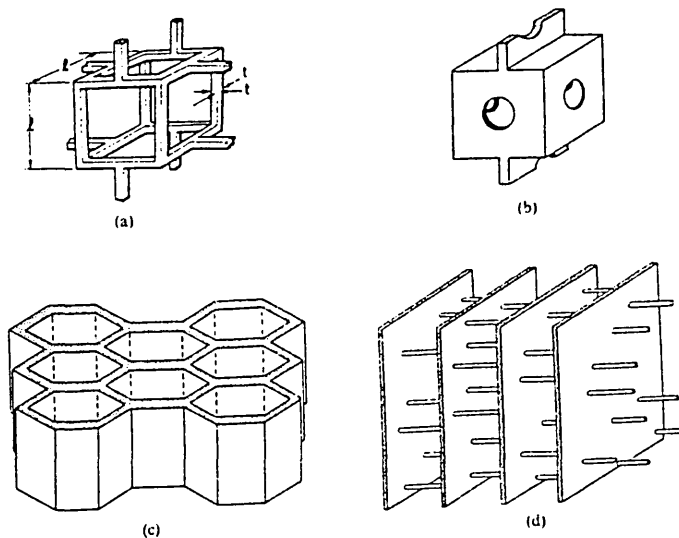
These two studies show the general type of structures found in cancellous bone and Singh gives an indication of the range of the trabecular plate thickness, however there is insufficient detail to form a realistic model design.

Enrico Lozupone(1985)[30] carried out a detailed examination of 87 individual trabeculea isolated from two separate regions of the calcaneus. The first group were taken from the perpendicular bundle of trabeculea located forward of the central waist and were almost entirely cylindrical. The second group were taken from an area within the posterier and central waist region (the ultrasonic measurement area), and were laminar.

The mean trabecular thickness for the laminar sections was measured as 313mm, SD = Ý135mm, with a maximum of 600mm. This result is within the SL resolution of 0.3mm, however there is no indication of the trabecular microarchitecture nor information regarding pore size. A further factor that must be considered is that the samples were all elderly and no indication of the donors general status is given. This also applies to the work that Singh carried out.

More recently, Hans[31] et al(1995) looked at the microarchitecture of the calcaneus in relation to ultrasonic measurements. In a 2D study of 17 elderly (64 - 92years) calcaneum measurements were made of the trabecular thickness and separation (pore thickness). Structure was represented by measuring nodes and terminii to indicate connectivity. The mean trabecular thickness was given as 85mm, SD = Ý21mm, and the separation 907mm, SD = Ý260mm. The connectivity measurements did not contain sufficient information to recreate the trabecular structure.

There is more information in the literature regarding the structure of cancellous bone in the spine and iliac crest, the two most common biopsy sites, however work by Amling[32] et al showed that there was no correlation between the structure of the calcaneus and the spine or iliac crest, and so this data is of no use.

Although these studies give a general indication of the structure of the calcaneus, there is insufficient data to form a design for normal or osteoporotic trabecular bone and a specific histomorphological examination must be carried out.

4.3 Histomorphometry

4.31 Introduction

Bone histomorphometry[33] is derived from histology, the study of bone by light microscopy, and morphology, the study of form or structure. Initially, histology of cancellous bone gave only qualitative information. This was enhanced by morphometry to give quantitative measurements of past and present bone cellular activity and the structural components.

Typically, analysis is carried out on a section of bone mounted on a glass slide. The bone sample is cleaned, embedded in a supporting resin then sectioned on a microtome. The section is viewed on a transmission microscope and measurements taken using graticules and grid systems. Each section of the sample provides 2D information. For 3D data, serial sections must be used. More recently, microscopes with video cameras attached are being used in conjunction with computerised image analysis software, developed to perform the measurements. These techniques have also been used as the basis for a computerised 3D reconstruction of porous bone structures[34] (Odgaard 1990).

4.3.2 Sample Preparation and Sectioning [35]

Since the cellullar activity of the trabeculae is of interest, the samples must be prepared and embedded without affecting the bone surface. The biopsy is fixed in a formaldahyde solution, washed, then dehydrated using ethanol ready for embedding. The embedding

resin must be strong enough to support the sample during sectioning, flexible enough to allow thin (10-30μm) sections to be taken, and have no effect on the cellular structure. A 9:1 mixture of methyl and butyl methacrylate is generally used, the butyl makes the normally brittle methyl methacrylate more flexible. The biopsy is soaked in the polymer at 4°C for up to 4 weeks, depending on the use of vacuum, to degas, then polymerised at 30°C for several days with a final cure at 60°C.

Once the embedding is completed, the sample is cut on a heavy duty Jung K microtome. A finger must be lightly held on the top of the sample during cutting to prevent the section from curling up before it is transferred to a glass slide for storage.

This is a long and involved procedure and care must be taken throughout to maintain the cellular surfaces during embedding and prevent damage or distortion to the very fragile sections after cutting.

4.3.3 Measurements

The main parameters measured in bone histomorphology are: shown in table 4:1

Table 4:1 The main Histomorphological parameters used for trabecular bone

Trabecular Bone Volume	$\dfrac{\text{Volume of Trabeculae} \times 100}{\text{Volume of Trabeculae and marrow}}$
Osteoid Volume	$\dfrac{\text{Volume of Osteoid} \times 100}{\text{Volume of Osteoid and Mineralised bone}}$
Osteoid Surface	$\dfrac{\text{Length of Surface occupied by Osteoid} \times 100}{\text{Total length of trabecular surface}}$
Osteoblastic surface	$\dfrac{\text{Length of surface occupied by active osteoblats} \times 100}{\text{Total length of trabecular surface}}$
Resorption Surface	$\dfrac{\text{Length of Trabecular surface occupied by resorption lacunae} \times 100}{\text{Total length of trabecular surface}}$
Osteoid Index	$\dfrac{\text{Osteoid Volume} \times 100}{\text{Osteoid Surface}}$
Trabecular Thickness	Mean thickness measured by linear intercept
Marrow Star Volume	Mean length of lines radiating from a given point in the marrow space to intersection with a trabeculum

54

Volumes, bone or marrow, are expressed as a percentage of the whole and dimensions such as trabecular thickness are averaged. A point counting system is used to determine volumes, a grid with an array of points is superimposed over an area of the sample and the number of points covering the trabeculae counted. The grid is moved to a different area, or field, and the process repeated. When sufficient fields have been counted the number of points over the trabeculae are expressed as a percentage of the total, indicating the relative volumes.

A similar system called the Linear Intercept method is used to estimate thickness. Instead of points, a series of parallel lines are superimposed on the sample and the parts of the line that cross trabeculea are measured . Successive fields are interrogated until an accurate mean measurement is obtained.

These measurements are good indicators of the overall state and structure of bone but do not give the detailed dimensional information required for the SL design.

4.4 In vitro study of calcaneal trabecular bone

4.4.1 Aims of Analysis

Since the structural information required for an SL model design is not readily available a specific analysis of the calcaneum must be undertaken. The aim of this analysis was to provide detailed data for the model and determine its form dependent on whether the trabecular and pore thickness are within the resolution of the SL process. The two options are; a full 3D reconstruction of cancellous bone, or an extruded structure based on a 2D cancellous framework using the maximum SL resolution.

Initially, the frequency and distribution of trabecular and pore thickness must be measured and this will determine the choice of design option. A full structural data set

would be required for option one, the 3D reconstruction. Alternatively, for the second option, the trabecular framework or 'skeleton' must be provided.

4.4.2 Method

From a series of calcaneus cancellous bone samples, previously measured ultrasonically *in vitro*[40], two samples, one high and one low relative density, were selected for analysis. The samples consisted of a 20mm diameter cylindrical core, 15mm long, without the cortical shell. The cores were halved using a diamond saw, forming two semi-cylindrical sections, one to be sectioned horizontally, the other vertically.

The cellular activity on the bone surface is of no interest therefore the lengthy procedures normally used for histomorphometry described in section 4.3.2 need not be used and a modified approach, similar to that used by Odgaard (1990), was employed

The samples were embedded in a black resin that could be cut to leave a clean surface which was then photographed. Each sample was serially sectioned and successive sections captured on film. This is a much shorter process as there is no mounting and a less viscous resin may be employed, greatly reducing the embedding time. Also, the risk of error in the pore size is reduced since the standard resin is flexible and the thin sections are very prone to distortion during cutting and mounting.

It is possible to capture the images digitally, using a video camera, rather than photographic film but a comparison of the two methods shows the photographic option to be the best and was incorporated in this study. The digital imaging software stores each file as a 512 x 512 pixel image with a 256 greyscale. On a 20 mm sample thisgives resolution of 39mm compared to 5mm resolving power of photographic film. (200 lines/mm @1000/1contrast for Kodak TMX100). The segments in a video camera's

detector array are rectangular giving visual distortion on the screen, although this can be calibrated out for measurement, it has implications for image manipulation.(There are cameras with square detectors but these are very expensive and not readily available.) Image brightness is recorded on a continuos scale on film which can potentially save far more information than the 256 grey levels of the digitizer.

Sectioning the four samples produced 140 images that were to be transferred from Leeds University, where the microtome is situated, to Sheffield Hallam University for analysis. This would have provided a large amount of digital data and it was felt that a photographic film would be a more secure method of transferring and permanently storing the data. This is especially important as this method of sectioning is destructive. The actual procedure followed can be divided into the following four sections; Sample Preparation, Resin Embedding, Equipment Setup and, Sectioning and Photography.

4.4.3 Sample Preparation

The previously de-fatted samples were soaked overnight in a dilute sodium hyperchloride solution. This cleaned the bone and caused it to become brilliant white to give a good contrast with the black resin.

4.4.4 Resin Embedding

There are a variety of casting resins available with a wide range of properties. e.g. number of components , viscosity, pot life, hardness etc. For this application the resin must have sufficient pot life and a low enough viscosity to completely fill the marrow pores without voids forming under vacuum. It must also be able to be coloured black to aid contrast.

The resin selected was Acrulite Casting Resin. This is a two part resin consisting of a liquid and a powder. The mixing ratio of the powder and liquid is not critical, the only effect is on the curing time. A few trial mixes were carried out and the best results obtained by using a ratio by weight of 2 parts powder to 4 parts liquid, with 0.3 parts of black graphite powder for colouring.

A square aluminum mould was constructed so that the samples could be cast with the flat section on the bottom and the sides of the block at right angles. This makes alignment of the sample in the micro tome easier. The resin was mixed, then allowed to stand for a short period to allow most of the air to escape. The sample was held in the centre of the mould by a short rod and the resin poured over the bone until the mould was full. This was to prevent the sample moving during the filling process. After filling the mould was then placed under vacuum to remove the air. Care was taken since if the initial vacuum was too high, the resultant air bubbles would disturb the position of the bone and cause the resin to spill over. The vacuum was gradually increased until all the air had been removed, (approximately 20 mins), the sample was then left over night to fully harden. The mixing, casting and de-gassing was carried out in a fume cupboard.

4.4.5 Equipment Setup

The micro tome was a heavy duty Jong type, capable of cutting 30μm slices, with a specially made camera attachment bracket. The bracket allowed a 35mm SLR camera to be positioned directly above the cutting plane so that the sample could be photographed after successive sections. A small lamp was attached to the mount to give an even light across the sample. A test piece was placed in the micro tome and cut down until the top surface was completely flat. The sample holder was then manually moved along its guide until it was directly under the camera. The camera height was adjusted to put the sample surface in the closest focal plane thus giving the largest image size. Once the positioning and focus had been set, the camera was locked in position. To find the optimum f stop and shutter speed settings a series of test exposures using kodak TMX 100, a high contrast 100 ASA black and white film, were taken. Speed settings of 1/2,

1/4, 1/8, and 1/16 of a second were used at f 4, 5.6, 8, and 16. The test film was developed using the standard method, the optimum contrast was determined as f8 at 1/8 of a second and the camera set accordingly.

Sections were removed from the test piece at 10 , 20 ,and 30μm thickness to check the cut surface, 10 and 20μm left good finishes whilst 30μm left a slightly ragged edge . The slice thickness was set to 20μm. The camera and micro tome were now fully prepared.

4.4.6 Sectioning and Photography

A block was placed in the holder and aligned so that the cutting plane was parallel to the bone sample, and that the position of the final cut would be well above the jaws of the holder. The sample blocks had been cast with sufficient depth to allow for this. The camera was loaded with a 36 exposure film and one cut was taken from the sample. The micro tome was then manually rotated until the sample was directly beneath the camera. Two exposures were then taken with a graduated glass slide placed on the sample for calibration, one for each orthogonal axis. The slide was placed upside down so that the markings would be next to the sample and thus in focus. The first exposure of the sample was taken. The micro tome was switched on for the required number of cuts ready for the next exposure.

Table 4:2 Sections per exposure for the cancellous bone samples

	Number of cuts/exposure	cut depth μm	Number of exposures	Exposure spacing μm	Sample depth mm
Horizontal	15	20	33 + 2	300	9.9
Vertical	30	20	33 + 2	600	19.8

59

The sample was again manually positioned beneath the camera and the second exposure taken. This procedure was repeated for the rest of the sample. The whole process was then repeated for the other three samples. As a check the first film was developed before the other three samples were sectioned. The results were as expected so the remaining samples were sectioned and the films developed.

The films contained a large amount of structural data from the bone samples which could be extracted using computer image analysis techniques if required. In order to carry out some initial measurements the high and low density horizontal sections were printed on to 8 x 10 sheets, scaled up by a factor of ten. One sheet from each density was scanned on to a computer disc in Bitmap format, using an Hewlett Packard Scan Jet llp, ready for the initial analysis.

4.5 Structural Analysis

4.5.1 Computerised Image Analysis

The purpose of the initial analysis was to provide data on the frequency and distribution of the trabecular thickness and pore diameter and hence determine the design. The bitmap images of the high and low density sections were analysed using Ominet, an Industrial image analysis system supplied by BUEHLER UK Ltd.

The scanned images were in 256 Greyscale form and needed to be converted into binary (black and white) by threshholding. A certain grey level (0 = black, 255 = White) is set as the threshold, all areas of the image with a grey level lower than the threshold become black, and similarly those with a higher level become white. The threshold level is adjusted manually whilst viewing the image to get the most accurate setting.

Once the images were binarised they were superimposed with a blue grid of 50 parallel lines that would be used to interrogate the image. (see figures 4:3 and 4:4) Using the 'logical AND' function between the colours in the image, the portions of the grid covering the white solid, and the black pores were isolated; i.e.

Black AND blue equals black - this leaves the grid segments covering the white solid.

White AND blue equals white - this leaves the grid sections covering the black pores.

The respective grid segments for pore and solid (trabeculae) were measured and counted for both the high and low density samples, see table 4:2 and figures 4:5 and 4:6.

Table 4:3 Mean trabecular and pore thickness

	SOLID		PORE	
	High Density	Low Density	High Density	Low Density
Mean Thickness (mm)	0.240	0.242	0.521	0.985
STD Deviation (mm)	0.181	0.229	0.386	0.786
Object count	1022	506	1084	553
% of Tot 0 - 0.1mm	24.85	38.74		
% of Tot 0.1 - 0.2mm	35.61	24.90		
% of Tot 0.2 - 0.3mm	16.92	12.65		
% of Tot < 0.3mm	77.38	76.29		

Figure 4:3 High Density Sample
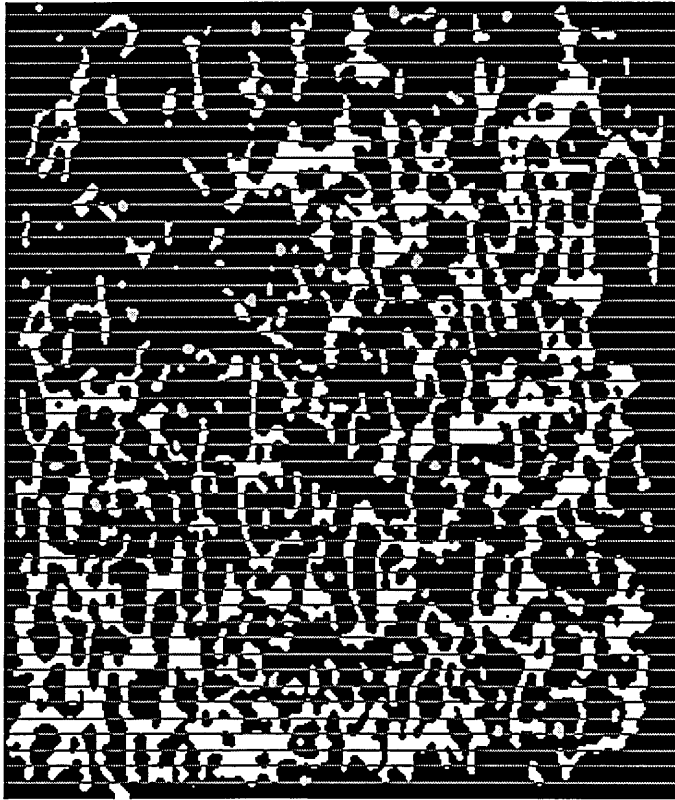
Figure 4:4 Low Density sample
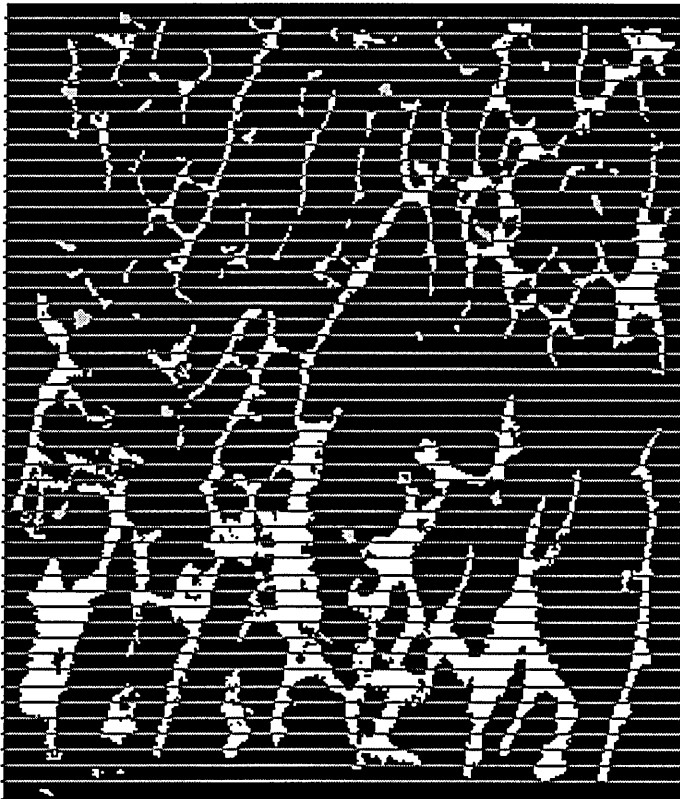
Figure 4:5a High Density Trabecular size and distribution
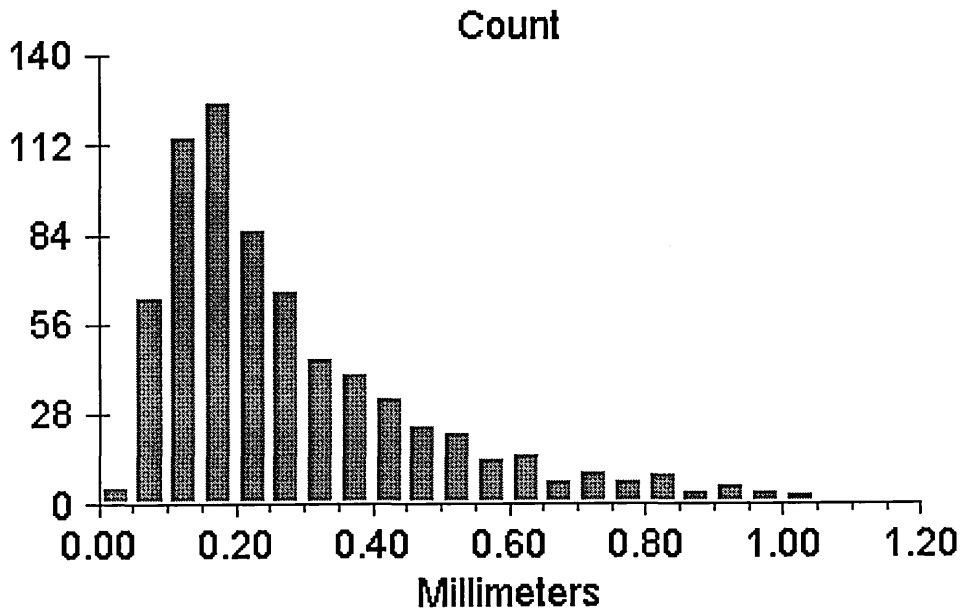
Figure 4:5b Low Density Trabecular size and distribution
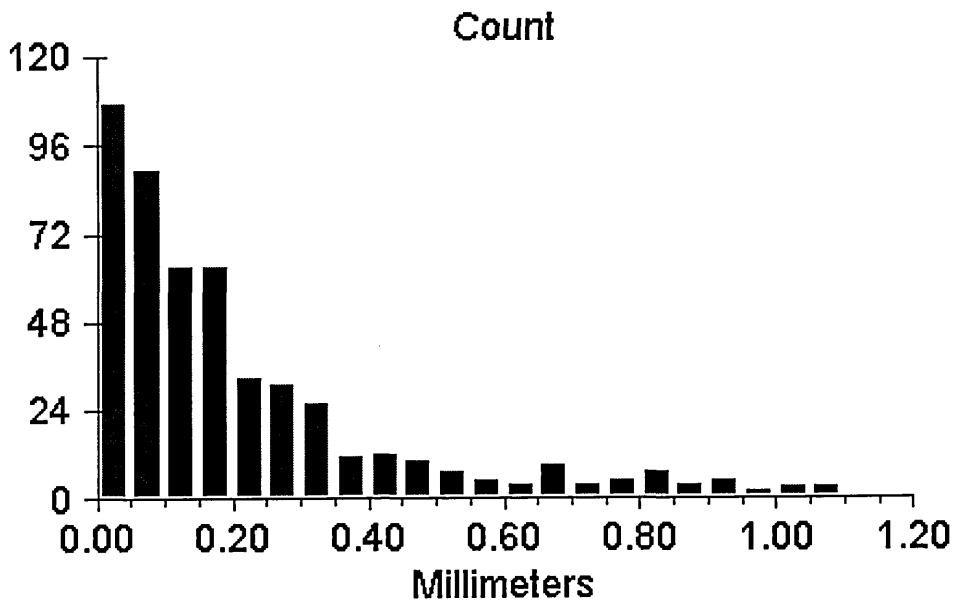
Figure 4:6a High Density Pore size and distribution
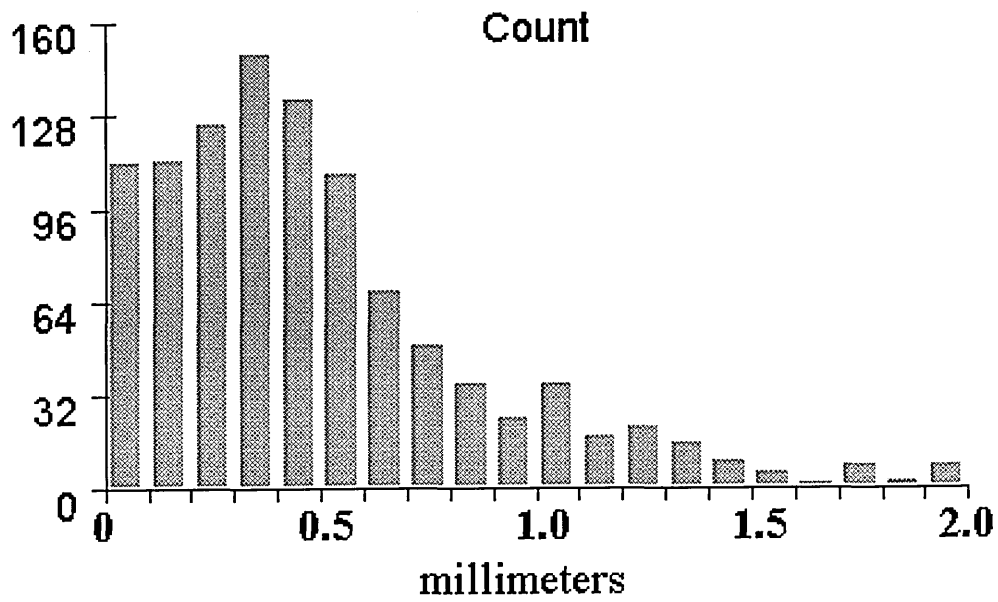
Figure 4:6b Low Density Pore size and distribution
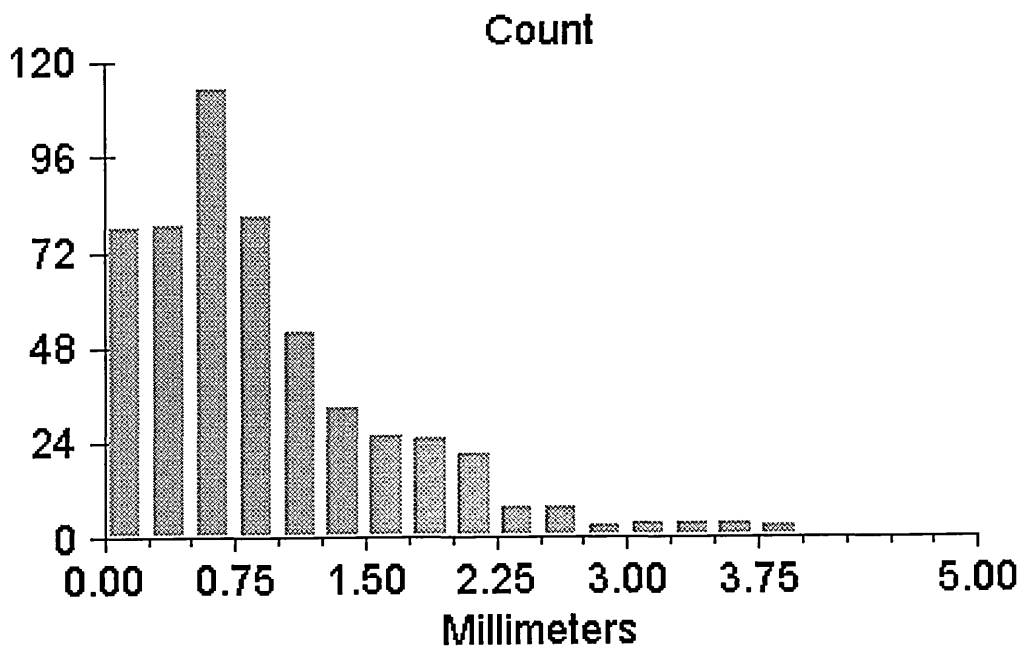
4.5.2 Conclusion

The mean trabecular thickness for high and low density samples were measured as 0.24mm which is below the 0.30mm resolution of the SL system. The percentage below 0.30 mm for the high and low density samples are 77.38% and 76.29% respectively, and below 0.20mm, 60.46% and 63.64% respectively.

This shows that a full 3D reconstruction is not possible since the thickness of the majority of trabeculae in both the high and low density samples was outside the resolution limits of the SL system.

The high density sample had 52.53% of the trabeculae in the 0.1 to 0.3 mm range, compared to 37.55% for the low density sample, which has a greater amount, 38.74% compared to 24.85%, in the 0.0 to 0.1mm range. The total segments counted for the high density sample was twice that of the low density sample, 1022 and 506 respectively. The thinner trabeculae and higher framework perforation indicates that both type I and type II osteoporosis were present in the low density sample.

4.5.3 Accuracy

The accuracy of the results is dependent on three main factors, distortion of the image during the photographic process, greyscale setting during thresholding, and the resolution of the measurement system.

Thresholding the images was very straight forward due to the contrast enhancing measures taken during sample cleaning and the use of a black resin.

The image distortion was checked using a high precision square grid. The grid, marked on a 4" x 4" glass plate, consisted of 0.1mm lines forming 1mm squares with a tolerance of 1μm. The grid was photographed and processed as for the samples and the

4.5.2 Design Considerations

The mean trabecular thickness for high and low density samples were measured as 0.24mm which is below the 0.30mm resolution of the SL system. The percentage below 0.30 mm for the high and low density samples are 77.38% and 76.29% respectively, and below 0.20mm, 60.46% and 63.64% respectively.

This shows that a full 3D reconstruction is not possible since the thickness of the majority of trabeculae in both the high and low density samples was outside the resolution limits of the SL system.

The high density sample had 52.53% of the trabeculae in the 0.1 to 0.3 mm range, compared to 37.55% for the low density sample, which has a greater amount, 38.74% compared to 24.85%, in the 0.0 to 0.1mm range. The total segments counted for the high density sample was twice that of the low density sample, 1022 and 506 respectively.

The thinner trabeculae and higher framework perforation indicates that both type I and type II osteoporosis were present in the low density sample.

4.5.3 Accuracy

The accuracy of the results is dependent on three main factors, distortion of the image during the photographic process, greyscale setting during thresholding, and the resolution of the measurement system.

Thresholding the images was very straight forward due to the contrast enhancing measures taken during sample cleaning and the use of a black resin.

The image distortion was checked using a high precision square grid. The grid, marked on a 4" x 4" glass plate, consisted of 0.1mm lines forming 1mm squares with a

tolerance of 1mm. The grid was photographed and processed as for the samples and the image measured. There was no noticeable distortion within the resolution of the Ominnet measurement system.

The resolution of the measurement system is determined during calibration of the image and is the equivalent distance of one pixel. For this analysis, the resolution was Ý0.05mm. At first glance this figure seems large compared to the mean trabecular thickness (0.24mm), however, even in the worst case of all the measurements being low there will still be at least 60% below the SL limit of 0.3mm.

CHAPTER FIVE

STL Model Design and Manufacture

5.1 Introduction

The initial analysis results determined that the design of the SL model would be based on the second option. This involved processing the 2D scanned sample images into a 3D solid model that can be converted into the SL format.

5.2 Overview

Firstly, the basic trabecular bone structure images for both the high and low density samples were reduced to a skeleton. The skeletal elements were joined together to form a practical, fully connected, structure which was then dilated to within the SL resolution limit of 0.3mm. The skeletonisation and dilation were carried out using the image manipulation routines in Imagery, dedicated histomorphological analysis software. Both images had previously been converted to binary during the Ominet Image analysis.

In order to import the structural detail into a CAD package for solid modeling, the bit map images had to be converted into vector format. Firstly, each image was converted to EPS(Encapsulated Post Script) format using Corel Trace, the EPS file was then imported to Corel Draw and exported in vector form as AutoCAD.DXF. Once in AutoCAD, the images were precisely scaled, mirrored about both axis to give the model a practical size, and an outer shell added for support and protection.

The final images were taken to the School of Engineering at Sheffield Hallam University and imported into MEDUSA, the School's main CAD 3D solid modeling software, for extrusion. Although importing the 2D images into MEDUSA caused no

problem, any attempt to extrude into a solid model caused the software to crash. It was not possible to identify the problem in MEDUSA and so the images were taken to the Centre for Rapid Prototyping at Nottingham University and analysed on a UNIGRAPHICS system. This system has more advanced software, and the hardware has greater processing power and memory.

The problem with the images had occurred during conversion into vector format. The number of entities, or data points, created in each image was too high, using up a lot of internal memory and taking a long time to perform the modelling calculations.

The images were data reduced manually in AutoCAD and then returned to Nottingham University where the extruded solid models were created. The 3D models were then converted into the STL format ready for model manufacture.

5.3 Morphological image processing

The framework of the basic trabecular bone structures was extracted using morphological image processing techniques[36]. The structure or spatial form of an image may be modified by operations such as erosion, dilation and skeletonisation. The image must be in bitmap format and, for most applications, in binary . These techniques are also used in industrial applications such as surface coating analysis and quality control inspection of high density printed circuit boards.

5.3.1 The Bitmap format

An image in the Bitmap format consists of an array of rectangular blocks called pixels arranged in a grid. The pixels are identified by X and Y coordinates, hence the term map, and the file contains information about colour, brightness etc. for each pixel. The

resolution of the image is dictated by the number of pixels in the array, common sizes are 320 x 200, 640 x 480, 1024 x 786, and the colour levels, typically 2, 16 or 256. High resolution colour images require correspondingly greater memory space compared to low resolution black and white (binary) images. Since the basic block of a bitmap image is a rectangle, any circular or non orthogonal lines will have a characteristic jagged edge. This is demonstrated in figure 5:1 which shows orthogonal ,circular and diagonal lines at pixel level.

Figure 5:1 The BITMAP format at pixel level
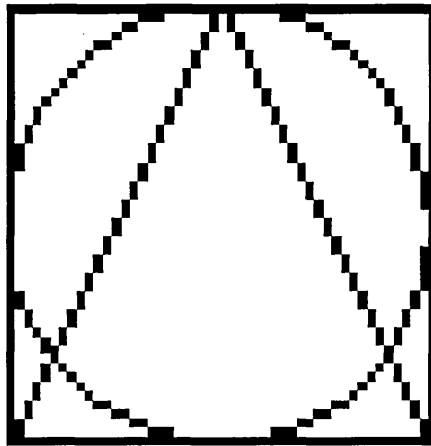
This is the main disadvantage of bitmaps and can only be overcome by using the vector format. There are also implications for resizing images and these are discussed in the section on conversion to vector format.

The advantage of the bitmap format is that it needs relatively simple software routines to manipulate the pixels within the image. Morphological operations make use of this by simply superimposing a mask over each pixel in turn then altering its binary value according to the pattern formed in the mask. Commonly found file extensions for bitmap files are; .BMP, .PCX, .TIFF, .GIF, and .JPEG (used on the internet).

5.3.2 Morphological Operations

All morphological operations are variants of two basic operators, dilation or erosion (thinning or skeletonisation), and are carried out by placing a mask over each pixel in turn and setting its binary condition according to the conditions of the surrounding pixels. For example to remove a single black pixel from a white image a 3 x 3 pixel pattern is placed over each pixel in turn. If the following pattern is found the central pixel is turned to white.

0	0	0			0	0	0
0	1	0	becomes		0	0	0
0	0	0			0	0	0

Black = 1   White = 0

Pattern recognition is performed by using a pixel stack. The pixel stack is formed by convolution of the central pixel and its eight surrounding neighbours, read in the following order;

3	2	1
4	X	0
5	6	7

The binary state for each pixel is used in the stack and this forms a unique numerical code for the pattern, in this case 100000000. This code is then used as an address in a look up table that dictates what condition the central pixel (X) should be set to.

The output of the look up table is held in a separate register (Y) until all the pixels have been looked at then the whole image is updated, i.e. X = Y. In this case the look up table would give Y = 0 for address 100000000 and Y = X for all the rest. Each operator or variant is associated with its own look up table.

It should be noted that when the X register is updated from the Y register, the original contents are not normally saved and that the previous image is lost. It is therefore advisable in processes that use multiple operations to save the intermediate images. Once each operation is successfully completed the image should be saved under a different name, at least until the final image is produced.

This is a very simple example, some operations require a mask larger than 9 elements and the edges of the image need special conditions, however it does show the basic concept and highlights the need to save important images.

5.3.3 Fundamental operations

Binary morphological operations are carried out by dilation or erosion of an image. This is achieved by the addition or removal of pixels of a given condition within the Image.

5.3.4 Dilation

Dilation in the general form consists of the addition of a single ring of boundary pixels for each iteration. This means that a section across any two points on the boundary will show an increase of two pixels. Consider two circles, one solid, one doughnut. Both receive a ring of pixels around the outside circumference, the doughnut also receives a ring around the interior circumference. If sufficient iterations were carried out the inner circumference would eventually disappear as the doughnut became a solid circle. See figure 5:2. This property is used for closing operations described later.

Figure 5:2 Dilation

72
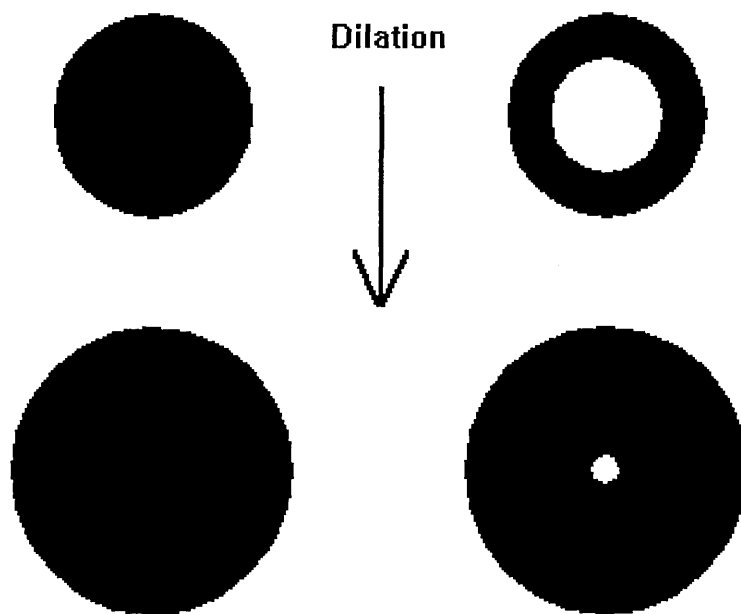
5.3.5 Erosion

Erosion can be subdivided into three operations, smoothing , thinning and skeletonisation. Smoothing operations are used to clean up noisy images, the single pixel removal described in section 5.3.2 is an example of a smoothing operation. Thinning is the compliment of dilation and involves the removal of a boundary layer of pixels. The solid circle thins towards the central pixel whilst the doughnut thins towards the midpoint between inner and outer circumferences. Thinning performed on shapes such as an hour glass can cause separation of features, see figure 5:3, this can be used for opening operations.

Figure 5:3 Erosion (Thinning and Skeletonisation)

THINNING
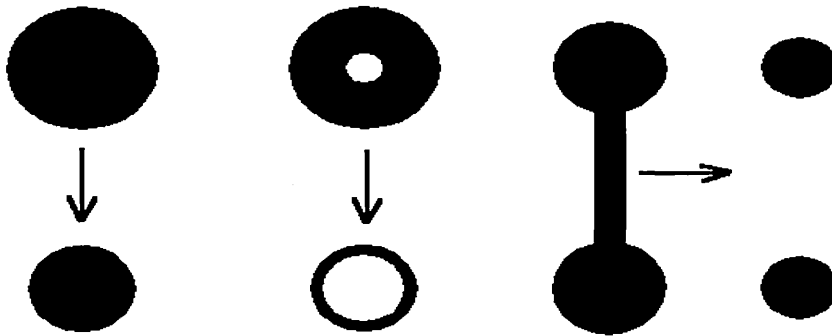
SKELETONISATION

5.3.6 Skeletonisation

Skeletonisation is a special form of thinning that maintains connectivity, thereby forming a 'stick figure' representation of the original object. The whole image is eroded in the usual way except that when any area reaches one pixel thickness, further erasure is prevented and eventually the image is reduced to a skeleton one pixel wide. Solid squares and circles reduce to a single pixel, ellipses and rectangles reduce to a line equidistant from the longest side and triangles transform to a star shape.

5.3.7 Opening and Closing

Dilation and erosion used in conjunction can provide smoothing operations, dilation followed by erosion can close small holes and erosion followed by dilation can open small gaps. See figure 5:4.

Although these operations were not used on the STL design they have been described as they do show that using complimentary operations on bitmaps can permanently alter the image.

Figure 5:4 Smoothing operations (opening and closing)
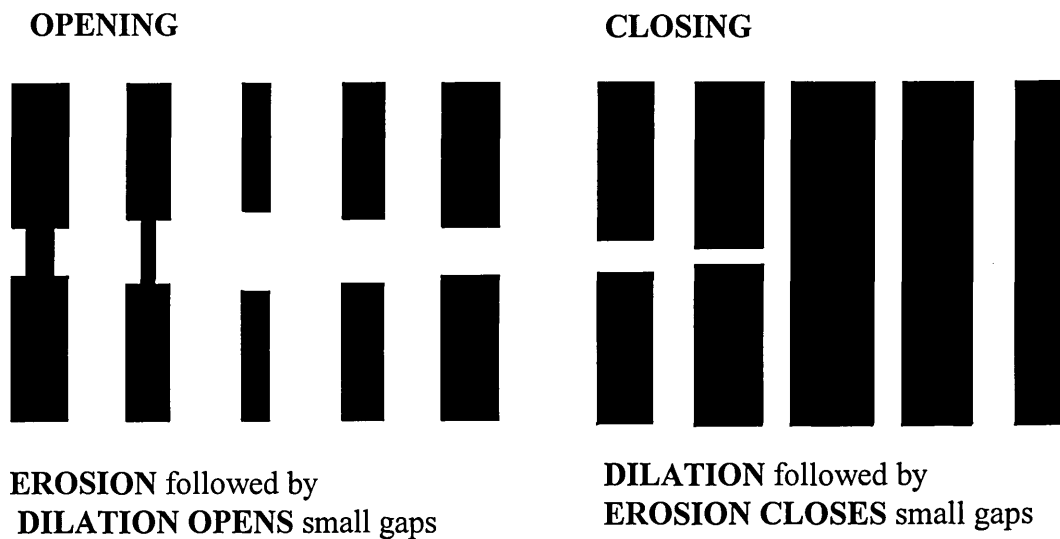
OPENING   **CLOSING**

EROSION followed by
DILATION OPENS small gaps

DILATION followed by
EROSION CLOSES small gaps

The images of the samples were transformed using Imagery, a specifically designed histomorphological analysis software obtained from Leeds University. Calibration was carried out using the images of the graduated glass slide where one pixel was equivalent to 0.05mm. The basic bone images were smoothed then skeletonised. The isolated elements of the skeleton were joined together to form a complete structure which was then dilated by 3 iterations. Each iteration added two pixels to the line width giving a total of 7 pixels. Each pixel is the equivalent of 0.05 mm giving a total line width of 0.35mm, which is within the SL resolution of 0.3 mm. See figure 5:5 . The dilated images formed the last stage of processing as bitmaps and must then be converted into the vector format to continue the STL model design.

Figure 5:5 The basic bone structural Bitmap images(low density)

a) The bone section
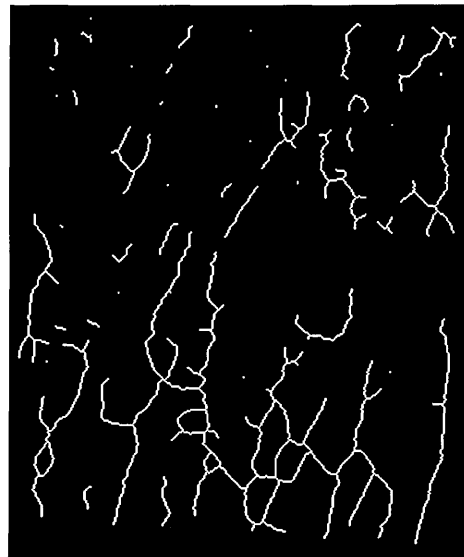
b) Skeletonisation
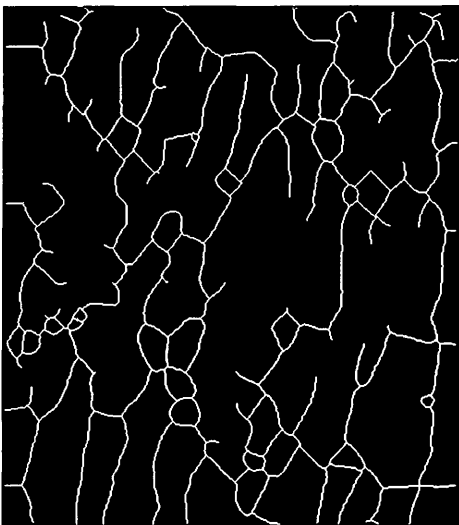
c) Linking
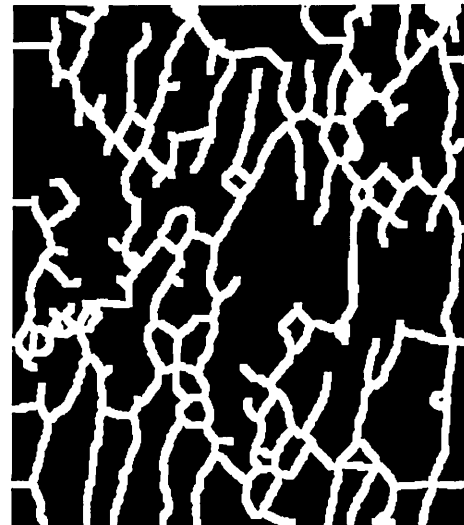
d) Dilation to 0.35mm

5.5 *File Conversion from Bitmap to Vector formats*

An image in the vector format consists of objects made up of predefined elements called entities. The entities, lines, circles, etc. are stored as vectors with coordinates of their position within the image. A series of entities, forming any shape, can be linked together to form a polyline, the area within the polyline becoming an object. Since vector coordinates can be given for the x, y and z axes, 3 dimensional objects can be described. Image transformations are performed by mathematical calculation of the entity vectors and are therefore inherently more accurate than bitmap changes. For instance, if a bitmap image with single pixel detail were reduced to 50%, the detail would disappear. If the image was then enlarged to its original size it would be still be the 50% image but twice the size. The standard vector file formats are .DXF and .IGES. The accuracy of a vector format image is as high as the number of decimal places the processor can work to. Practically, the accuracy is set by the resolution of the output device, (plotter, printer, modelling system, etc.) and the minimum number of decimal places to give the required resolution are used. This is because more decimal places require more time and processing power to calculate. Also, more memory is needed and complex images can have huge file sizes (30 Mbytes and upwards). For this reason output files are usually limited to a maximum 16 decimal places and typically 6 places are used.

Conversion of a bitmap to vector format is carried out by tracing. This can be done manually or by use of tracing software. The manual method involves tracing over an enlarged printout of the image using a digitizing tablet. This is very time consuming and the accuracy depends upon the hand and eye of the operator. Tracing software is much faster and more accurate and this was the method used.

5.5.1 Vector conversion

The images needed to be converted into AutoCAD.DXF so that they could be prepared for 3D modeling. This was accomplished in two stages using COREL 4. Firstly, the images were traced using Corel trace, which outputs files in encapsulated postscript format, EPS, a standard file interchange format. Secondly, the EPS files were imported into CorelDRAW and exported as AutoCAD.DXF.

CorelTRACE is a designated package for the conversion of bitmaps to vector format. The areas of an image to be traced are selected by colour and a trace is drawn around the perimeter of each one. Working on the principle that a curve can be represented by a series of straight lines, the trace file forms a polyline consisting of line entities. The start and finish of each entity is positioned exactly on the interface between the colour selected and the background. The precision of the trace , i.e. how well the trace follows the original image, is set by the distance the line entities are allowed to deviate from the actual edge. This deviation can be either side of the boundary. See figure 5:6

Figure 5:6 Trace Precision

High precision gives high entity count.

Low precision gives low entity count.
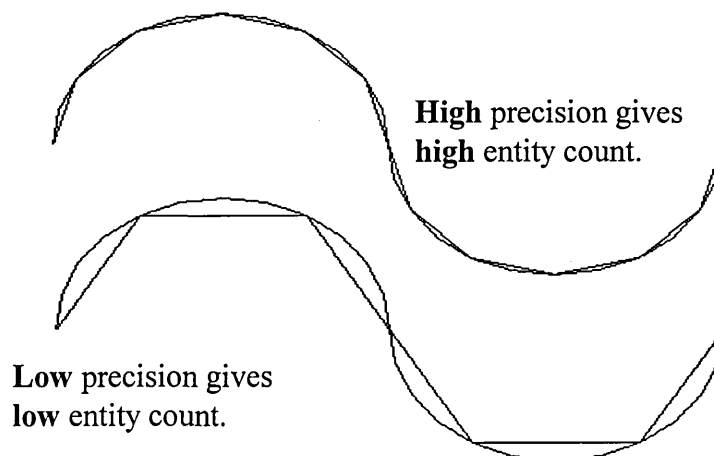
There are five preset precision options and the highest setting was selected to ensure that the trace deviations would maintain the 0.35 mm width. When a lower resolution was used certain parts of the geometry were reduced to less than the 0.3mm SL resolution. Use of the high resolution setting presented problems for the solid modelling which are described later. Once the two images had been traced the output EPS files were imported into CorelDRAW then exported as AutoCAD.DXF

5.6 Final design drawing

5.6.1 2D - AutoCAD

The vector format files of the two structural images were now ready to be transformed into the final design and this was drawn in AutoCAD. The SL model had to be large enough to accommodate the 19 mm diameter transducers used in the measurement system and have a width similar to a normal calcaneum. The measurement faces were set at 30mm and the width set to 28mm. The structure was surrounded by a 2mm jacket, mimicking the cortical outer shell, which gave overall dimensions of 34mm x 32mm, and the extrusion depth set to 34mm. The width was set slightly lower so that only the two measurement surfaces would be square, all the rest being rectangular. This was done to reduce the possibility of measurements being taken across the wrong axis. The size of the sample images were approximately one quarter full-scale and so each one was mirrored about both axes to form the complete structure. The images were cropped to the exact dimensions, 14mm x 15mm, and a 2mm jacket added to the two outer sides. The pore surface area of each quarter image was measured, as an indication of porosity, before being mirrored up to form the full size model. The final design

drawings were now complete and were saved in the AutoCAD.DXF format ready for transfer to the solid modelling system.

5.6.2 Solid modelling - MEDUSA

The two dimensional images needed to be extruded to form a three dimensional solid model which would then be converted into the STL format. At the time the processing power required to run solid modelling software was not generally available in PC format and a work station had to be used. The school of Engineering at Sheffield Hallam University were using a modelling package called Medusa and agreed to perform the modelling.

The AutoCAD.DXF files for the high and low density models were imported into MEDUSA without any problems. Within the files the outline of each pore is described by a polyline made up of line entities. The protocol of modelling packages is such that the area within an enclosed polyline is classed as solid, this means that as far as Medusa is concerned, the pores are solid and the solid structure is a void. Due to this, the extruded model would consist a series of 'solid' pores. This is overcome by subtracting the 'solid' pores from a solid cube with the outside dimensions of the model, leaving the correct structure.

The low density design was selected and extruded to 34mm. Although the extrusion was successful it did take quite a long time and the system seemed to be working hard. This could indicate possible problems with the file conversion or format and it was therefore decided to check the high density design before going any further.

The high density design was selected and an attempt was made to extrude the image. However, after 15 to 20 mins the system crashed with an undisclosed error. The system

was rebooted and a second attempt was made with the same result. The Engineering School staff felt that the problem was most likely to do with the tortuous geometry of the images but, as the error message was undisclosed there was no easy way of pinpointing the fault and a different approach had to be found.

5.6.3 Extrusion - Unigraphics

The AutoCAD.DXF files were sent to the Centre for Rapid Prototyping in Manufacturing at the University of Nottingham for further investigation. Using a HP 9000 series workstation with the latest version (Version 10) of Unigraphics modeling software, the files were checked and the problem identified. The geometry of the images was not at fault, it was purely the number of entities created during the conversion to vector format. Nottingham University advised that it would make subsequent modelling and conversion to STL format much easier if the entity count was reduced.

5.6.4 Data Reduction - AutoCAD

The entity counts of both images were reduced manually using AutoCAD. The original images were traced over on a separate layer using the polyline command. Use of the snap mode ensured that the trace faithfully followed the original structure and visual inspection allowed the entity count to be kept to a minimum whilst still retaining adequate precision. This was a simple but time consuming process. Once the trace had been completed the trace layer was frozen and the original image deleted leaving only the reduced count structure. The size of the data reduced files were approximately 10 % of the originals.

5.6.5 STL Files - Unigraphics

By this time it had been decided to use the Rapid Prototyping Centre at Nottingham University to manufacture the SL models and so they would carry out the solid modelling as well. The data reduced files were taken down to Nottingham University and 3D solid models produced which were then converted into the STL format ready for manufacture.

5.7 MODEL MANUFACTURE

5.7.1 Bureau Services

The models were manufactured at the Centre for Rapid Prototyping in Manufacturing at Nottingham University. 3D modelling was performed using Unigraphics Version 10 on a HP 9000 Series 700 workstation and the models built on a 3D Systems Inc SLA 250. This centre was selected rather than the Rover group, the only other SL bureau, as Nottingham provided better 3D modelling facilities and data exchange was much easier using the Joint Academic Network (JANET). Costs were approximately equal for the two service suppliers.

5.7.2 Small Pore Drainage

The SL engineers at Nottingham expressed concern that the smaller pores may cause problems with drainage of the unused resin, especially in the high density model. To test this, a single low density model was produced and left to drain. It was found that several of the smallest pores (<0.2 mm dia) could not be drained even with a pressurised air jet. The problem was caused by the extrusion of the pore forming a long capillary.

This could easily be over come in the low density model by simply removing the smallest pores, making little difference to the over all structure, and the design was altered accordingly. Since the high density model had a greater percentage of smaller pores, removal of those pores would have altered the structure by so much as to be unacceptable. It was therefore decided to continue with the low density model only.

5.7.3 Low Density Model production

At least five models would be needed for intermodel precision tests, for possible use as a phantom, and a further five for marrow mimic trails. Using the revised low density design, 10 models were built on the SLA taking approximately 40 hours.

To look at the effect of structure and density, a further six models were made, based on the original low density design, with the following alterations;

Basic design 70% porosity   See Figure 5:7 a and b

Basic design dilated to 50% porosity   See Figure 5:8a

Basic design dilated to 30% porosity   See Figure 5:8b

Basic design perforated to 80% porosity   See Figure 5:9a

Basic design perforated to 85% porosity   See Figure 5:9b

80% porosity dilated to 70% porosity   See Figure 5:10a

85% porosity dilated to 70% porosity   See Figure 5:10b
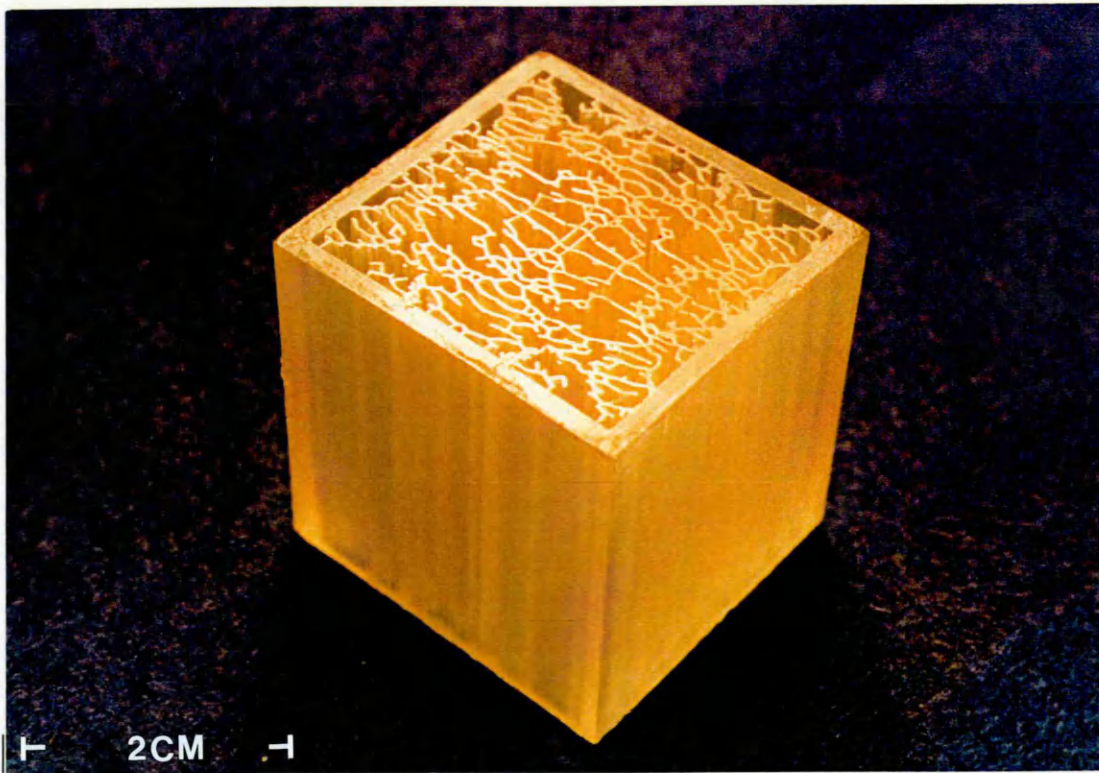
Figure 5:7a The Stereolithography model
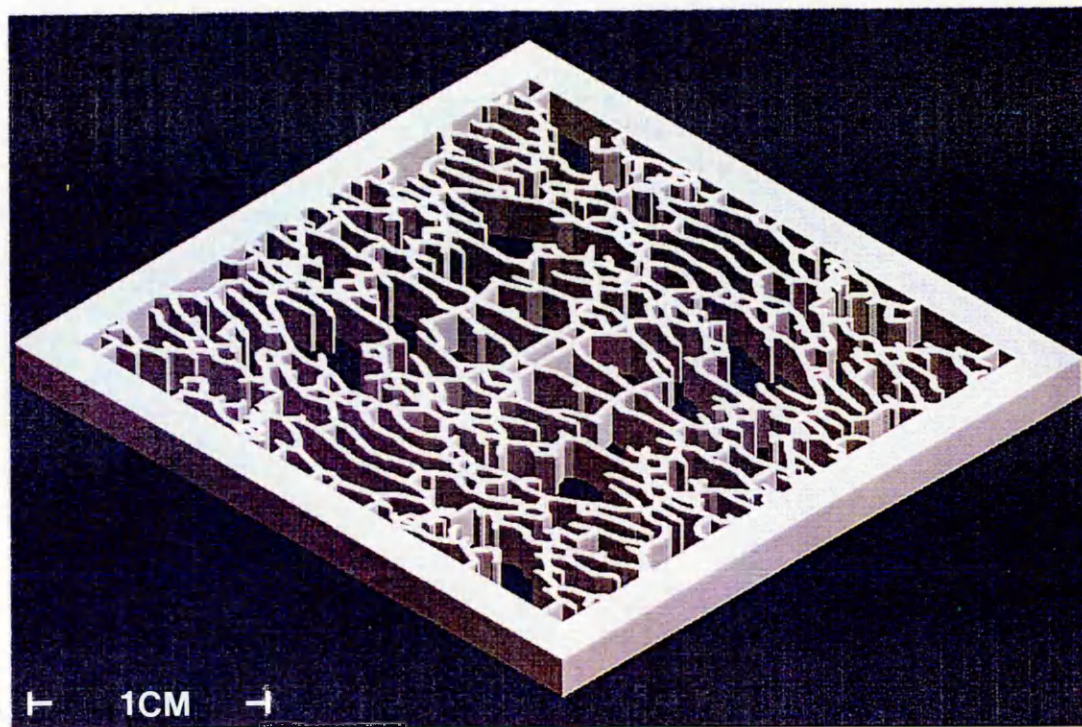
Figure 5:7b Section of the basic model CAD extrusion
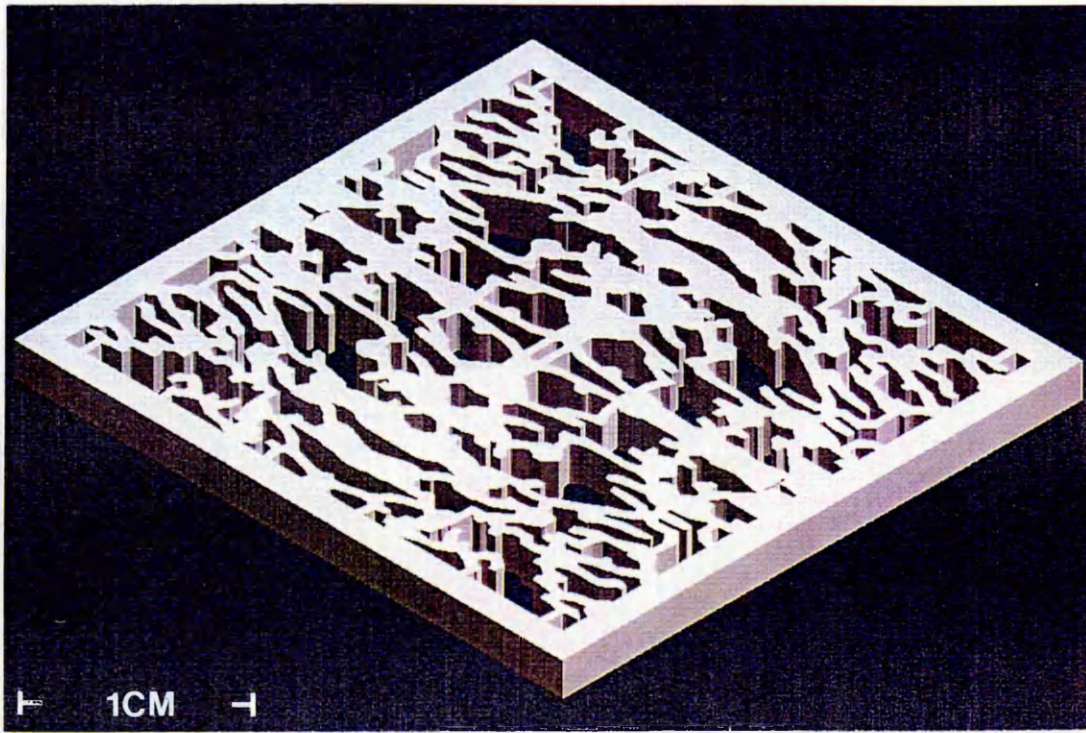
Figure 5:8a Basic model dilated to 50% porosity
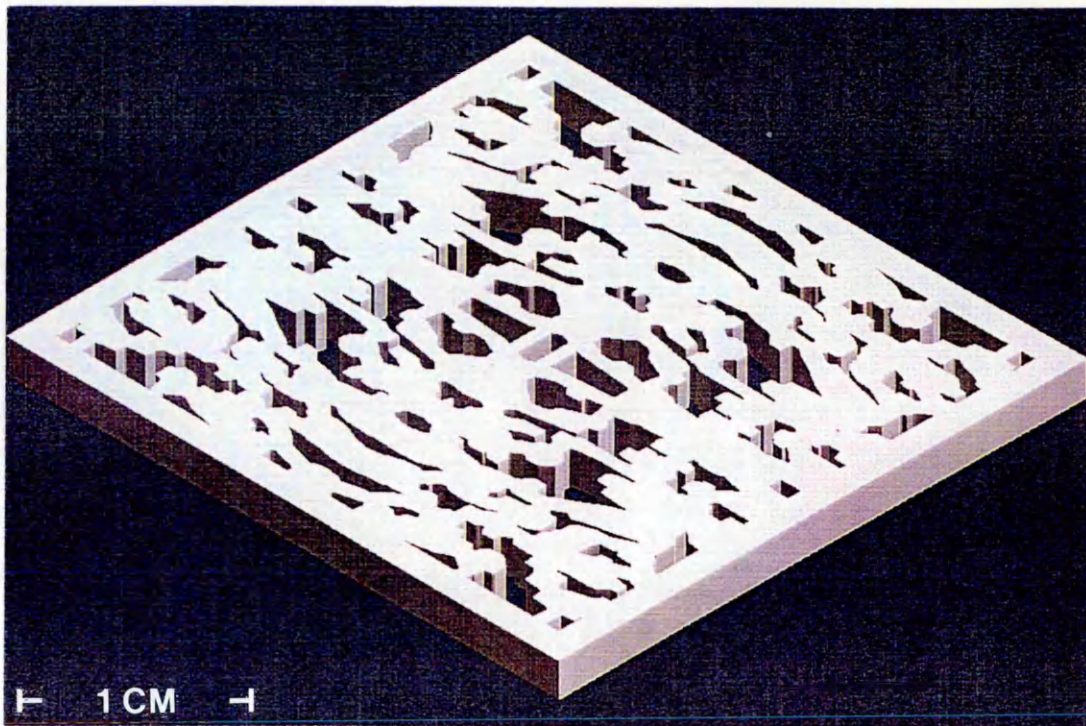
Figure 5:8b Basic model dilated to 30% porosity

84
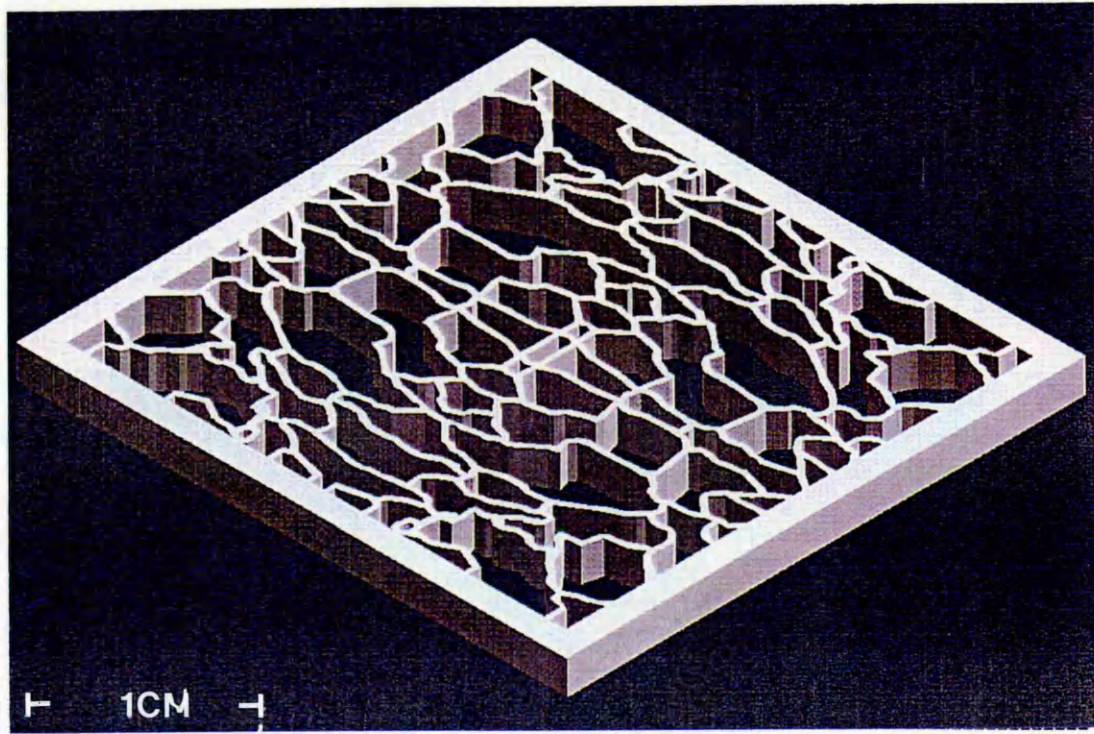
Figure 5:9a Basic model perforated to 80% porosity
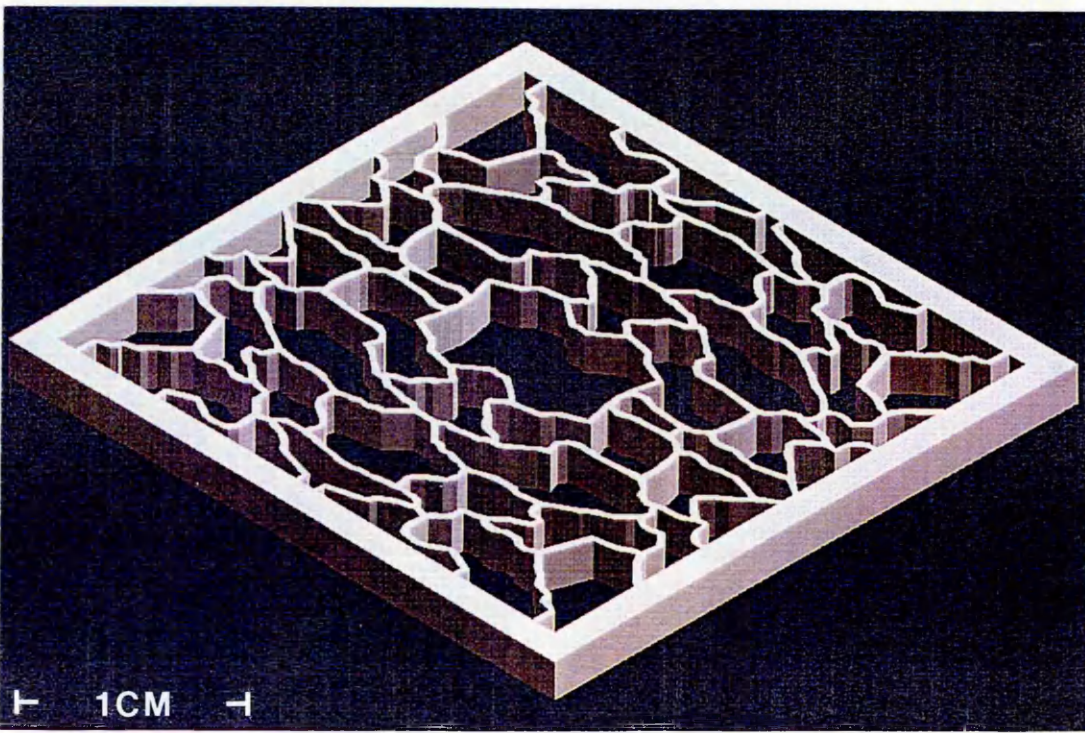
Figure 5:9b Basic model perforated to 85% porosity

85
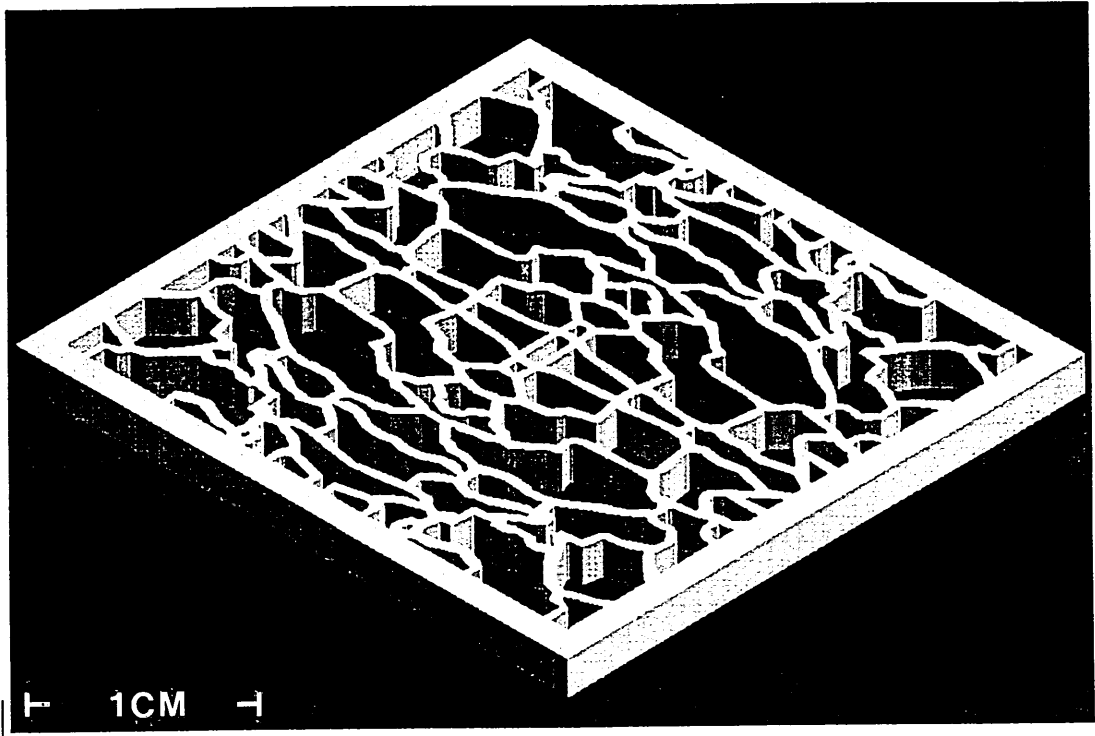
Figure 5:10a Dilation of 80% to 70% porosity
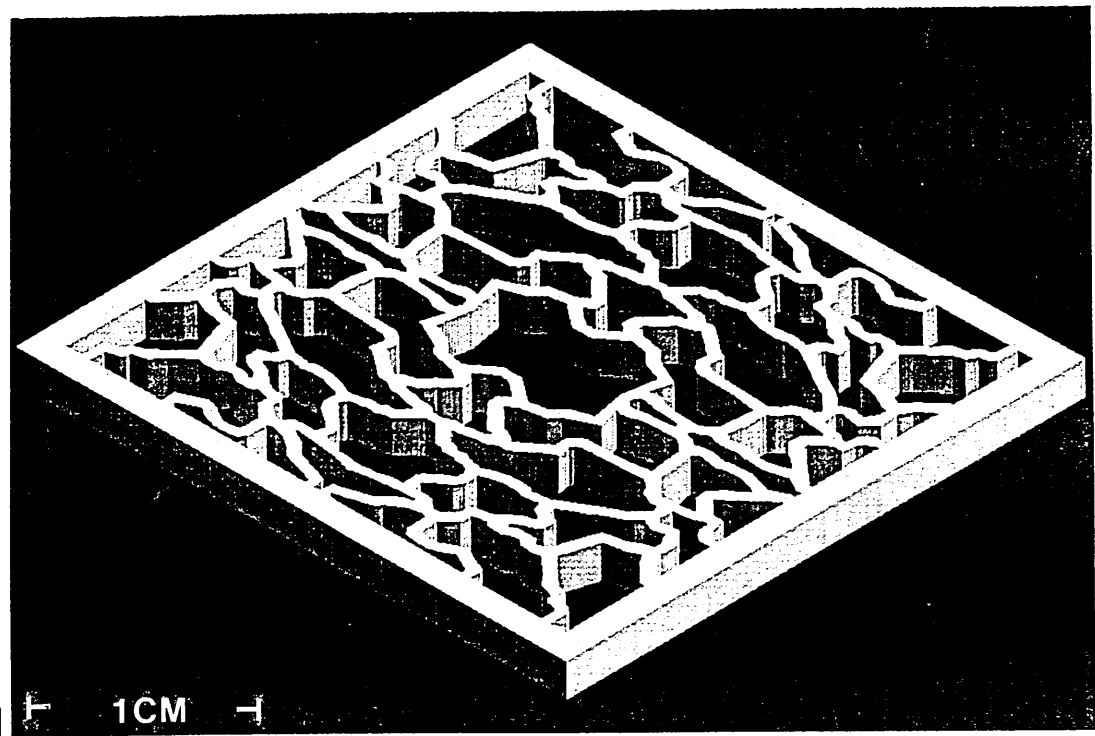
Figure 5:10b Dilation of 85% to 70% porosity

86

CHAPTER SIX

SL MODEL EVALUATION

6.1 Overview

The first stage of the evaluation of the completed SL models was to find a suitable

marrow mimic. Using four of the ten basic models, various materials were investigated

and castor oil was selected as the most suitable. Five of the remaining six models were

then tested for repeatability and stability. These tests showed the models to be stable

however the perspex boxes used to house the models were causing problems with the

BUA measurements. The last basic model and the six structural variations were then

tested without the perspex housings.

6.2 Test Equipment

All the testing was carried out using CUBAR (Contact Ultrasonic Bone Analyzer

Research). This is a research version of CUBA clinical[37] and consists of a computer

controlled pulse generator and a Thurlby digitizer. The system works in the time domain

and the digitized received pulse gives both BUA and velocity information. The software

obtains the amplitude spectrum data in the range 0.2 to 0.6 MHz by using a fast Fourier

transform. The 19mm diameter transducers are 1MHz broadband with silicone pads for

coupling, and mounted on a sliding caliper with a digital vernier gauge. (See figure 1.4)

6.3 Marrow Mimic

The structure formed by the stereolithographic resin represents the mineralized solid

part of the calcaneus and a compatible material to act as the marrow fat must be found.

The following properties are required:

1)   Compatibility with SL resin

2)   Acoustic properties similar to marrow at room temperature.(see table 6:1)

3)   Low variation with temperature.

4)   Ease of use, non toxic and no special handling precautions.

5)   Readily available.

Table 6.1 Physical and Acoustic properties of Materials

MATERIAL	VELOCITY $m\,s^{-1}$	ATTENUATION $dB\,MHz^{-1}\,cm^{-1}$	DENSITY kgm^{-3}
Subcutaneous Fat	1450	0.5	952
Water[1]	1480	-	1000
Castor Oil[2]	1472	-	969
Synthetic Oil	1474	-	840
Silicone Oil	1577	-	960
Silicone Rubber	1045		1080
note: no 1 Wells 1997, no 2 Njeh 1995			

6.3.1 Water

Water is used extensively in ultrasonic measurements and its sonic characteristics are well documented. An added advantage of using water is that attenuation is not frequency dependent and so BUA measurements would relate to the bone structure only. To test the compatibility of the SL models with water, a model was immersed in degassed water for several days. Inspection showed barrel distortion of the model due to water ingress. The model was no longer rigid and could be easily squeezed with finger pressure, returning to roughly the same barrel shape on release. Due to the hygroscopic nature of the resin, water cannot be used as a marrow mimic.

88

6.3.2 Gelatine

Clarke et al[15] (1994) used a geletine/water mix for the cancellous bone phantom. This was selected as a compromise between ultrasonic parameters and the ability to form solid granules, fundamental to that method of manufacture. The extra preparation and difference in ultrasonic coefficients make gelatine unsuitable for this application.

6.3.3 Agar gel

During his work on phantoms, Njeh [14](1995) looked at several materials including Agar gel, lard and Castor oil. The Agar gel was mixed with graphite powder, distilled water and n-propanol, the relative proportions affecting the ultrasonic velocity and attenuation. This material has a semi-solid consistency with comparable acoustic coefficients but is complicated to make.

6.3.4 Lard

Household lard is similar to marrow fat however cycling between solid and liquid states causes inconsistency in the ultrasonic attenuation.

6.3.5 Castor Oil

Castor oil has a very comparable density ($969Kg\ m^{-3}$) and velocity ($1472\ ms^{-1}$). It is readily available, liquid at room temperature and requires no preparation. This makes castor oil a very practical possibility for the marrow mimic material.

6.3.6 Synthetic oil

Synthetic engine oil has similar properties to castor oil and so has the potential to be marrow mimic.

6.3.7 Silicone

Silicone rubber was looked at as a possible mimic as this would provide an excellent barrier to the outside world. Use of liquids or semi-solids require the model to be housed in a container, for protection, and to prevent spillage or contamination of the marrow mimic. This is an important consideration as ultra sound measurements involve the use of coupling agents, usually water, waterbased gels or oils and are, therefore, somewhat messy.

Silicone rubber is used in conjunction with Stereolithography to form molds for casting and a sample was acquired from the Rapid Prototyping Centre at Nottingham. The density and velocity were measured as $1080Kgm^{-3}$ and $1045ms^{-1}$ respectively. The low velocity was felt to be acceptable when compared to the convenience of a solid marrow mimic. The model would also be more realistic as the stiffer silicone rubber is very similar to soft tissue.

Using the facility at Nottingham University one of the SL models was cast into a block of silicone rubber, oversized by 5mm in all directions. The model was returned to Sheffield and tested ultrasonically.

The results showed an unacceptably large attenuation of 40 dB at 0.2 MHz. This amount of attenuation indicates a large mismatch in acoustic impedance, usually associated with the presence of air although no bubbles could be seen in the rubber block. A second model was prepared, paying special attention to the evacuation during

90

casting to ensure the removal of all the air, and tested. The attenuation at 0.2 MHz was similar to the first. A further model was immersed in silicone oil and degassed overnight before being tested. Again the low frequency attenuation was very high. This result was surprising and could not be readily explained as the acoustic impedance of the silicone oil is similar to castor and synthetic oil (see table 6.2). It would appear that the SL model is not compatible with silicone and since the SL models were not retrievable from the rubber block, it was decided that further testing was impractical.

A different material must be used as the marrow mimic.

Table 6.2 Acoustic impedance of Silicone, Castor and Synthetic oils.

	VELOCITY ms^{-1}	DENSITY Kgm^{-3}	IMPEDANCE $Kgs^{-1} m^{-2}$
SILICONE OIL	1577.2	960	1.514×10^6
SYNTHETIC OIL	1473.75	840	1.238×10^6
CASTOR OIL	1551.76	914	1.418×10^6
WATER	1480	1000	1.480×10^6
notes: Velocity measurements of oils taken in perspex box 52mm and include 2 x 0.6mm windows Density measured by weight of known volume. Acoustic Impedance Z calculated by: Z = Velocity x Density			

6.3.9 Synthetic and Castor oil Evaluation

Since silicone proved unusable, the choice of marrow mimic material lay between castor and synthetic oil. In order to evaluate the two oils further, a perspex box was designed to accommodate the SL models. The overall dimensions of the box, 52mm x 54mm x 54mm, allowed the model to be surrounded by 5mm of oil in all direction. Small lugs were incorporated in the box to hold the model in position and acoustic windows were machined inside the faces of the measurement axis.

Two SL models were placed in the specially made perspex containers, one filled with castor oil, the other with synthetic oil, and degassed. The models were placed in a water bath set at 30°C and daily readings taken. After 3 days the readings became repeatable at 70 dBMHz^{-1} and 1738.21 ms^{-1} for castor oil, and 76 dBMHz^{-1} and 1679.16 ms^{-1} for synthetic oil.

The two models were then tested over a range of temperatures, 19°C to 45°C, and the respective coefficients derived.

Fig 6.1 BUA versus Temperature for Castor and Synthetic oils
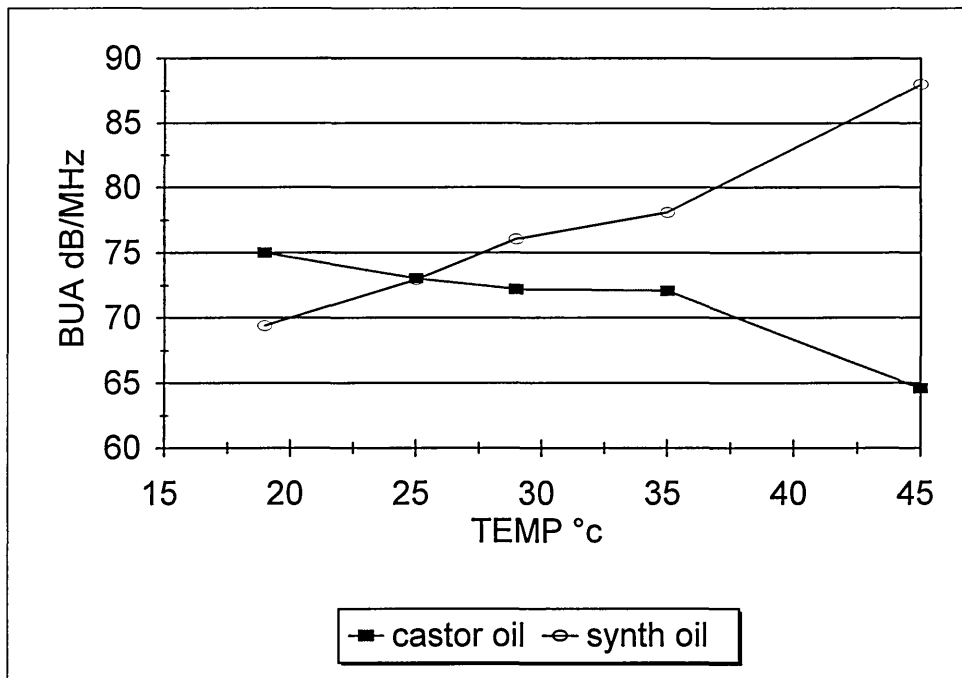
Table 6.3 Temperature coefficients of BUA and Velocity in castor and Synthetic Oil

	CASTOR OIL	SYNTHETIC OIL
BUA (dB/MHz/°c)	- 0.4	0.71
VELOCITY (m/s/°c)	- 4.8	- 4.3

Castor oil was selected as the marrow mimic as it has the smallest temperature coefficient for BUA, approximately half that of synthetic oil, the velocity coefficients being approximately equal.

6.4 Cancellous bone model evaluation

The cancellous bone models, consisting of the SL model immersed in castor oil in a perspex container, were prepared for ultrasonic evaluation. The initial tests were carried out on five of the remaining six basic models, looking at repeatability and overall stability. Once the models were proved stable, the last basic model and the six structural variants were then prepared and tested.

6.4.1 Repeatability tests

The 5 basic models were placed in a water bath set at 30° C and measured five times over a period of seven days. BUA and velocity were measured using CUBAR with each daily reading consisting of the average of five consecutive measurements of each model. The transducers were set at 90mm separation and placed in a jig, aligned with the acoustic windows in the perspex boxes, to give exact repositioning for each measurement. The results are given in table 6:4 for BUA and table 6:5 for velocity. The inter and intra model precision for velocity (0.69% mean) showed stability and repeatability for all the models however the reduced precision of the BUA (8.5%) caused some concern. The variability was attributed to reverberations within the perspex box and so it was felt that more accurate measurements would be obtained without the housings.

6.4.2 Structural Model evaluation

The last basic model and the six structural variations, described below, were prepared

and measured in a bath of castor oil at room temperature. The results are in table 6:6.

Model 6   Basic structure with 70% porosity.

Model 7   Basic structure dilated to 50% porosity.

Model 8   Basic structure dilated to 30% porosity.

Model 9   Basic structure perforated to 80% porosity.

Model 10   Basic structure perforated to 85% porosity.

Model 11   Model 9 (80%) dilated to 70% porosity.

Model 12   Model 10 (85%) dilated to 70% porosity

6.4.3 RESULTS

The results of the ultrasonic tests are as follows:

Table 6:4 Repeatability - BUA dBMHz^{-1}

MODEL	1	2	3	4	5	MEAN	SD	CV%
DAY 1	77.52	100.90	99.74	83.91	98.82	92.18	10.73	11.64
2	88.67	91.97	99.34	80.67	111.39	94.41	11.62	12.31
3	81.53	96.38	97.77	84.92	101.63	92.45	8.72	9.43
4	82.28	84.41	86.13	92.98	100.64	89.29	7.51	8.41
5	84.64	95.00	99.50	83.88	95.94	91.79	7.08	7.72
MEAN	82.93	93.73	96.50	85.27	101.68	92.02	7.82	8.50
SD	4.11	6.12	5.85	4.60	5.84			
CV%	4.95	6.53	6.06	5.39	5.74			

Table 6:5 Repeatability - Velocity ms^{-1}

MODEL	1	2	3	4	5	MEAN	SD	CV%
reading								
1	1982.48	1965.38	1954.28	1985.65	1961.49	1969.86	13.61	0.69
2	1956.67	1953.14	1948.22	1986.89	1957.88	1960.56	15.19	0.77
3	1962.67	1966.31	1941.34	1980.99	1956.89	1961.64	14.42	0.74
4	1989.47	1979.83	1968.81	2007.56	1968.79	1982.89	16.27	0.82
5	1985.92	1966.38	1947.32	1972.48	1953.25	1965.07	15.38	0.78
MEAN	1975.44	1966.21	1951.99	1986.71	1959.66	1968.00	13.55	0.69
SD	14.76	9.45	10.46	12.95	5.89			
CV%	0.75	0.48	0.54	0.65	0.30			

Table 6:6 Basic model and structural variation measurements

Model	BUA dBMHz^{-1}	VEL ms^{-1}	POROSITY %	Trab Surf Area mm^2	Trabecular number
6	81.36	2000.61	70	55696	18
7	74.18	2378.17	50	38454	13
8	53.93	2498.60	30	30022	11
9	79.89	2130.47	80	38522	13
10	75.13	1930.08	85	35360	10
11	79.71	2216.96	70		
12	85.49	2076.47	70		

DISCUSSION

7.1 Introduction

The ultimate aim of the use of ultrasound bone densitometry is to determine those at risk of fracture due to osteoporosis. Fracture risk is related to skeletal strength which is determined by the amount of bone material (relative density/porosity) and the form of the internal structure (architecture). Previous evidence shows that BUA measurements have a structural component as opposed to the purely densitometric measurements obtained with ionizing radiation techniques. If this structural information can be quantified, the quality of fracture risk predictions will be enhanced.

To quantify the structural aspect of BUA, the attenuation mechanisms, thought to be predominately scattering, must be better understood than at present and this requires the use of a physical bone mimic whose structure can be carefully controlled. This study has examined the Stereolithography process as a means of producing structures comparable with those of cancellous bone, based upon histomorphometric analysis of the calcaneous.

7.2 The Stereolithography process

The initial investigation of Stereolithography indicated the suitability of this process for use as a cancellous bone phantom. The rod lattice test pieces demonstrated the ability to produce the complex, high precision 3D structures associated with cancellous bone. The ultrasonic properties of the cured resin, although not exactly the same as natural bone, were acceptably similar. Ultrasonic tests of subsequent models based on the calcaneus showed the combination of SL resin and castor oil gave results very compatible with natural cancellous bone tissue.

The key features of the SL system over other model manufacturing methods are:

- Virtually any 3D structure can be produced, including direct use of histomorphometric data.

- The 3D computer file used to produce the model allows the accurate extraction of all structural data.

- The exact specification of the internal structure and the ability to make small precise alterations allows the independent study of individual structural parameters.

The main limitations with the system are, firstly, the smallest laser spot size, 0.3 mm, which is slightly larger than the trabeculea found in the calcaneus, and secondly, small pore resin drainage difficulties. Since this study is looking at the large scale effects of structure, these limitations are thought to be negligible, and in any case are much less than with the other modelling systems.

Through use of the Stereolithography process, the seven structural models used in this study are probably the first realistic mimics of cancellous bone, created with a precise, predefined internal structure.

7.3 Repeatability

The first five basic models were used in a short term repeatability test and the low variance in the velocity, (intra = 0.75%, inter = 0.69%), shows that the combination of the SL resin and Castor oil is stable and reproducible. The higher than expected variance in BUA, (intra = 6.53%, inter = 8.5%), was attributed to high frequency reverberations found on the attenuation response curve. The reverberations were thought to be occurring within the perspex box and the 2 mm outer jacket of the SL structure. To

reduce this effect as much as possible the structural variation models were measured in a bath of castor oil without being encased in a perspex box.

The ability of SL to form complex structures and exactly replicate them shows the potential to use this system to manufacture calibration and quality assurance phantoms. Practically, a phantom would need to be housed in some form of casing for protection but it is felt that the reverberation effect could be minimised through design optimisation.

Long term repeatability tests must also be carried out. For the modelling application, the use of a castor oil bath was found to be adequate and further investigation was beyond the scope of this work.

7.4 Attenuation mechanisms in cancellous bone.

The current thinking at present is that scattering is the dominant attenuation mechanism with frictional interaction (Biot theory) [38] also a contender. The Biot theory looks at visco elastic effects in porous media and includes structural parameters such as pore size, trabecular spacing, permeability and tortuosity. Williams et al(1996)[39] used this to model the change of BUA with porosity. The results showed a BUA peak at 65% to 70% porosity but the attenuation level was under estimated by a factor of approximately 100. They concluded that some other factor, possibly scattering, was responsible for the majority of the attenuation.

The correct prediction of the BUA peak strengthens the argument that the complexity of the structure is a factor in the BUA/porosity relationship.

The composite material used by Clarke et al(1994)[15] exhibited a parabolic relationship between porosity and BUA with the peak at 50% porosity. It was suggested that

scattering was the main attenuation mechanism and that the position of the BUA peak was determined simply by the number of scatterers. Below 50% porosity the isolated pores cause the scattering, however above 50% porosity the pores will begin to combine leaving the solid frame work as the net scatterer. As the porosity increases the amount of solid, and hence the attenuation, will decrease.

Although we can be certain that the pores will combine, the point at which this combination affects the number of isolated pores is purely intuitive since Clarke *et al* have no precise internal structural data for the models used. The only way to test this would be by destructive histomorphology, unlike the SL method were such data can be readily extracted from the computer model. There is then, no conclusive proof ,one way or the other, that the number of scatterers is responsible for the BUA/porosity relationship.

Further more, as mentioned by Clarke *et al*, cancellous bone is a combination of two continuous, interspersed phases not the single dispersed phase of the composite model, so even if the scatterer number is responsible for BUA in this case, it may not be so for cancellous bone.

Hodgskinson *et al* (1996) [40], in a study of the relationship between BUA and porosity in cancellous bone, suggested that surface area would be a better indicator of BUA. Scattering takes place at the interface between the bone and marrow therefore more surface area means more attenuation. Surface area also takes some account of the complexity of the structure as well as the number of scatterers, as a simple structure will have a lower surface area than a more complex one for the same porosity.

In a comparison between natural tissue, perspex models and the SL models, shown in figure 7:1, Hodgskinson *et al* found the BUA peak for natural tissue was at approximately 75% porosity. This was explained by assuming that the surface area

would continue to increase as the porosity increased due to the greater complexity of the structure, until perforation eventually began to remove complete elements, causing the surface area to decrease. This argument would hold good for Clarke *et al*'s composite model and is in keeping with structural aspect found by Williams *et al*.
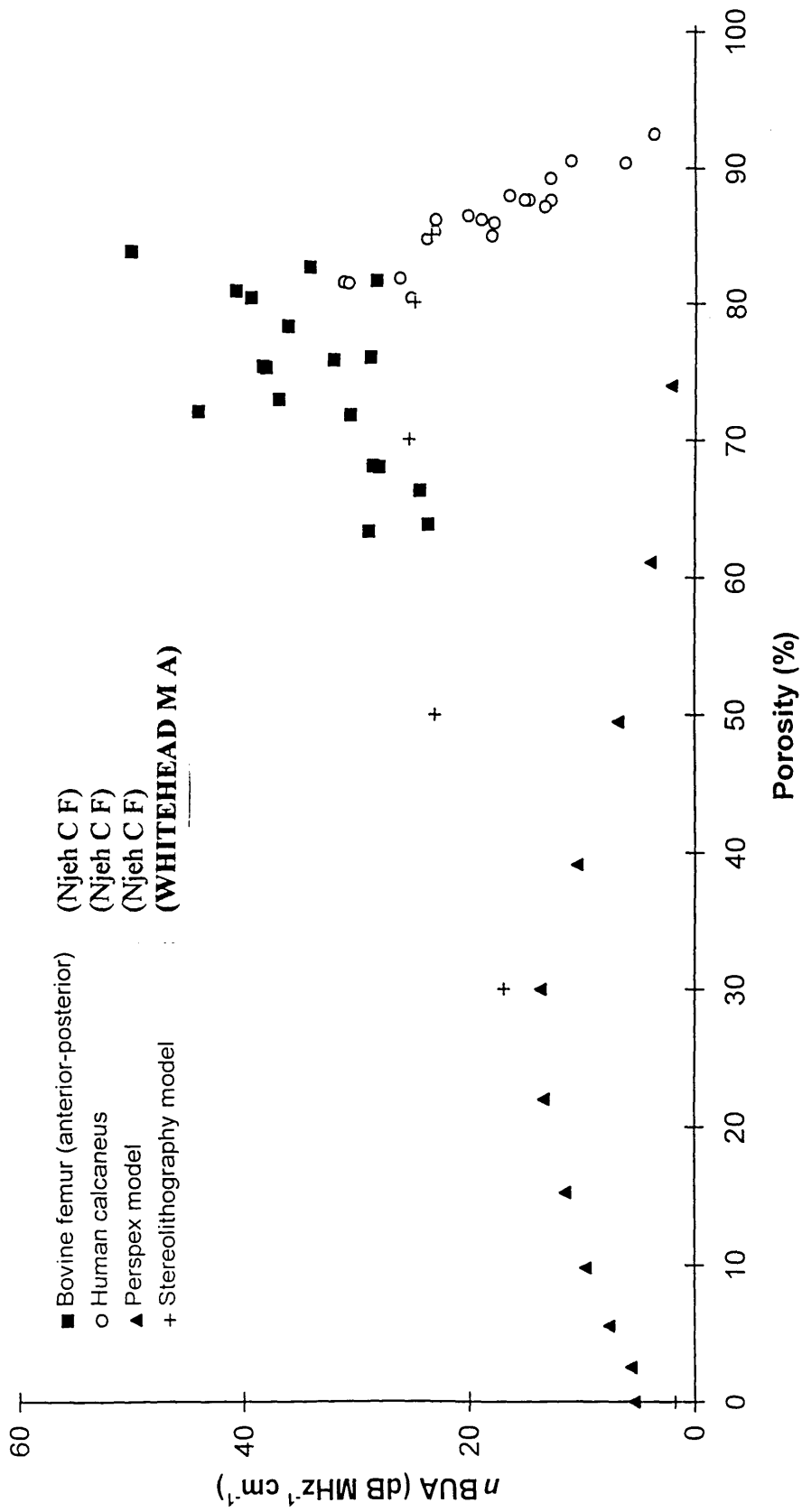
Figure 7:1 Comparison of width normalised BUA (nBUA) for natural tissue, perspex and stereolithographic models (from Hodgskinson et al 1996)[40]

7.5 The Stereolithography structural models.

The structural variation models were used to find the ultrasonic velocity and BUA for varying porosity, maintaining the structure of the basic model. The results, shown in figures 7:2 and 7:3 for Velocity and BUA respectively, are very compatible with human cancellous bone, thus validating the use of the SL process.

The velocity readings (figure 7:2) show a linear relationship with porosity which, allowing for experimental errors, agrees with that proposed by Clarke *et al*, and are within those quoted for natural tissue. (1600 - 2500 ms^{-1},Wells 1977).

The relationship between BUA and porosity (figure 7:3) is non linear with a peak BUA at 70% porosity. This is comparable with natural tissue which has a peak BUA at 75% porosity as shown in figure 7:1.

The other two modelling systems, Njeh's drilled perspex and Clarke *et al*'s epoxy composite, compare less favorably, with BUA peaks at 30% and 50% porosity respectively. This is most probably due to the fact that the SL model is based on the actual structure of the calcaneus, rather than the unnatural, regular forms of the other two models. Also, since the SL model is a 2D extrusion rather than a full 3D reconstruction of cancellous bone, some difference in BUA response is to be expected, and this may account for the 5% shift in porosity for peak BUA.

If, as Clarke *et al* suggested, BUA is directly related to the number of scatters, it would be fair to expect a good correlation between the two. In both cancellous bone and the SL models, the scattering occurs at the bone/ marrow interface and so the number of trabecular plates represents the number of scatters. The mean number of plates in each SL model was calculated using 30 evenly spaced linear intercepts along the ultrasonic measurement axis and the results are shown in figure 7:4

Figure 7:2 The relationship between velocity and porosity for the SL models
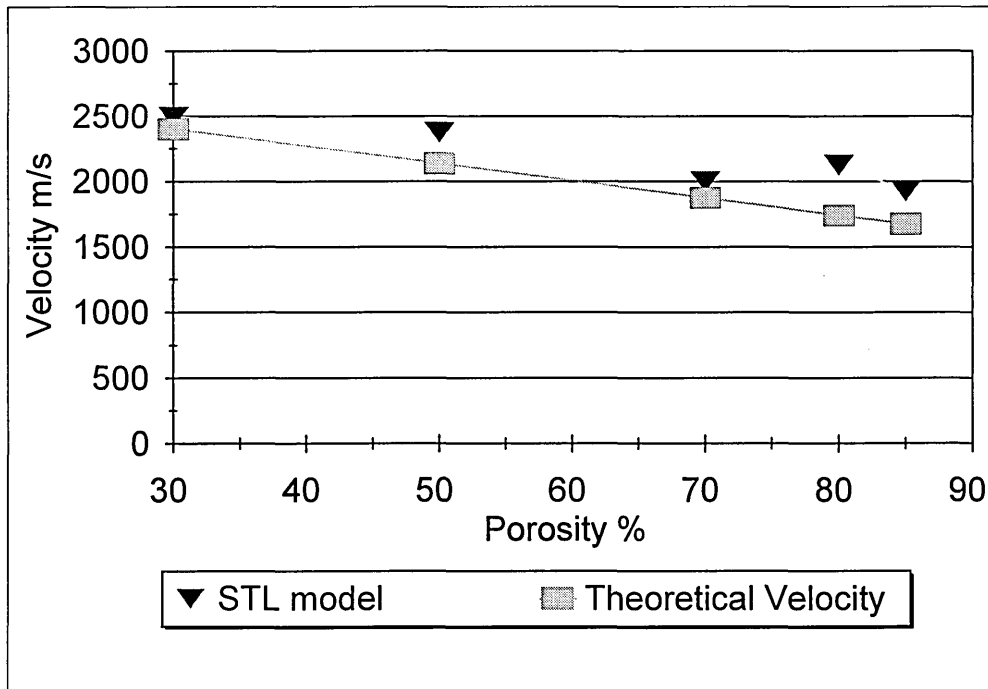
Figure 7:3 The relationship between BUA and Porosity for the SL models
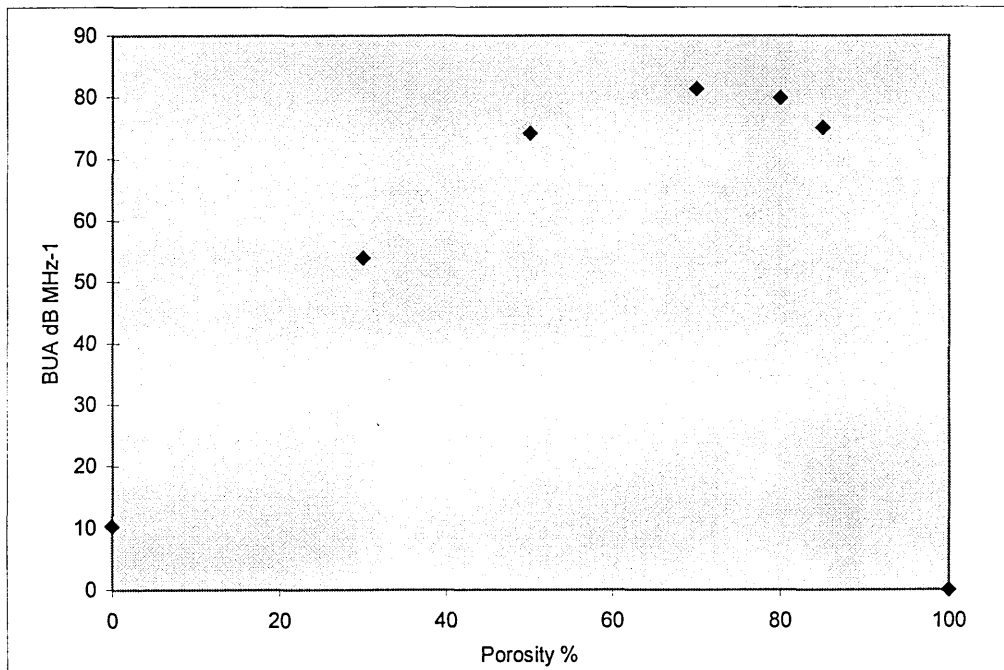
Figure 7:4 The relationship between trabecular plate number and porosity
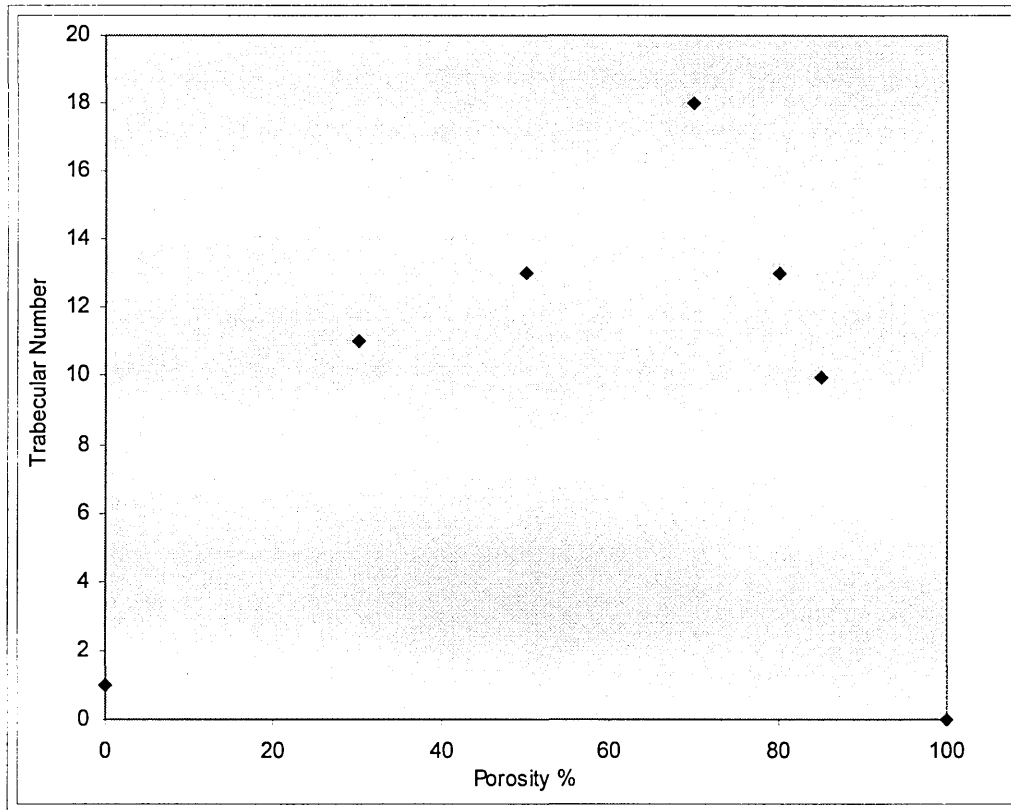
Figure 7:5 The relationship between trabecular surface area and porosity
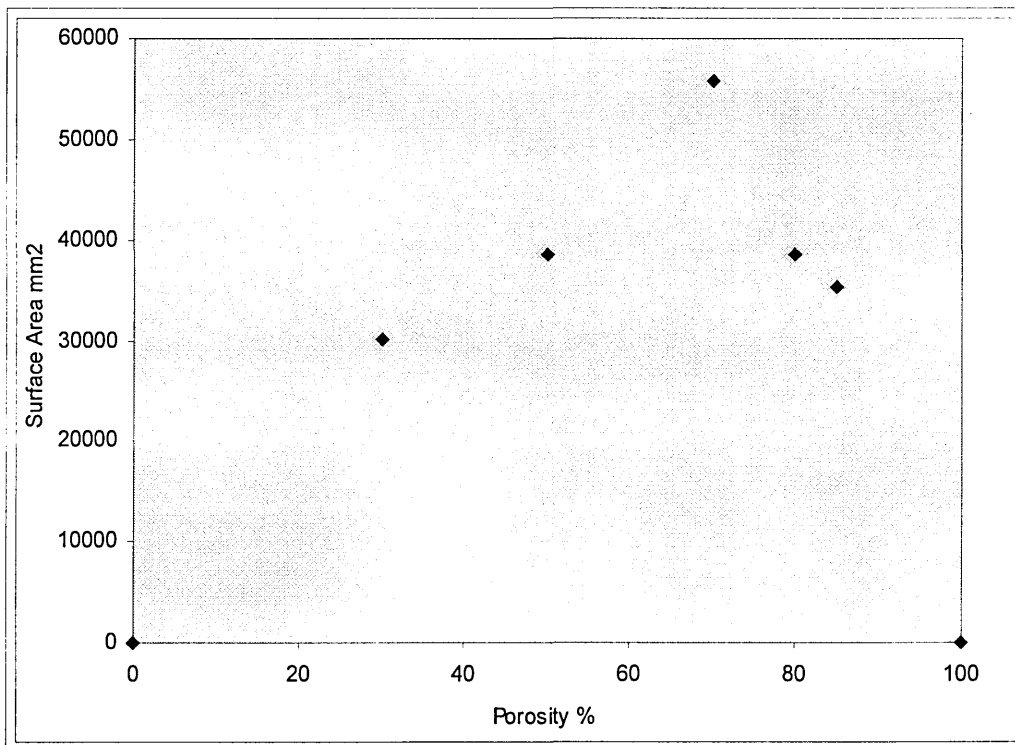
The correlation coefficient between BUA and the number of trabecular plates was $r^2 = 0.89$ which is significant and tends to confirm that scattering is the main attenuation mechanism. However, 11% of the attenuation is still unaccounted for and trabecular number alone cannot explain the results obtained by Williams *et al*.

To introduce a structural aspect, as proposed by Hodgskinson *et al*, the relationship between trabecular surface area and BUA was investigated. Surface area gave a higher correlation, $r^2 = 0.92$, with BUA than the number of plates, as shown in figure 7:6.

Figure 7:6 The relationship between trabecular surface area and BUA
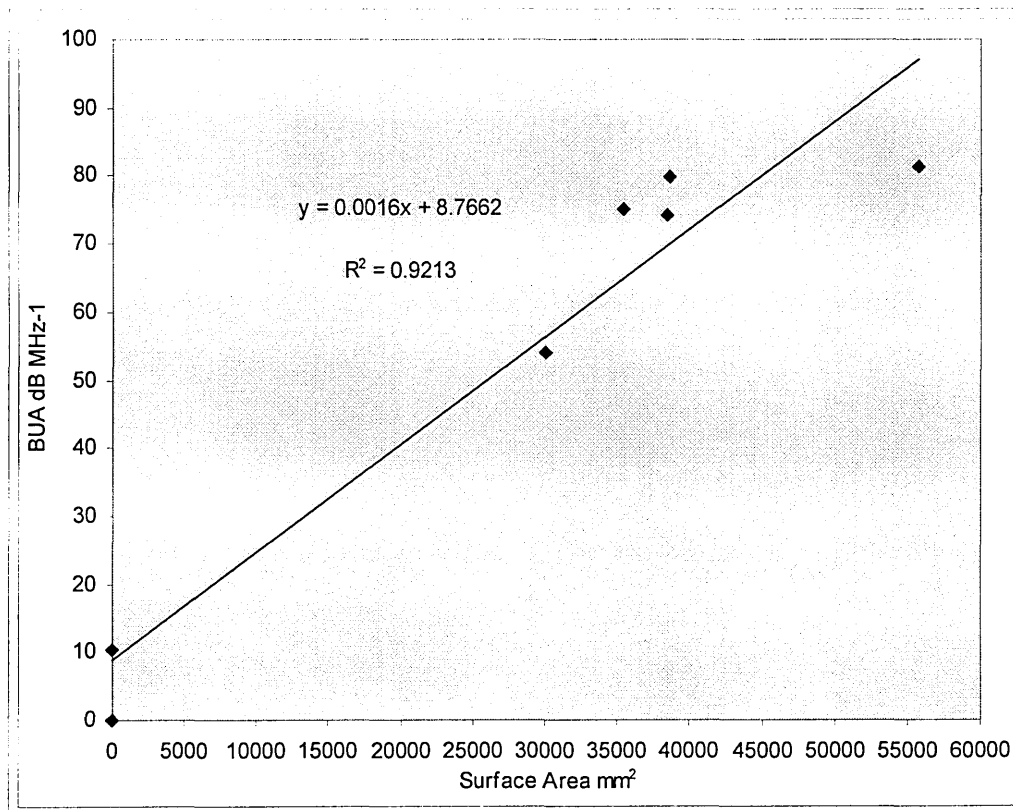
The better correlation of surface area with BUA lends support to the idea that the scattering mechanism is dependent not only on the number of scatterers but the

106

complexity of the structure as well. This could explain the findings of both Clark *et al* and Williams *et al*. Further more, since surface area is an architectural parameter it will take into account the nature of the structure, i.e. continuous indispersed, or single dispersed phase.

The actual surface area measurements, shown in figure 7:5, were measured on a computer from the digital data used to produce the SL models. This demonstrates a key advantage of using the SL process to model cancellous bone as previously impractical complex structural measurements can be very accurately extracted from the computer model.

Another feature, the ability to make controlled alterations, was demonstrated by producing 3 models with the same porosity but different structures, the basic 70% porosity model(6) and two variations (11 and 12)

The basic design had been perforated to produce the 80% and 85% models, these two models were then further altered by dilation to a specified 70% porosity, to give a total of three different models with the same porosity. The BUA results confirmed the structural dependence showing a range of 6 dBMHz^{-1} which is equal to 7% of the basic model. (Of the 3 BUA readings the worst case %CV was 3.5% showing the inter model variation to be significant). The small number of samples precluded further conclusions being drawn.

These results confirm the structural dependence of BUA in cancellous bone and that the attenuation mechanism is governed by the complexity of the structure rather than simply the number of scatterers. For the SL models, 92% of the BUA can be accounted for by trabecular surface area, the remaining attenuation may be attributable to a different

structural parameter or some other separate attenuation mechanism, such as absorption, diffraction or phase cancellation.

It must be noted that the 2D extrusions used in this study are not exactly representative of the continuous 3D form of trabecular bone and that the structures produced by dilation would not be found in a real calcaneal sample.

Essentially the models used in this study are a family based on the low density calcaneal core sample. Within that family 92% of BUA can be explained by trabecular surface area, and it may well be that a similar family based on a different structure will show the same correlation. What is not known is whether the high intra family correlation would hold good for inter family samples.

Since this study is concerned with the use of ultrasound in the measurement of osteoporosis this is a very important question as real patients are from different families and each will have a unique trabecular bone structure.

The correlation between BUA and trabecular number for the SL models was found to be 0.89, however Hans et al[31] (1995) analysed 17 human samples and found a correlation of only 0.65 between the same two parameters. This shows that there is a correlation between the two, but the difference between the correlation of the SL model and human bone samples is significant. It is more than likely that a difference would be seen in the correlation of other parameters including trabecular surface area.

In light of this the author feels that it would be fair to say that trabecular surface area is a significant indicator of BUA in cancellous bone but to draw any deeper conclusions based on the SL models would be unsafe.

CHAPTER EIGHT

CONCLUSIONS AND FURTHER WORK

8.1 Conclusions

The conclusions of this study are as follows:

- **The suitability of the Stereolithography system**
  The Stereolithography process has been shown to be capable of producing complex 3D structures similar to human cancellous bone and the ultrasonic properties of the cured resins are within acceptable limits.

- **The modified histomorphological procedure**
  The modified histomorphological method proved successful in providing the detailed human calcaneal structural data required to produce a basic design for the SL model.

- **Stability and repeatability of the basic SL model design**
  The combination of the basic SL model design and castor oil as a marrow mimic is stable and repeatable. The ultrasonic properties, velocity and BUA, of the basic model are comparable with human cancellous bone.

- **The ultrasonic characteristics of the variable porosity models**
  The ultrasonic characteristics of the variable porosity models were extremely similar to those of natural tissue, showing the validity of using the SL process as a modelling medium.
  The relationship between velocity and porosity was found to be linear and, within experimental limits, followed the model proposed by Clarke *et al*.
  BUA showed a non linear relationship with porosity with minima at 0 and 100% porosity and a maxima at 70% porosity.
  The structural dependence of BUA was confirmed.

- **The prediction of BUA from structural parameters**
  The main attenuation mechanism in cancellous bone is assumed to be scattering and is governed by architectural complexity as well as porosity.
  For the models used in this study, trabecular surface area was found to be the best indicator of BUA with a correlation coefficient $r^2 = 0.92$.

For the SL models   **BUA = 0.0016 Trabecular Surface area x 8.76**
$$(r^2 = 0.9213)$$

8.2 Further work

This study has shown the ability of the SL process to model cancellous bone like structures over the extreme range of porosity and this opens the door for deeper analysis to be carried out.

The next stage is to produce more complex 3D structures, based on the actual structure of calcaneal cancellous bone, to give a better understanding of the interaction with ultrasound. The data for such models may be obtained by histomorphological methods or preferably, by use of high definition medical imaging systems such as Magnetic Resonance Imaging (MRI). This would allow the direct use of digital, *in vivo*, architectural data as a basis for a 3D model design. Defined changes to structure and porosity can then be produced and used to form a theoretical model.

The limiting factor of the SL system at the moment is that the minimum wall size is larger than the smaller trabeculea and this precludes full reconstruction of cancellous bone structures. Theoretically the laser spot size could be reduced by tighter focusing and this would be worth investigating. Narrowing the focus of the beam reduces the working envelope but this should still be large enough to produce calcaneal sized models.

Alternatively, the field of Rapid Prototyping is evolving and new systems are being developed. One such system, the MM-Pro[41], uses thermoplastics and claims to give a free standing wall thickness of 0.1mm and this or similar systems should be investigated for ultrasonic modelling suitability.

Development of the full 3D reconstruction of cancellous structures would allow precise modelling of actual cancellous samples, *in vivo*, and lead to a much deeper understanding of the ultrasonic attenuation mechanism in the calcaneus.

LIST OF REFERENCES

1   The National Osteoporosis Society. The new approach to osteoporosis, a guide for general practitioners: NOS 1990

2   Tothill P (1989) Methods of bone mineral measurement. *Phys. Med. Biol. 34, 543-72*

3   Concensus Development Conference. (1994) *The American Journal of Medicine 94 ,646*

4   Genant HK and Cann CE (1981) Reply on spinal mineral loss after menopause *JAMA vol 246 (20) ,2322-2323*

5   Langton C M, Palmer S B and Porter R W (1984) The measurement of broadband ultrasonic attenuation in cancellous bone. *Eng. Med. 13, 89-91*

6   Baran D T, Kelly A M, Karellas A, Gionet M, Price M, Leahey D, Steuterman S, McSherry B and Roche J (1988) Ultrasound attenuation of the os calsis in women with osteoporosis and hip fractures. *Calcif. Tissue Int 43(3), 138 142*

7   Massie A, Reid D.M and Porter R.W (1993) Screening for osteoporosis:comparision between dual energy x-ray and broadband ultrasound attenuation in 100 perimenopausal women. *Osteo. Int 3, 107 - 110*

8   Baran D T,McCarthy C K, Leahey D and Lew R (1991) Broadband ultrasound attenuation of the calcaneus predicts lumbar and femoral neck density in caucasian women: A preliminary study. *Osteo. Int 1, 110 - 113*

9   Gluer C C, Vahlensieck M, Faulkner K G, Engelke K, Black D and Geneant H K. (1992) Site-matched calcaneal measurement of broadband ultrasound attenuation and single X-ray absorptionmetry: Do they measure different skeletal properties? *J. Bone and Mineral Research 7(9), 1071-1079*

10   Waud C E, Lew R and Baran D T.(1992) The relationship between ultrasound and densitometric measurements of bone mass at the calcaneus in women. *Calcif. Tissue Int 51, 415-418*

11   Langton C M, Evans G P, Hodgskinson R and Riggs C M.(1990) Ultrasonic, elastic and structural properties of cancellous bone. Current research in Osteoporosis and bone mineral measurements. *Bath conference, 10-11.*

12   Gluer C C, Wu C Y and Genant H K.(1993) Broadband ultrasound attenuation signals depend on trabecular orientation: An In Vitro study. *Osteo. Int 3,185-191*

27   **Rapid News Europe 1996.** *Service and equipment suppliers guide. Vol 4 (1),39-73. Published by Rapid News Publications, Trafford Press Ltd, Manchester*

28   **Singh I, (1978).** The architecture of cancellous bone. *J. Anat. 127(2) 305-310*

29   **Gibson L J and Ashby M F(1988)** Cancellous Bone. Cellular Solids, structure and properties. *Pergoman Press 316-330*

30   **Lozupone Enrico (1985).** The structure of the trabeculea of cancellous bone, *Anat. Anz. Jena,159,211-229*

31   **Hans D, Arlot M E, Schott AM, Roux J P, Kotzki P O and Meunier P J.(1995)** Do Ultrasound measurements on the Os Calsis reflect more the bone microarchitecture than the bone mass?: A two dimensional histomorphometrical study. *Bone Vol 16(3), 295-300*

32   **Amling M, Herden S, Posl M, Hahn M, Ritzel H and Delling G (1996)** Hetrogeneity of the skeleton: Comparison of the micro architecture of the spine , the iliac crest, the femur and the calcaneus. *Journal of Bone and Mineral Research 11(1),36-45*

33   **Eriksen E F, Axelrod D W and Flemming M (1994)** Bone histomorphology: An official publication of the American Society for bone mineral research.*Raven Press New York*

34   **Odgaard A, Andersen K, Flemming M and Jorgen G. Gundersen H(1990)** A direct method for fast three dimensional serial reconstruction. *Journal of Microscopy 159(3), 335-342*

35   **Nordin B E C. (editor) 1996** Calcium, Phospate and Magnesium Metabolism. *Chapter 14 section 2, Histological methods, 564-567. Published by Churchill Livingstone, Edinburgh London and New York*

36   **S Levialdi 1984** Digital image analysis Chapter 15:Morphological image processing. *Pitman 1984 pp449-490*

37   **Langton C M, Ali A V, Riggs C M, Evans G P and Bonfield W (1990)** A contact method for the assesment of ultrasonic velocity and broadband attenuation in cortical and cancellous bone. *Clin. Physiol. Meas., 11(3), 243-249*

38   **Biot M A.(1956)** Theory of propagation of elastic waves in a fluid saturated porous solid-I and II. *J. Acoustic Soc. Am. 28, 168-91*

39   **Williams J L, Grimm M J, Wehrli FW, Foster K R and Chung H-W (1996)** Prediction of frequency and pore size dependant attenuation of ultrasound in trabecular bone using Biot's theory. *Mechanics of Poroelasticity ed A P S Selvadurai (Dordrecht: Kluwer Academic) pp 263-271*

113

13   Gluer C C, Wu C Y, Jergas M, Goldstein S A and Genant H K. (1994)
Three quantitative ultrasound parameters reflect bone structure. *Calcif. Tissue
Int 55, 46-52*

14   Njeh C F 1995 The dependence of ultrasound velocity and attenuation on the
material properties of cancellous bone. *PhD Thesis: Sheffield Hallam University.*

15   Clarke A J, Evans A J, Truscott J G, Milner R and Smith M A 1994 A
phantom for quantitative ultrasound of trabecular bone *Phys. Med. Biol. 39 (16)
77-87*

16   Hull C. 1986 Apparatus for the production of three dimensional objects by
stereolithography. *U.S. Patent 4575330, March 11*

17   HIGH SPEED MODELLING SHFTS UP A GEAR 1991. Article in
Engineering Computers May 1991

18   Hull C.(1988) Stereolithography: Plastic parts from CAD Data without tooling.
Modern Casting 78(8), 38

19   Amick S D (1991) Stereolithography reduces the time from design to
manufacture. *Proc. Inter. Conf. Computer intergrated Manufacturing ICCIM'91
202-205*

20   Waymire P B.(1991) 3 Dimensional reconstruction of Human body parts with
stereolithography from computerized axial tomography and/or nuclear magnetic
resonance imaging. *Proc. 49th ann. tech. conf. antec '91 37,2597-2598*

21   Selective Layer Sintering Agent AMSYS, Sunderland, UK

22   Laminated Object Manufacturing systems. Agent UMAK, Birmingham, UK

23   Woo-Jong Lee. Yong Ham Lee and Yoo Suk Hong (1992) Geometric
conversion procedure for rapid prototyping system. *Jour.of.Des.and.Manu 2(2),
83-92*

24   Gargiulo E. P. and Belfiore D. A. (1991) Photopolymer solid imaging process
accuracy. *Proceedings of the winter annual meeting of the American Society of
Mechanical Engineers, Intellegent Design and Manufacturing for Prototyping.
1991 PED-Vol 50, 81-95*

25   Ehrmann J S. (1991) Optics for Vector Scanning. *Beam deflection and
Scanning Technologies SPIE Vol 1454,245-255*

26   Miller J.F. (1994) CAD Requirements for Rapid Prototyping. *Tutorial notes
from Rapid Prototyping and Manufacturing 94,EDS Unigraphics, Woking UK.*

40   **Hodgskinson R, Njeh, Whitehead M A and Langton C M (1996)** The non linear relationship between BUA and porosity in cancellous bone. *Phys. Med. Biol. 41(1996), 2411-2420*

41   **MM-Pro system.** Sanders Prototype, Inc., P. O. Box 540, Wilton, NH 03086. USA. Phone: 603-654-5100 FAX: 603-654-2616.

APPENDICES

Appendix   A   Conference contributions

Appendix   B   Papers submitted for publication

Appendix   C   Published papers.

APPENDICES

Appendix   A   Conference contributions

Appendix   B   Papers submitted for publication

Appendix   C   Published papers.

APPENDIX A

1   Boutinaud RX, Holden G J, Whitehead M A and Langton CM. (1993)

     Comparison of Biot and Scattering Theory for the Propogation of Ultrasound

     through Porous Media.

     Annual Review of Progress in Physical Acoustics and Ultrasonics.

     Sheffield 1993.

2   Whitehead M A, Hodgskinson R and Langton C M. (1994)

     Development of a Cancellous Bone Phantom for Ultrasonic Characterisation

     and Quality Assurance.

     Measurement of the Acoustic properties of Biological Tissues.

     London 1994.

3   Holden G J, Boutinaud R X, Whitehead M A, Langton C M and Njeh C F.

     (1994)

     Ultrasonic Prediction of Structure and Material Properties of Cancellous Bone.

     Biological Tissue. Institute of Physics.

     London 1994

4   Langton C M, Whitehead M A, Hodgskinson R and Holden C J. (1994)

     Development of a Cancellous Bone Phantom for Ultrasonic Characterisation and

     Quality control.

     Ultrasonic Assesment of Bone.

     AEA Bath 1994.

APPENDIX B

The following is being prepared for publication:

Langton CM, Whitehead M A, Bennett D K and Langley G. (1997)

Development of a Cancellous Bone Structural model by Stereolithography for

the Ultrasonic Characterisation of the Calcaneus.

The non-linear relationship between BUA and porosity in cancellous bone

R Hodgskinson†, C F Njeh‡, M A Whitehead§ and C M Langton†

† Centre for Metabolic Bone Disease, Hull HU3 2RW, UK
‡ Bone Densitometry Services, Queen Elizabeth Medical Centre, Birmingham B15 2TH, UK
§ Health Research Institute, Sheffield Hallam University, Sheffield, UK

Abstract. There is growing interest in assessing the clinical value of ultrasound in the prediction and management of osteoporosis. However, the mechanism of ultrasound propagation in cancellous bone is not well understood. The Biot theory is one approach to modelling the interaction of sound waves with cancellous structure, and porosity is one of its input parameters. In this paper we report the relationship between broadband ultrasonic attenuation (BUA) corrected for specimen thickness (nBUA) and porosity in a porous Perspex cancellous bone mimic, a stereolithography cancellous bone mimic and in natural human and bovine tissue. nBUA and porosity have a non-linear parabolic relationship. The maximum nBUA value (nBUA$_{max}$) occurs at approximately 30% porosity in the Perspex mimic, approximately 70% in the stereolithography mimic and approximately 75% in natural cancellous bone. We discuss the effect of structure on the form of the nBUA–porosity relationship.

1. Introduction

Non-invasive assessment of osteoporosis relies principally on the use of bone mass measurements, which may be measured accurately and precisely by ionizing radiation techniques such as dual-energy x-ray absorptiometry (DEXA) and quantitative computerized tomography (QCT) (Tothill 1989). Although bone mass shows a strong correlation with compressive strength, as much as 25–30% of the observed variance in strength is due to other factors such as bone micro-structure, architecture and state of remodelling (Kleerekoper *et al* 1985, Mosekilde 1989). Ultrasound is currently being assessed as an alternative method of evaluating skeletal status, following reports that it provides information about structure in addition to density (Langton *et al* 1990a, Tavakoli and Evans 1992, Gluer *et al* 1993). This sensitivity to structure has the potential of increasing the reliability of predicting those at risk of fracture. The ultrasound parameters used to characterize cancellous bone are broadband ultrasound attenuation (BUA) and ultrasound velocity (V).

Previous research has focused on clinical measurements of ultrasound velocity and BUA, and their comparison with bone mineral density (BMD) assessed by a variety of absorptiometry techniques. Correlations between BUA and DEXA vary, in general, between 0.46 and 0.89 (Hans *et al* 1993). This range encompasses both intra- and inter-site comparisons with little indication that the degree of correlation differs between the two. Variation in correlation coefficient has been attributed to various factors, including precision variability, differences in the populations studied and differences in the densitometry equipment used.

The mode of interaction of ultrasound with cancellous bone is still not fully understood. BUA in porous media, such as cancellous bone, is thought to be due to both absorption and scattering. Various theories have been developed to explain the attenuation process in cancellous bone; these include 'single scattering', 'multiple scattering' and 'Biot theory' models. Single scattering theory calculates the attenuation caused by a single obstacle, it is then assumed that the total attenuation is this value multiplied by the number of obstacles. Multiple scattering is a modification of single scattering, taking into account the interaction of the scatterers. Both theories are only valid for very low concentrations of isolated scatterers and therefore not applicable to the study of cancellous bone. The Biot theory (Biot 1956, 1962) analyses the relative motion of the porous structure (trabeculae framework) and the interspaced fluid (marrow) induced by the ultrasonic wave. This approach considers the energy loss due to the frictional interaction of the marrow flowing within the trabecular framework, and the inelasticity of the trabecular framework. Porosity is an important parameter in the Biot theory. As part of an investigation of the relevance of the Biot theory in understanding ultrasonic attenuation, we report here on the relationship between attenuation (nBUA) and porosity in cancellous bone samples and two physical mimics of the natural tissue.

2. Methods

The aims of this work were to:

- develop a cancellous bone mimic (phantom) which could be used to study the behaviour of ultrasound through a porous material;
- investigate the effect of porosity on BUA;
- to make preliminary observations on the effect of structure on the BUA parameter.

2.1. Development of cancellous bone phantoms

In the clinical environment there is a distinction between *test objects* and *phantoms*. A test object is designed to evaluate equipment performance while a phantom is designed to mimic the material properties of a natural tissue, with particular reference to the parameter to be measured. Hence, bone phantoms will be different depending on the parameter of interest, and whether ultrasound, x-rays or magnetic resonance is the measuring technique. The requirements of cancellous bone phantoms for ultrasound are:

- material and ultrasonic properties must approach those of cancellous bone;
- air bubbles must be absent, because they are highly attenuating to ultrasound and will create anomalous results;
- they should be durable and stable and allow controlled variation in their properties.

Cancellous bone is both heterogeneous and anisotropic, making it difficult to model. Two types of phantom were investigated; a milled porous Perspex block and a more complex mimic, created by laser polymerization of a photosensitive resin (stereolithography) and based on histomorphometric data from the human calcaneus.

2.1.1. Perspex block models

Our previous ultrasonic measurements of Perspex have demonstrated it to be a good cortical bone mimic. A cancellous bone phantom was manufactured by introducing a symmetrical array of holes into a Perspex block, initially having zero porosity. Thirty-six (6 × 6) vertical holes were drilled in a 41 mm cube of

Perspex. The number of holes was kept constant and the porosity increased by enlarging the hole diameter from 1 mm (2.5% porosity) to 5.5 mm (74% porosity) in steps of 0.5 mm (figure 1).
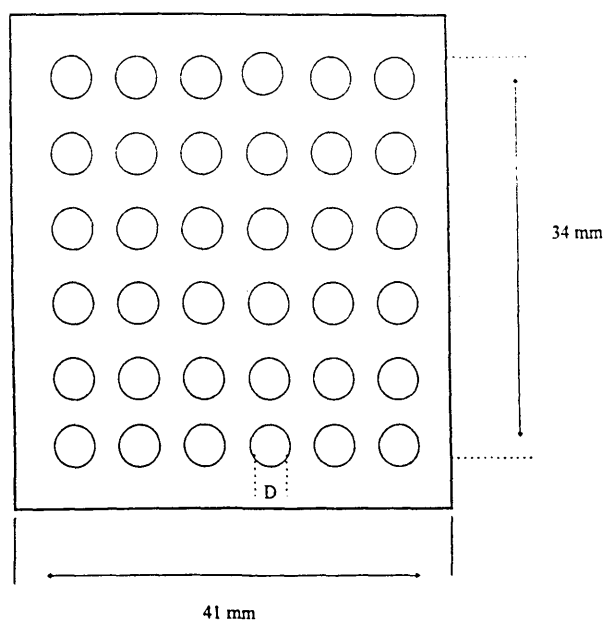

Figure 1. A diagrammatic representation of the Perspex models employed in this study. Porosity was varied by changing the hole diameter (*D*).

2.1.2. Stereolithography models The process of stereolithography (SL) modelling utilizes a photosensitive resin (in this study Ciba Geigy: XB 5154) polymerized using a scanning laser, the movement of which is controlled by a series of computer-generated 'slice-files'. The liquid resin is contained within a vat possessing a variable-height tray. In the first instance the tray is positioned towards the top of the liquid volume so that a resin layer of approximately 0.1 mm lines the tray. The laser polymerizes the resin according to structural information in the first 'slice-file'. The tray is then lowered by 0.1 mm and fresh liquid resin flows over the cured resin. Polymerization is repeated using the next 'slice-file'. Successive polymer layers fuse to each other, the process being repeated until the required three-dimensional structure is formed.

It is possible to create many complex three-dimensional geometric shapes using the SL system. For the purpose of this study we wished to create a structure similar, in its structural complexity, to cancellous bone. We employed a modified image of human calcaneal cancellous bone (figure 2) to do this. The trabecular elements of a skeletonized image were dilated so that all trabeculae were of 0.3 mm thickness, producing a structure of 70% porosity. This is referred to hereafter as the *basic SL model*.

0.3 mm was the lateral resolution of the SL system used, governed by the laser spot size. In our experience, the majority of trabeculae in the human calcaneus have a thickness below 0.2 mm. However, we were not attempting to create an exact replica of the cancellous bone, only an approximation of the overall structural complexity.

To create a series of mimics with a range of porosity values, the trabecular elements of the basic SL model were further dilated or perforated. Perforation involved the removal
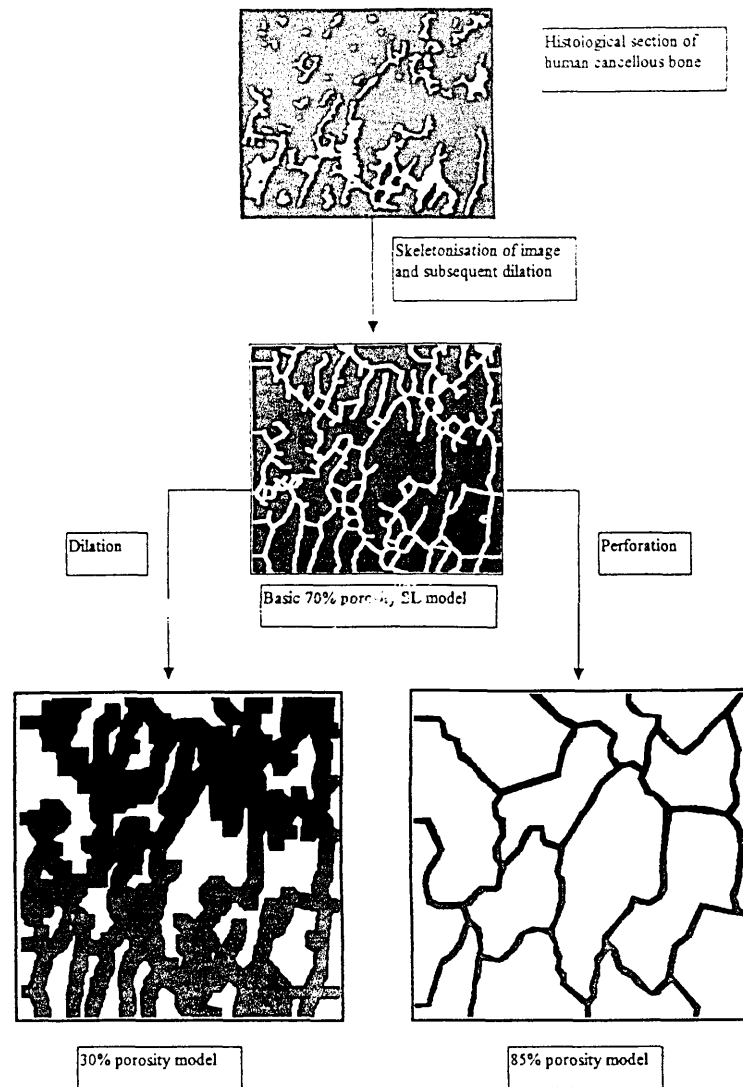
Figure 2. Flow diagram summarizing the construction of the stereolithography models. The figure includes the 70%, 30% and 85% models. Intermediate 50% and 80% models were also created.

of whole trabecular elements from the basic model. Using these two methods we produced five samples of 30%, 50%, 70%, 80% and 85% porosity.

2.2. Preparation of cancellous bone samples

Proximal bovine femora and human calcanei were investigated. The bovine samples were obtained fresh from a local butcher. After removal of soft tissue, 20 mm cubes were excised from the trochanter, neck and head of each femur, using an EXAKT cutting grinding system, under constant irrigation. Final smoothing was done on fine (1000 grit) carborundum paper with the specimens immersed in water.

The human samples were obtained from 20 cadavers (10 male and 10 female) with an age range of 59 to 90 years. No pathology information was available. Following removal of

external soft tissue, a coring drill of 21 mm internal diameter was used to remove samples in the medio-lateral direction. The region of bone removed was the same as that through which ultrasound would pass in the clinical measurement. The cortical end plates were removed using the EXAKT system, producing cylinders of cancellous bone with parallel end faces. At this stage the specimens still contained the bone marrow (un-defatted).

2.3. Apparent density measurements for natural tissue

Apparent density is defined as the ratio of defatted, dehydrated tissue mass to total specimen volume. To obtain the defatted tissue mass, the soft tissue and marrow were removed from the specimens. This involved subjecting each specimen to a high-pressure water jet and compressed air. This process was repeated until no fat was visible in the marrow spaces. The specimens were then tumbled overnight in an excess of 2:1 chloroform–methanol mixture (Brear *et al* 1988) to remove any residual fat and then dried at 60–70 °C to constant weight. The specimen external dimensions were measured using a micrometer and the volume calculated. The dry weight divided by the volume gave the apparent density (kg m^{-3}).

We have converted apparent density to porosity for the purposes of this study. This was done by dividing each apparent density by the density of cortical bone, which we assumed to be 1900 kg m^{-3}. This bone fraction was converted to pore fraction by subtraction from unity and finally expressed as a percentage porosity.

2.4. BUA measurements

Ultrasound measurements were carried out using the contact ultrasonic bone analyser (CUBA) system (Langton *et al* 1990b), consisting of an IBM-compatible PC with dedicated menu-driven software, interfaced to a spike generator (transmitter) and digital receiver. Two 1 MHz (nominal frequency) broadband ultrasonic transducers, one acting as a transmitter and the other as a receiver, were mounted on a hand-held sliding calliper incorporating a digital vernier gauge to measure specimen thickness. Two pairs of transducers, of 19 mm and 13 mm diameter respectively, were used during the investigation. The 19 mm diameter transducers were used for investigation of the phantoms while the 13 mm diameter transducers were used for the cancellous bone specimens, commensurate with their smaller lateral dimensions. All measurements were performed with the samples immersed in degassed water.

To determine BUA, the amplitude–frequency spectrum for a selected portion of the received time domain signal was calculated using a fast Fourier transform (FFT) algorithm. The amplitude–frequency spectrum of the signal through a reference material (degassed water without the specimen) was first recorded and stored as the reference trace. The measurement sample was then placed in the water and a second amplitude spectrum recorded.

This method corrects for the frequency dependence of both transducer efficiency and beam profile for a particular pair of ultrasound transducers (Langton *et al* 1984). In the frequency range of 0.2 MHz to 0.6 MHz, the attenuation is linearly proportional to frequency. Linear regression of ultrasound attenuation against frequency between 0.2 MHz and 0.6 MHz is preferred and the slope computed to give the BUA index with units of dB MHz^{-1}. To obtain a true volumetric parameter, BUA is divided by the specimen thickness to give nBUA (dB MHz^{-1} cm^{-1}).

Inclusion of air substantially increases the ultrasound attenuation since the air interface effectively acts as a total reflector. The samples were therefore thoroughly degassed under

water at a pressure of 1 bar. Each specimen was deemed to have been fully degassed when no air bubbles were visible on the sample surface. In practice. degassing overnight was always sufficient to achieve this. Caution was exercised in transferring the specimens to the measurement bath so as not to introduce air. A wetting agent (Tepol) was added to the water during degassing to enhance air removal (Njeh 1995).

The cancellous bone mimics were ultrasonically tested in one direction only. The human calcaneal specimens were also tested in one direction. corresponding to the medio-lateral direction in the heel. The cubic bovine femoral samples were tested in the three orthogonal directions.

3. Results

Table 1 summarizes the densities and the ultrasonic characteristics of the materials employed in, or relevant to, this study.

Table 1. The densities and the ultrasonic characteristics of the materials related to this study.

| Material	Density $(kg\ m^{-3})$	BUA $(dB\ MHz^{-1}\ cm^{-1})$	Velocity $(m\ s^{-1})$
Cortical bone[a]	1800–2000	3.50	3000–4000
Perspex	1180	5.34	2657
Stereolithography resin	1120	2.50	2800
Fat	952	0.50	1580
Water	1000	0.00	1540

[a] Note that although the properties quoted here are for the materials at zero porosity, cortical bone is generally defined as having a porosity < 30%. Velocity was not measured in this study. Values are drawn from the literature and from other studies we have performed.

Figure 3 shows the relationship between nBUA and porosity for the cancellous tissues. In each case the human calcaneal samples, tested in the medio-lateral direction, are plotted with bovine femoral samples tested in the (a) proximal-distal direction, (b) medio-lateral direction and (c) antero-posterior direction. Generally, the calcaneal samples have high porosity in the range 80–95%, the femoral samples have relatively lower porosities, 60–85%. The calcaneal samples show a significant negative relationship between nBUA and porosity (table 2) whereas the relationships for the femoral bone are significantly positive (table 2).

Table 2. The relationship between nBUA and porosity for bovine and human samples. ($\log BUA = a + b \log porosity$.)

| Sample	Intercept a	Coefficient b	R^2 (%)
Bovine femur PD	−3.41	+2.68	41.4
Bovine femur ML	−3.27	+2.61	61.8
Bovine femur AP	−1.33	+1.53	39.5
Human calcaneus	+24.9	−12.2	86.8

The region of overlap between the two types of cancellous bone (80–85% porosity), contains only five of the 18 bovine femoral samples and four of the 20 human calcaneal samples. In this region the calcaneal samples attain a peak nBUA (nBUA$_{max}$) value of
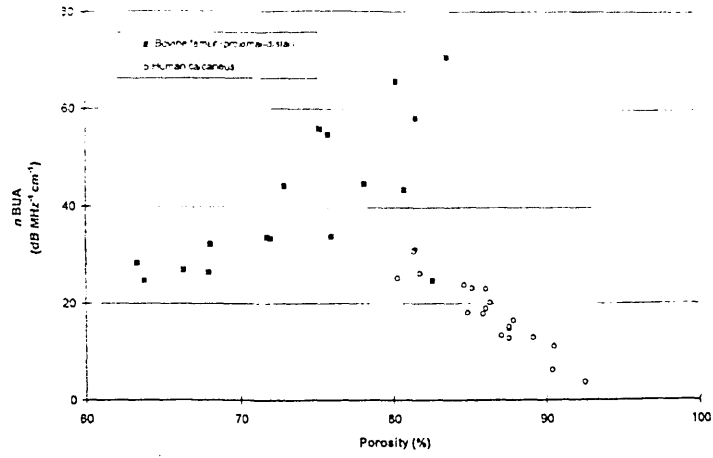
(*a*)
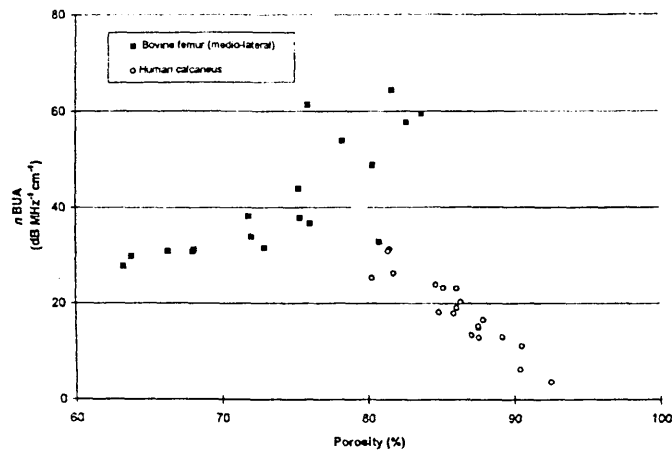
(*b*)
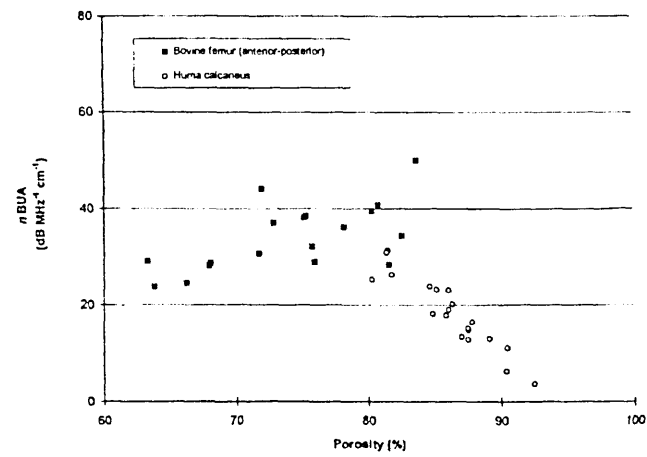
(*c*)

Figure 3. The relationship between nBUA and porosity for the human and (a) bovine specimens tested in the proximal-distal direction (PD); (b) bovine specimens tested in the medio-lateral direction (ML) and (c) bovine specimens tested in the antero-posterior (AP) direction.

approximately 30 dB MHz^{-1} cm^{-1}. For the femoral samples in the same porosity range, the nBUA$_{max}$ value varies depending on the direction in which the cubes were tested. In the proximal-distal direction it is $\approx$70 dB MHz^{-1} cm^{-1}, medio-lateral $\approx$65 dB MHz^{-1} cm^{-1} and antero-posterior $\approx$40 dB MHz^{-1} cm^{-1}. These observations are reflected in the regression analysis of the relationships between nBUA and porosity for each separate femoral direction, excluding the calcaneal data. The slopes of the regression lines are given in table 2. The highest gradient is for the proximal-distal direction and the least is for the antero-posterior direction. The relationships for bovine femoral bone show a statistically significant positive trend.

Figure 4 shows the relationship between nBUA and porosity for the porous Perspex mimic and the stereolithography mimic. Included on this graph are the human and bovine AP data. All the curves show similar non-linear characteristics with minima (nBUA$_{min}$) at high and low porosity and an nBUA$_{max}$ value which is markedly different in the three cases; Perspex approximately 15 dB MHz^{-1} cm^{-1}, natural tissue 50 dB MHz^{-1} cm^{-1} and the stereolithography model 25 dB MHz^{-1} cm^{-1}. The porosity value at which the peak occurs ($\phi_{BUA max}$) is similar in the natural tissue and the stereolithography model (approximately 70–75%). The value for the Perspex mimic is substantially lower at approximately 30%.
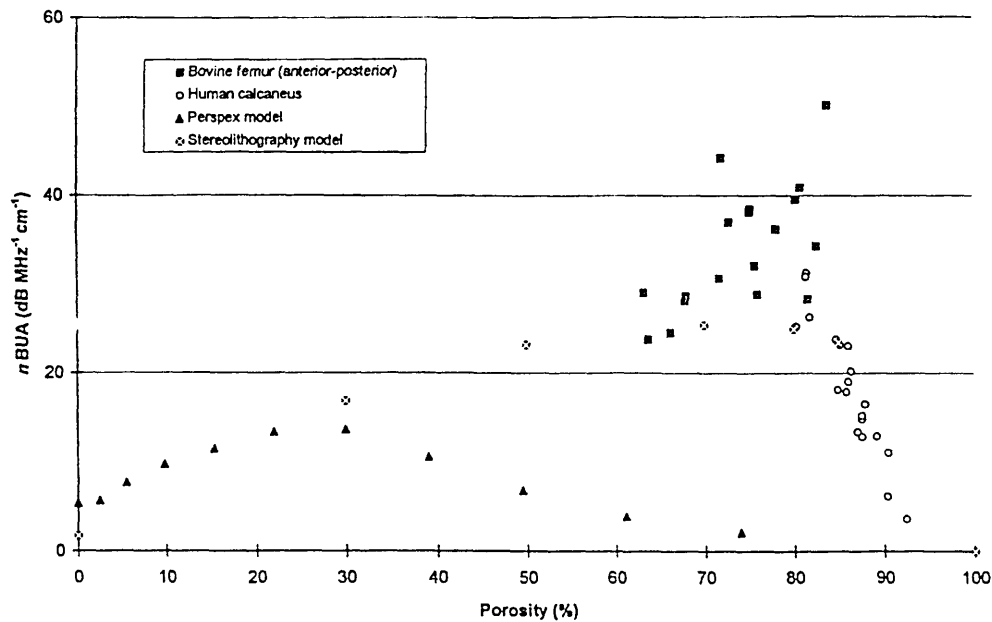

Figure 4. The relationship between nBUA and porosity for the natural tissue (human calcaneal and bovine femoral AP), the stereolithography models and the porous Perspex models.

4. Discussion

The results obtained in this study show clearly that the relationship between a measure of the density of a porous structure (porosity) and the broadband ultrasonic attenuation is not a simple linear function. Using bovine and human cancellous bone to increase the range of porosity available, we have demonstrated a peak attenuation at approximately 75% porosity for natural cancellous bone. We have also demonstrated a peak nBUA similar to that for

natural cancellous bone in the stereolithography model (the structure of which was based on histomorphometry of the natural tissue) and a very much lower peak attenuation porosity (30%) in porous Perspex.

Williams *et al* (1994) have reported results of a theoretical study which used Biot parameters to model the change in attenuation with porosity. The parameters considered included permeability, tortuosity, mean trabecular plate separation and a measure of dynamic pore size. The results showed a peak attenuation at between 65–70% porosity, however, the magnitude of the attenuations were grossly underestimated by a factor of approximately 100. The authors conclude that although the Biot theory may describe the fundamental interaction of ultrasound with cancellous bone other factors may be influencing the attenuation, either related to Biot's theory or unrelated to Biot's theory (such as diffraction, scattering or phase cancellation).

Clarke *et al* (1994), demonstrated a peak BUA at 50% porosity in a gelatine/epoxy resin cancellous bone phantom. Porosity was changed by varying the number of iso-dimensional gelatine particles and it was suggested that the peak in BUA occurred when there was a peak in the number of scatterers. Above 50% porosity the dispersed gelatine phase became the continuous phase. In the natural tissue, porosity can vary due to changes in *pore size* as well as the *number of pores*. Clarke *et al* (1994) mention that any peak attenuation in cancellous bone may occur at a porosity value other than 50% because the mode of porosity variation in the natural tissue is likely to be far more complex. Firstly, there is, of course, no true dispersed phase in three dimensions, both the bone framework and the interspersed marrow are continuous. Secondly, the marrow spaces in bone have a range of dimensions and morphology.

Clarke *et al* (1994) base their explanation of the parabola on the number of isolated scatterers present and suggest that scattering is the dominant process causing attenuation. Williams *et al* (1994) also suggest scattering as one of the processes which could account for the much larger experimental attenuation values compared to their theoretical calculations. The scattering process will take place at the boundaries between the bone and marrow, and it is therefore the surface area available for scatter which will determine the amount of attenuation. The increase in nBUA with increasing porosity, noted below 75% porosity in the study reported here, could be explained by an increase in the surface area. This may be produced either by increasing the diameter of existing marrow spaces or by the introduction of new, essentially isolated (at least in two dimensions) marrow spaces into the bone framework. nBUA will continue to increase as long as bone surface area increases. The complex cancellous bone geometry may explain the greater porosity value at which peak nBUA occurs, compared with simpler geometries such as the milled Perspex used in this study and the phantom of Clarke *et al* (1994). Cancellous bone can become extremely tortuous and convoluted before extensive perforation on the trabecular elements occurs. Eventually, the perforation of plates and rods will decrease the surface area for scattering and so cause a decrease in nBUA. This process will be the dominant factor above 75% porosity.

Our observations that the stereolithography model displays a similar $\phi_{BUA\,max}$ to natural bone, on which its structure was modelled, supports the explanation that the complexity of the structure determines the position of the nBUA peak. Also, bearing in mind that the stereolithography structures were created using calcaneal histomorphometric data, the calcaneal data and the stereolithography data fit together extremely well (figure 4).

This study also demonstrates the difference in the relationship between nBUA and porosity in the bovine samples due to testing direction. We have no clear explanation for this but the calcaneus is highly stress-oriented proximal-distally and antero-posteriorly,

whereas the femur is stress-oriented to withstand loads primarily in the proximal-distal and medio-lateral directions. The *least* discontinuity between the femoral and calcaneal data sets was seen when using the antero-posterior bovine values. Both sets of data were taken normal to the two major stress directions in the two bones, again highlighting the dependence of attenuation on cancellous structure. The variation in BUA with testing direction may well help to explain the poor correlations observed between DEXA and BUA, as any measure of bone mineral density through a given volume of tissue should be independent of direction.

These are preliminary results only. We intend to use both theoretical modelling of the interaction of ultrasound with cancellous bone and physical testing of a range of structurally controlled stereolithography models in further studies. We believe this work has demonstrated the potential of stereolithography models, with controlled cancellous-like structure, to be developed as quality-control phantoms for ultrasonic assessment of cancellous bone.

Acknowledgments

References

Biot M A 1956 Theory of propagation of elastic waves in a fluid-saturated porous solid—I and II *J. Acoust. Soc. Am.* **28** 168–91

Biot M A 1962 The mechanics of deformation and acoustic propagation in porous media *J. Appl. Phys.* **33** 1482–98

Brear K, Currey J D, Raines S and Smith K J 1988 Density and temperature effects on some mechanical properties of cancellous bone *Eng. Med.* **17** 162–7

Clarke A J, Evans A J, Truscott J G, Milner R and Smith M A 1994 A phantom for quantitative ultrasound of trabecular bone *Phys. Med. Biol.* **39** 1677–87

Gluer C C, Wu C Y and Genant H K 1993 Broadband ultrasonic attenuation signals depend on trabecular orientation: an in-vitro study *Osteoporosis Int.* **3** 185–91

Hans D, Schott A M, and Meunier P J 1993 Ultrasonic assessment of bone: a review *Eur. J. Med.* **2** 157–63

Kleerekoper M, Villaneuva A R, Stanciu J, Rao D S and Parfit A M 1985 The role of three dimensional trabecular microstructure in the pathogenesis of vertebral compression fractures *Calcif. Tissue Int.* **37** 594–7

Langton C M, Palmer C R and Porter R W 1984 The measurement of broadband ultrasonic attenuation in cancellous bone *Eng. Med.* **13** 89–91

Langton C M, Evans G P, Hodgskinson R and Riggs C M 1990a Ultrasonic, elastic and structural properties of cancellous bone *Current Research in Osteoporosis and Bone Mineral Measurement* ed E F G Ring (Bath: British Institute of Radiology)

Langton C M, Ali A V, Riggs C M, Evans G P and Bonfield W A 1990b A contact method for the assessment of ultrasound velocity and broadband attenuation in cortical and cancellous bone *Clin. Phys. Physiol. Meas.* **11** 243–9

Mosekilde Li 1989 Sex differences in age-related loss of vertebral trabecular bone mass and structure-biomechanical consequences *Bone* **10** 425–32

Njeh C F 1995 The dependence of ultrasound velocity and attenuation on the material properties of cancellous bone *PhD Thesis* Sheffield Hallam University

Tavakoli M B and Evans J A 1992 The effect of bone structure on ultrasonic attenuation and velocity *Ultrasonics* **30** 389–95

Tothill P 1989 Methods of bone mineral measurements *Phys. Med. Biol.* **34** 543–72

Williams J L, Grimm M J, Wehrli F W, Foster K R and Chung H-W 1996 Prediction of frequency and pore size dependent attenuation of ultrasound in trabecular bone using Biot's theory *Mechanics of Poroelasticity* ed A P S Selvadurai (Dordrecht: Kluwer Academic) pp 263–71